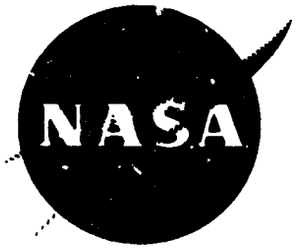

NASA CR-134796

EFFECT OF HYDROGEN ON THE MECHANICAL PROPERTIES OF TITANIUM AND ITS ALLOYS

F. H. Beck

Department of Metallurgical Engineering

The Ohio State University
Research Foundation
Columbus, Ohio 43212

June 1975

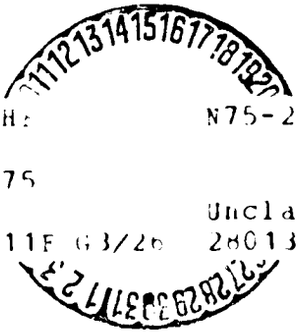

NATIONAL AERONAUTICS AND SPACE ADMINISTRATION
Lewis Research Center

Grant No. NGL-36-008-051

FINAL REPORT

1 Report No.	2 Government Accession No.	3. Recipient's Catalog No.
NASA CR-134796		

4 Title and Subtitle	5. Report Date
EFFECT OF HYDROGEN ON THE MECHANICAL PROPERTIES OF TITANIUM AND ITS ALLOYS	June 1975
	6. Performing Organization Code

7 Author(s)	8. Performing Organization Report No.
F. H. Beck	RF Project 2267 No. 16
	10. Work Unit No.

9 Performing Organization Name and Address	11. Contract or Grant No.
The Ohio State University Research Foundation 1314 Kinnear Road Columbus, Ohio 43212	NGL-36-008-051
	13. Type of Report and Period Covered Contractor Report 1/72-6/75

12 Sponsoring Agency Name and Address	14. Sponsoring Agency Code
National Aeronautics and Space Administration Washington, D.C. 20546	

15 Supplementary Notes

Project Manager, Hugh R. Gray, Materials and Structures Div.,
NASA Lewis Research Center, Cleveland, Ohio

16 Abstract

Occluded hydrogen resulting from cathodic charging of commercially pure titanium and titanium alloys, Ti-8Al-1Mo-1V and Ti-6Al-4V, caused embrittlement of the alloys. Embrittlement was a function of the interstitial hydrogen content rather than the amount of precipitated titanium hydride.

The effects of hydrogen concentration on the critical strain for plastic instability along pure shear directions was determined for alloys Ti-8Al-1Mo-1V and Ti-5Al-2.5Sn. Hydrogen, in concentrations below that necessary for spontaneous hydride precipitation, increased the strain necessary for instability formation or instability failure. The strain rate sensitivity also increased with increasing hydrogen concentration.

The effect of hydrogen on slip and twinning was determined for titanium single crystals. The critical resolved shear stress for prism slip was increased and the critical resolved shear stress for $\{11\bar{2}2\}\langle 11\bar{2}3\rangle$ twinning was decreased with increasing hydrogen concentration.

17 Key Words (Suggested by Author(s))	18 Distribution Statement
Mechanical Properties Stress Corrosion Cracking Hydrogen Embrittlement, Hydrides Titanium Titanium Alloys	Unclassified - unlimited

19 Security Classif. (of this report)	20 Security Classif. (of this page)	21 No. of Pages	22 Price*
Unclassified	Unclassified	145	$5.75

* For sale by the National Technical Information Service, Springfield, Virginia 22151

FOREWORD

This grant (NASA Contract NGL 36-008-051) covers the period July, 1966, through June, 1975. During the period July, 1966, through December, 1971, the grant was administered by R. H. Raring, NASA Hq, Washington, D.C., and was concerned primarily with the electrochemistry and stress corrosion cracking of titanium and titanium alloys in aqueous solutions. Detailed results of the research completed during the 1966 - 1971 period are contained in two dissertations (also submitted in total as special reports) and in two publications as follows:

Ph.D. Dissertation: "Some Aspects of Stress Corrosion Cracking of Alpha-Beta Alloys in Aqueous Environments," E. L. Owen (see also Contract Report No. 8, 1970).

Ph.D. Dissertation: "The Electrochemistry of Titanium in Acid Solutions and Its Relation to Stress Corrosion Cracking," R. C. May (see also Contract Report No. 9, Sept., 1971).

Publication: "Dissolution of Ti-6Al-4V at Cathodic Potentials in 5N HCl," E. L. Owen, R. C. May, F. H. Beck, and M. G. Fontana, Corrosion, Vol 28, No. 8 (Aug., 1972), 292-295 (see also Contract Report No. 11, Jan., 1973).

Publication: "Role of pH on the Stress Corrosion Cracking of Titanium Alloys," M. Inam Khokhar, F. H. Beck, and M. G. Fontana, Corrosion, Vol 29, No. 11 (Nov., 1973), 429-432 (see also Contract Report No. 13, Feb., 1974).

This report covers the period January, 1972, through June, 1975, during which time the project was administered by Dr. H. R. Gray, NASA Lewis Research Center. Research during the 1972-1975 period was concerned with the effect of hydrogen on the mechanical properties of titanium and its alloys. The report is prepared in three sections as follows:

Section 1: Cathodic charging of hydrogen into titanium and hydrogen embrittlement.

Section 2: M.S. Thesis, "The Effect of Hydrogen on Plastic Instabilities in Titanium," G. R. Stadler (see also Contract Report No. 15, June, 1974).

Section 3: Ph.D. Dissertation, "The Effects of Hydrogen on Slip and Twinning in Pure Titanium Single Crystals," John W. Fu.

Other contributors to the above research include Professor M. G. Fontana, Professor J. W. Spretnak, R. R. Roberts, Masuo Mori, and John F. Gloz.

TABLE OF CONTENTS

TABLE OF CONTENTS (continued)

TABLE OF CONTENTS (continued)

LIST OF FIGURES

LIST OF FIGURES (continued)

LIST OF FIGURES (continued)

LIST OF FIGURES (continued)

LIST OF TABLES

LIST OF TABLES

I. CATHODIC CHARGING AND HYDROGEN EMBRITTLEMENT

INTRODUCTION

Prior work showed that cathodically charged titanium alloys were severely embrittled, whereas commercially pure titanium (cathodically charged under the same conditions) was not embrittled. The difference in behavior was attributed to differences in hydrogen concentration.

On the basis of fracture surface appearance, May et al.[1] suggested that Ti-8Al-1Mo-1V alloy wire (0.56 mm) failed by two modes of fracture when strained in tension subsequent to cathodic charging for six hours at -850 mV(SCE) in 5N HCl solution. Inspection of a fracture surface revealed the presence of two zones. An outer zone could be recognized as extending from the surface of the wire a measurable distance inward and was characterized by limited topographic relief. This outer zone was concentric about an inner zone which was characterized by dimple-cone type relief. The outer zone displayed brittle fracture, while the inner zone failed by a ductile mode of fracture. If a hydrogen gradient is assumed to exist between the surface and the center of a cathodically charged sample, then the boundary between the fracture zones might define a critical hydrogen concentration characteristic of embrittlement. Also, the role of hydrogen in the embrittlement of these materials could be complicated by the reactivity of titanium and hydrogen to form titanium hydride. Hence, the question arises whether embrittlement would be the result of internal precipitation of a hydride phase as suggested by Owen et al.[2] or whether it would be more directly attributable to the presence of atomic hydrogen as an interstitial species in the titanium lattice.

The primary goal of this series of experiments was the documentation of a procedure as an effective means of increasing the hydrogen content of a specimen. Optical microscopy combined with low-angle electron reflection-diffraction and the analytical technique of ion microanalysis were used to analyze the cathodically charged specimens for titanium hydride and atomic hydrogen.

Mechanical determinations on charged specimens were in the form of tensile, hardness, and bend tests.

EXPERIMENTAL PROCEDURES

MATERIAL AND HEAT TREATMENT

The materials used in this investigation were commercially pure titanium, Ti-8Al-1Mo-1V alloy, and Ti-6Al-4V alloy. These materials

were received in the mill-annealed and cleaned condition. The commercially pure wire was straightened by straining 1.5% in tension and subsequently annealed in a vacuum of 10^{-7} mmHg for three hours at 973 K, followed by furnace cooling. The commercially pure titanium sheet was reduced from a thickness of 1.0 mm to a thickness of approximately 0.31 mm by cold rolling followed by annealing for two hours at 973 K in a vacuum of 10^{-7} mmHg and furnace cooled. Sheet material of Ti-6Al-4V was reduced to a thickness of 0.64 mm by a series of three 12% reductions and then annealed for nine hours at 1191 K in a vacuum of 10^{-7} mmHg and furnace cooled. Table I lists the geometric forms, thicknesses, and chemical compositions of the test materials.

Table I - Chemical Analyses, Heat Treatment, and Size of Test Materials

Material	Heat Treatment	Thickness or Diameter (mm)		Element (wt.%) C	Fe	Mn	Al	V	Mo	O	N	H
Unalloyed titanium	annealed	0.31	sheet	0.01	0.16	----	----	----	----	0.062	0.004	----
Unalloyed titanium	annealed	0.56	wire	0.012	0.205	----	----	----	----	0.047	0.017	11 ppm
Ti-8Al-1Mo-1V	annealed	0.64	sheet	0.02	0.13	----	7.85	1.05	1.1	0.08	0.008	102 ppm
Ti-6Al-4V	annealed	0.64	sheet	0.03	0.13	----	6.4	4.3	----	0.108	0.012	58 ppm
Ti-6Al-4V	annealed	0.56	wire	0.015	0.088	0.20	6.08	4.11	----	0.12	0.010	41 ppm

CATHODIC CHARGING AND OPEN CIRCUIT EXPOSURE

All specimens were polished on 600-grit silicon carbide paper followed by degreasing in reagent grade acetone and rinsing in distilled water.

Cathodic charging was done in aqueous hydrochloric acid solutions of two concentrations: 5N HCl and 0.025N HCl (1.7 pH) buffered with 0.075N KCl. The charging was done under potentiostatic control at a potential of -850 mV(SCE).

Exposure at open circuit potential was done on unalloyed titanium only. For these specimens sheet material was stressed in tension to 80% of the yield strength during the exposures in 5N HCl for 24, 43 and 212 hours to determine the effect of stress on hydrogen occlusion.

RESULTS

TENSILE STRENGTH, ELONGATION, HYDRIDE LAYER THICKNESS, AND SURFACE HARDNESS DETERMINATIONS ON CATHODICALLY CHARGED Ti-6Al-4V SHEET

These experiments were made only on 0.64 mm annealed Ti-6Al-4V sheet prepared into tensile specimens having 1.3 cm wide x 5.1 cm long reduced sections. Subsequent to charging the specimens were tested in the Instron at a cross-head speed of 0.05 cm/min. Microhardness measurements were then made with a Tukon tester on polished cross sections of the specimens to determine the extent of hydrogen penetration and the hydride layer thickness.

Tensile data, hydride layer thickness, and surface hardness are reported in Table II and the hardness vs. distance from surface profile of one of the specimens is shown in Fig. 1. These data show that the specimens became more brittle with increasing charging time. Also the hardness on the specimen surface increased with charging time. The surface hardness was about 480 (Knoop Hardness Number) as compared to about 340 just below the surface hydride layer. There was a slight hardness gradient which decreased toward the specimen center. One other observation worthy of mention is that titanium hydride dissolved in 5N HCl solution and the hydride thickness remained almost constant even though the sample thickness kept decreasing.

Table II - Tensile Properties, Hardness and Hydride Layer of Cathodically Charged Ti-6Al-4V Annealed Sheet, 0.64 mm Thick

Series	Charging Time (hr)	UTS (MN/m^2)	Elongation (%)	Layer (% of specimen thickness)	Surface Hardness (KHN)
	0	1010	10.25	0	369
B1	1	1030	10	1.45	364
B2	4	1020	8.8	1.4	390
B3	24	1010	7.5	1.47	470
B4	97	972	6.5	1.6	500
A1	49	1030	8.9	0.6	369
A2	61	1030	7.6	1.37	371
A3	84	987	5.6	3.35	404
A4	144	1030	5.9	3.16	525
A5	196	965	4	6.6	513

A series specimens charged in 5N HCl solution
B series specimens chared in 0.025N HCl buffered with 0.075N KCl
All charging was done at a potential of -850 mV (SCE)

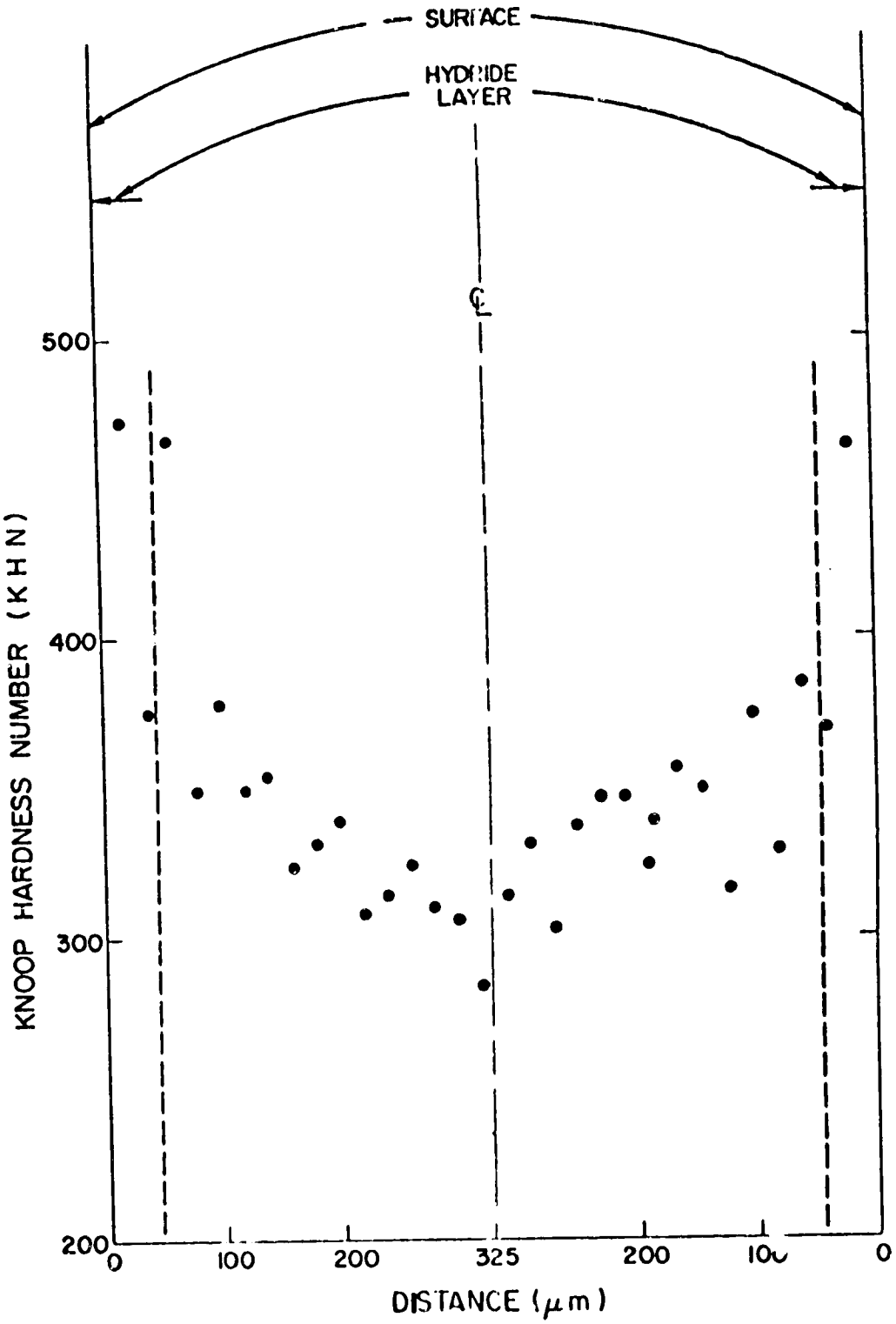

Fig. 1 - Hardness vs distance from surface

HYDROGEN DETERMINATION AND EMBRITTLEMENT OF CATHODICALLY CHARGED UNALLOYED TITANIUM, Ti-8Al-1M-1V AND Ti-6Al-4V AND UNALLOYED TITANIUM EXPOSED AT OPEN CIRCUIT POTENTIAL

Table III lists the results of cathodic charging of unstressed specimens and exposure at open circuit potential (B series unalloyed titanium specimens stressed to 80% of the yield strength during exposure) on embrittlement and surface hydrogen content. Embrittlement was determined by simple bend tests of the exposed specimens: severe embrittlement implies brittle failure with little or no deformation on bending, while no embrittlement implies that the specimens were bent 180° (plastically deformed) without fracturing. The alloy specimens were embrittled by cathodic charging while the unalloyed specimens were not embrittled.

Surface hydrogen was determined for some of the specimens by the method of ion microprobe analysis. Specific comments concerning these analyses are contained in the footnotes to the table.

DISCUSSION

TENSILE PROPERTIES, SURFACE HARDNESS, AND HYDRIDE LAYER THICKNESS

The surface hydride layer reported in Table II for Ti-6Al-4V was harder than the specimen center. Whether this was due to the hardness of the hydride plates or because the hydride plates were barriers for dislocations was not determined in these experiments, although it is generally accepted that hydride is a hard and brittle phase. If this is so, then hydride plates should serve as loci for crack initiation, and the presence of the hydride plates would, therefore, always mean premature failure. This was not the case in an earlier experiment on commercially pure titanium where the presence of hydride did not impair ductility. Smith and Otterson[3] have reported similar results.

Irving and Beevers[4] found that titanium hydride was not necessarily brittle, but the yield stress of the hydride increased with increasing nonstoichiometric vacancy concentration. The composition of the hydride in our study was not determined. The above authors also found that the hydride and titanium matrix boundary was probably a weaker point and would serve better for crack initiation than hydride itself. These results strongly suggested that cubic hydride was not brittle but was rather tough, and that cracks initiated on hydrid -titanium matrix boundaries because of a high stress concentration build up by possible dislocation interaction with hydride plates.

Table III - Effect of Cathodic Charging and Exposure at Open Circuit Potential on Bend Test Embrittlement and Surface Hydrogen of Some Titanium Materials

Test Number	Material	Geometric Form	Thickness or Diameter (mm)	Thermal Treatment	Solution	Potential (mV, SCE)	Time (hr)	Stress (% Y.S.)	Embrittlement	Surface H (ppm)
	*Ti-8Al-1Mo-1V	sheet	0.64	annealed	----	----	----	----	----	102
	*Ti-6Al-4V	sheet	0.64	annealed	----	----	----	----	----	58
B-2	Titanium	sheet	0.31	annealed	5N HCl	open cir.	24	80	none	**2.5
B-4	Titanium	sheet	0.31	annealed	5N HCl	open cir.	43	80	none	**6
B-9	Titanium	sheet	0.31	annealed	5N HCl	open cir.	212	80	none	**1.75
D-2	Titanium	sheet	0.31	annealed	5N HCl	-850	24	none	none	---
D-2	Titanium	wire	0.56	annealed	5N HCl	-850	24	none	none	---
D-5	Titanium	sheet	0.31	annealed	5N HCl	-850	56	none	none	**7
C-2a	Ti-8Al-1Mo-1V	sheet	0.64	annealed	5N HCl	-850	24	none	severe	+2,040
C-2b	Ti-8Al-1Mo-1V	sheet	0.64	annealed	5N HCl	-850	24	none	severe	+1,020
C-3a	Ti-8Al-1Mo-1V	sheet	0.64	annealed	5N HCl	-850	48	none	severe	+1,275
C-3b	Ti-8Al-1Mo-1V	sheet	0.64	annealed	5N HCl	-850	48	none	severe	+2,040
E-1	Ti-6Al-4V	wire	0.56	annealed	5N HCl	-850	24	none	severe	---
E-2	Ti-6Al-4V	wire	0.56	annealed	.025N HCl	-850	120	none	severe	---
E-3	Ti-6Al-4V	sheet	0.64	annealed	5N HCl	-850	24	none	severe	---

*These materials were used as standards for ion microanalysis. The hydrogen concentrations are bulk hydrogen determined by the producers. All values were normalized accordingly.

**These values represent ratios of the amount of hydrogen contained in the specimen relative to that contained in the standard. This method was used in the case of titanium sheet because of the lack of a hydrogen analysis for this material.

+These samples are identical except that "a" was stored in air and "b" in liquid nitrogen prior to hydrogen analysis. This was done in an effort to determine hydrogen losses in a charged sample due to outgasing during storage - no effect, just normal scatter.

Beachem[5] proposed a model for hydrogen embrittlement in steel in which hydrogen aided whatever deformation processes the matrix allowed. Hydrogen simply makes things happen. Microvoid coalescence, quasi-cleavage, or intergranular cracking are made easier because the hydrogen appears to lower the yield stress of the steel. A similar mechanism might operate for titanium; that is, hydrogen is needed to mobilize dislocations which pile up on hydride and titanium boundaries causing a build up of stress and crack initiation. Otherwise dislocations would be pinned in the matrix and no pile-up would occur on the titanium and hydride boundaries.

One possible explanation for dislocation mobilization by hydrogen is that more slip systems become available as the hydrogen concentration increases. It is known that the $(10\bar{1}0)$ plane is the slip plane for pure titanium, but as interstitial impurities increase the (0001) and $(10\bar{1}1)$ slip planes become operative.

Research performed over the last few years has shown that metals can be caused to fracture because of what are known as plastic instabilities.[6,7,8] This term refers to concentrated shear along certain characteristic or slip lines as defined by the continuum plasticity theory, these being directions of pure shear. The phenomenon is dependent on the stress state of the system, the strain rate, and the strain hardening exponent of the metal; it is also temperature dependent. Actually this phenomenon is a realistic means of understanding what has been to this time referred to as quasi-cleavage fracture.

Plastic instability studies may be very important in understanding the role of hydrogen on the stress corrosion cracking of titanium. This is particularly true in light of the evidence advanced by Beachem[5] (that hydrogen actually acts as a plasticizer in iron instead of an embrittler). Thus, Section II of this report will examine whether interstitial hydrogen can, in fact, cause titanium to behave more plastically (strain harden more quickly and thus reach the ideal plastic state sooner). This would mean that increased hydrogen would cause a decrease in the strain necessary to cause failure by instabilities.

The above phenomenon is based on a material strain hardening until that point where strain hardening is exhausted and thus the change in stress ($d\sigma$) reaches a maximum. At this point, the material acts in an ideally plastic manner along particular characteristics and, depending on the strength of the instability, failure occurs. Thus, a basic material parameter is the true strain necessary for formation of instabilities or fracture by instabilities.

HYDROGEN CONCENTRATION AND EMBRITTLEMENT

The sample preparation procedure was selected to minimize ambiguities regarding the identity of the surface film. Tomashov[9,10] indicates

that the air-formed film on titanium is TiO. Thus, it is assumed that the specimens used in this investigation had a thin surface film (approximately 16 Å) of TiO immediately prior to test initiation. Because titanium will not spontaneously passivate in 5N HCl solution,[11] the surface reaction must be either the reduction of the surface film to form titanium or titanium hydride, or the reduction of hydrogen ions. Experimental observations of changes in the current density with time tend to support the supposition that oxide reduction rather than hydrogen evolution predominates as the cathodic reaction during the early stages of cathodic charging. Observations of the current density indicate that the initially low value increases at least one order of magnitude during the first hour of a test. The increase in current density is accompanied by a corresponding increase in the rate of hydrogen evolution. Once the initial increase in current density is completed the current remains constant for the duration of the experiment. Probably this change reflects the formation of a surface hydride.[12,13,14]

The above reasoning suggests that the embrittled materials reported in Table III were probably covered with a surface film of titanium hydride during most of the time of the charging experiments. The dominant reduction reaction on the hydride surface appears to be hydrogen reduction. The fact that the surface hydrogen content of Ti-8Al-1Mo-1V alloy was increased approximately one order of magnitude in 24 hours of charging indicated that these conditions were conducive to hydrogen occlusion. Further, the fact that the alloy was embrittled under these conditions indicated that hydrogen occlusion was the cause of embrittlement. However, the question immediately arises as to why the alloys displayed embrittlement while the commercially pure titanium did not under identical conditions. One possibility is the lower solubility limit of hydrogen in pure titanium.

The spontaneous precipitation of internal hydrides in titanium alloys would be expected to occur at a supersaturation of several hundred ppm,[15] probably much less for pure Ti. Although the total hydrogen content of the pure titanium sample could be expected to increase with charging time, the amount of atomic hydrogen would remain below 100 ppm. Data in Table III support this reasoning. The vanadium plus hydride ratio for sample D-5 is 40 times that of the standard. Because this material is commercially pure, most of this increase represents an increase in the hydride concentration. The interstitial hydrogen content of the same sample was increased only seven times that of the standard, thus suggesting that most of the hydrogen in the pure titanium was present in the form of hydride. The fact that titanium exhibits ductile behavior when known to contain significant amounts of internal hydride indicates that embrittlement is due mainly to interstitial atomic hydrogen rather than to hydrogen in the form of hydrides.

The work of May *et al.*[1] tends to support the above result. He observed severe embrittlement of Ti-8Al-1Mo-1V alloy charged in 5N HCl for six hours. However, an identical sample stored for 15 days exhibited ductile behavior when subsequently tested. It has been established in

the present work that hydrogen in some form has an embrittling effect on titanium alloys. Hence it is not unreasonable to assume that the degradation observed by May was the result of hydrogen occlusion. The regeneration of ductility can be explained on the basis of redistribution of interstitial hydrogen, either by diffusion out of the sample or by precipitation as hydride phase, or by uniform homogenization within the entire sample thickness. Results of the present research are insufficient to permit a distinction between these two mechanisms.

A final consideration is the effect of stress on hydrogen occlusion. This is demonstrated by samples B-2, B-4, and B-9. As in the case of sample D-5, the amount of hydrogen present as atomic hydrogen is less impressive than the amount present in these stressed specimens of pure titanium as atomic hydrogen is less impressive thatn the amount present as hydride.

CONCLUSIONS

The effect of cathodically charged hydrogen on the tensile properties, hardness, and embrittlement of commercially pure titanium and titanium alloys, Ti-8Al-1Mo-1V and Ti-6Al-4V, was determined.

Cathodic charging in 5N HCl solution increased the total hydrogen content of commercially pure titanium, and of Ti-8Al-1Mo-1V and Ti-6Al-4V titanium alloys.

Hydrogen occlusion caused embrittlement of Ti-8Al-1Mo-1V and Ti-6Al-4V alloys.

Embrittlement was a function of the interstitial hydrogen content of the lattice rather than the amount of hydrogen precipitated as titanium hydride.

*Sample D-5 was not embrittled after 56 hours of charging in 5N HCl solution.

II. THE EFFECT OF HYDROGEN ON PLASTIC INSTABILITIES IN TITANIUM ALLOYS

INTRODUCTION

The effect of hydrogen on the properties of metals, including titanium and its alloys, has been investigated for many years. Of the several basic means by which hydrogen can gain entry into titanium hydrogen generated during corrosion is the most important and is most discussed in the literature. In addition to generating hydrogen, corrosion is the primary means for sharpening the notch or crack, for increasing the stress intensity, for producing ions capable of adsorbing on the surface and absorbing into the lattice, and/or for producing surface films thought to be vital to stress corrosion.

It is believed that premature failure of titanium in a corrosive environment follows the basic mechanisms of normal fracture. Exceptions to this would be those cases in which the stress corrosion is known to occur solely by anodic dissolution (an electrochemical process). Therefore, it is of primary importance to understand fracture mechanisms if one is to understand stress-corrosion failures.

As a background for the present study the basic theories of stress corrosion of titanium alloys will be reviewed. Since hydrogen absorption seems to play a vital role in the stress-corrosion cracking process, an attempt will be made to review literature concerned with the effect of absorbed hydrogen on the mechanical properties of metals. Finally, the basic modes of metal fracture and their importance to this study will be considered.

The experimental work performed in this research was designed to determine the effects of hydrogen concentration on the critical strain at which plastic instability along pure shear directions occurs. The materials used were titanium alloys Ti-8Al-1Mo-1V and Ti-5Al-2.5Sn.

LITERATURE REVIEW

TITANIUM STRESS CORROSION

A number of variables have been associated with the stress corrosion of titanium. These include environment, electrochemical potential, stress, metallurgical structure, alloy content, surface films, and heat treatment.

Reduced notch fracture toughness has been reported for titanium in hot salt, nitrogen tetroxide, methanol, and salt water environments.

Beck[16] found that Cl^-, Br^-, and I^- ions caused cracking and that the cations present were unimportant. He also observed that in an aqueous NaCl environment, as the potential was shifted in the active direction the crack velocity increased, while a shift in the negative direction caused the velocity to decrease until a point was reached at which the crack stopped propagating [~ -1000 mV (SCE)]. He reported this to mean that the mechanism was anodic dissolution dependent on the Cl^- ion mass transport. Powell and Scully[17] theorized that the OH^-/Cl^- ratio was critical and that at lower cathodic potentials the higher ratio caused a film formation which limited or eliminated ingress of hydrogen into the metal. Chen et al.[18] showed two areas of susceptibility in different concentrations of NaCl and KBr and showed that the propagation rate increased to about -500 mV (SHE) [~ -750 mV (SCE)] at which point the propagation decreased with increasing potential. Green and Sedricks[19] showed that the cracking velocity had two maximums for Ti-8-1-1 material in 3.5% NaCl solution and that the data agreed with that of Beck only in the region -800 to -200 mV (SCE) as shown in Fig. 2.

The stress state present is known to have an effect on the susceptibility of an alloy to stress-corrosion cracking. The procedural developments in fracture toughness testing have thus played an important role in the study of stress-corrosion cracking. Many authors are presently using stress intensity values at the onset of stress-corrosion cracking to compare titanium alloys for sensitivity. It is generally accepted that it is very difficult, if not in some cases impossible, to initiate cracking in titanium, thus most work has been done with a pre-existing crack; although Fontana et al.[20] demonstrated that initiation on smooth Ti-8-1-1 sheet in aqueous room temperature environments is possible. The triaxial tension state of a notch causes reduced ductility in the material tested and enhances those factors which lead to brittle-like failure.

The metallurgical structure as well as the alloy content have major roles in determining susceptibility. Lists have been compiled of those alloys susceptible in salt water,[21-25] generally alpha alloys are susceptible while alpha-beta alloys may or may not be. Stress-corrosion cracks in alpha-beta alloys normally follow the alpha phase or the interface. The alpha stabilizer, aluminum, has a marked effect on susceptibility. There is a transition to susceptibility at about 5-6 per cent aluminum and many investigators have related this to the formation of the ordered Ti_3Al phase.[26,27] R. A. Wood et al.[28,29] concluded that the size of the Ti_3Al particles was also important. They felt these particles cause a nonhomogeneous planar slip which leads to micro-void nucleation and coalescence by localized shear. The result is reduced fracture toughness and an enhanced chemical potential at the slip bands. They suggested the latter could contribute to sustain anodic dissolution. Yet, Swee et al.[30] have suggested that the role of Ti_3Al is to cause coplanar slip which they believe is a necessity for SCC. Lane et al.[31] reported that microstructures containing long coarse alpha were the most susceptible.

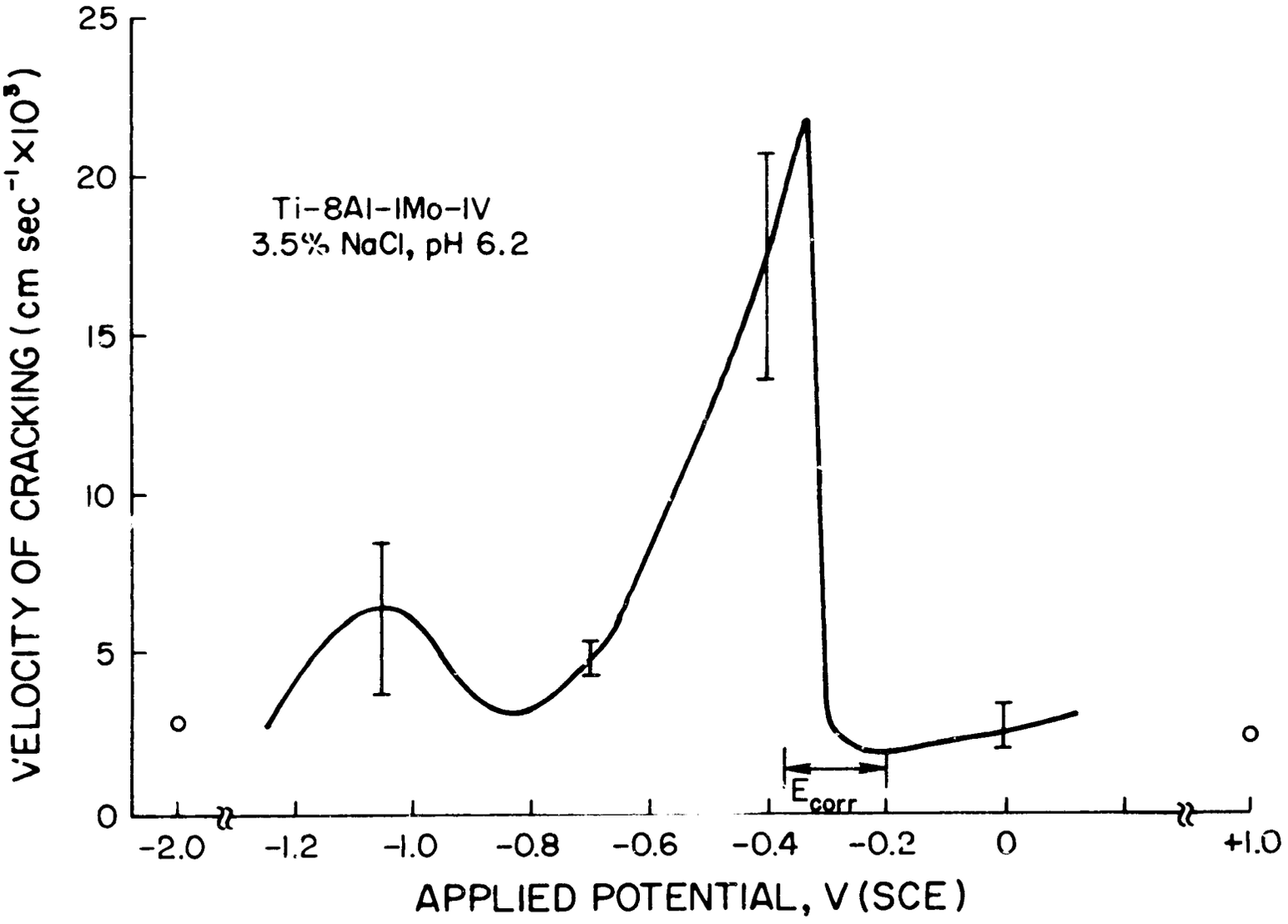

Fig. 2 - The effect of applied potential on the velocity of cracking of Ti-8Al-1Mo-1V alloy in a neutral 3.5% NaCl solution (after Green and Sedricks[19])

Heat treatment of the alloy is important to the resulting final microstructure and its susceptibility. The temperature range of 755-1089 K was determined to give the most susceptibility due to Ti_3Al precipitation.[22] Also the alpha platelet size and its effect as determined by Lane[31] can be controlled by heat treatment.

May et al.[32] discussed the importance of surface layers to stress corrosion. He attributes the hydride surface layer as being most important in the susceptibility and refutes the oxide layer theory presented by other investigators.[27] Green and Sedricks[19] stated that their investigation showed that stress-corrosion cracking in Ti-Al alloys was confined to an environmental regime in which surface films are relatively thin. They theorized that the increased susceptibility with increased aluminum content was related to a thinner surface film formation, and that on even the most metallurgically susceptible alloys stress-corrosion cracking can be controlled by controlling those factors (i.e., pH and potential) which influence film formation.

There are many proposed mechanisms for stress corrosion in titanium alloys. These include stress sorption, brittle film failure, anodic dissolution, and hydrogen "embrittlement."

HYDROGEN IN TITANIUM

It has long been an accepted fact that hydrogen absorption into many metals causes "embrittlement" of one form or the other. Many authors have attempted to explain the role of hydrogen on the mechanical properties of metals and a good review of the subject is presented by Cotterill.[33] Some related hydrogen embrittlement of steel to the variables in the Griffith crack theory. For example, hydrogen adsorbed on the crack surface lowers the surface energy term; or the pressure of gaseous hydrogen in a microcrack adds to the total energy released by the system. A theory proposed by Morlet et al.[34] introduced the possibility of the embrittlement being due not only to hydrogen in voids, but also to hydrogen in the triaxial stress region created by the voids. The precise mechanism involving this hydrogen in solution at these regions was not explained.

In a recent article, C. D. Beachem,[5] suggested that hydrogen in steel may well act as a "plasticizer" rather than an embrittler. Thus, hydrogen aids whatever deformation process the state of stress at a crack tip may dictate. Observations showed that cracks propagated entirely by microscopic plastic flow at the crack tip during stress-corrosion cracking and hydrogen-assisted cracking. Microvoid coalescence, quasi-cleavage, or intergranular fracture were shown to occur depending on the stress intensity and the hydrogen concentration at the crack tip. The relationships of these are shown in Fig. 3. These findings are well accepted by those who contend that plastic instability in a material is a reality. This theory will be covered later in this presentation.

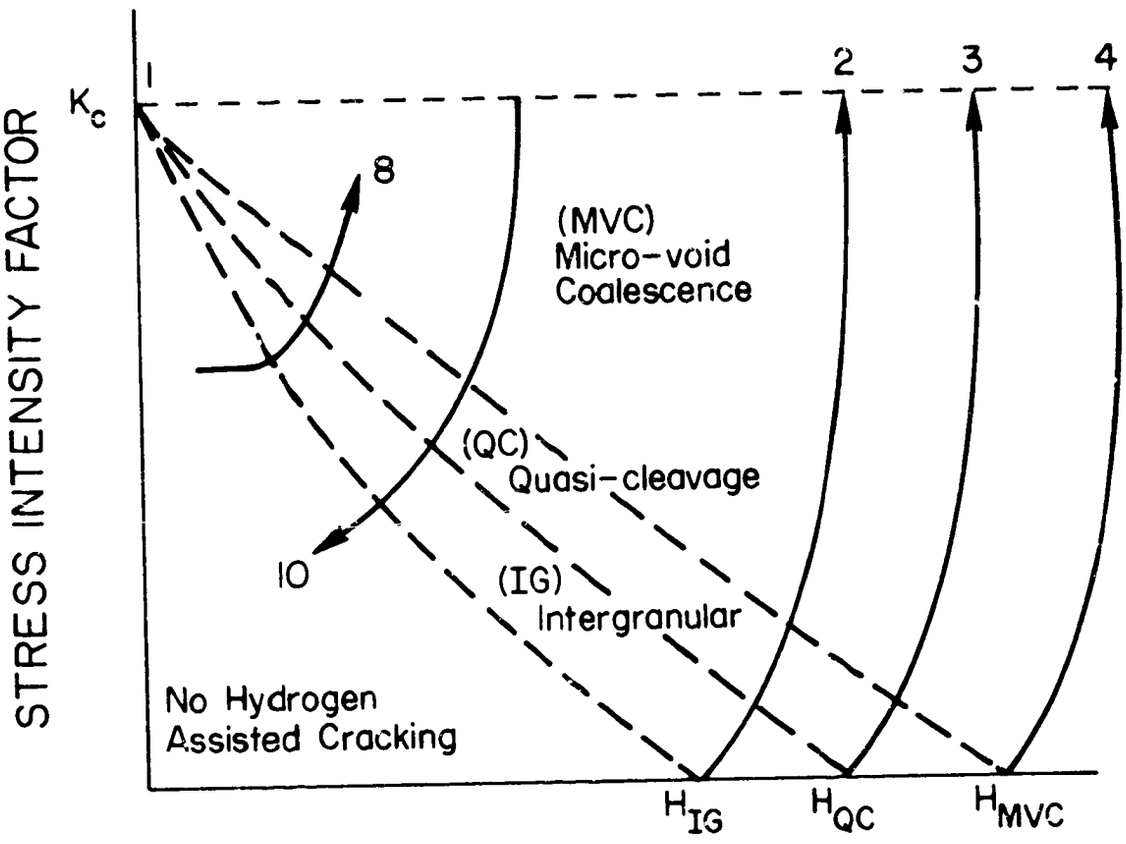

(1) No hydrogen

(2), (3), (4) Initiation in any of the three fracture modes depending on H_2 concentration

(8) Constant load with H_2 diffusing to crack tip causing shift to right

(10) Wedged specimens with decreasing stress intensity

Fig. 3 - Interrelationship between stress intensity and dissolved hydrogen content (after Beachem[5])

Unlike steel, which is classified as an endothermic occluder of hydrogen, titanium is an exothermic occluder. It is known to form a compound with titanium. Ideally the compound is TiH_2 but actually it is approximately $TiH_{1.5}$ - TiH_2.[35] Hydrogen in titanium has been associated with the embrittlement of the material. The embrittlement is divided into two categories depending upon the loading rate of the specimen. These are known as impact embrittlement and low-strain-rate embrittlement. Both types are believed to be due to the hydride phase precipitation. Williams[36] has related the impact embrittlement to hydrides formed on cooling to room temperature. If precipitation does not occur on cooling to room temperature a supersaturated condition exists and the action of strain can then cause hydride precipitation. This latter type is known as strain-induced hydride. Resistance to hydride precipitation has been associated with the solubility of hydrogen in the matrix and this solubility is apparently increased with certain alloy additions (i.e., aluminum). Boyd[35] made a thorough investigation of both the spontaneous and strain-induced hydrides formed in Ti-8-1-1. He believes that the effect of aluminum is to increase the activation energy of hydride nucleation, and that the strain-induced hydrides are nonequilibrium precipitates having lower activation energy for nucleation than the spontaneous hydrides. The general view of the mechanism of hydrogen embrittlement is one that the hydrides limit the amount of plastic deformation thus making the material less ductile. The effect is to cause a decrease in the reduction of area as the hydrogen concentration increases.

The data gathered on the mechanical properties of titanium and its alloy[37-39] show generally that the tensile and 0.2% offset yield strength increase with increased hydrogen concentration. However a point which is little emphasized is that--whether the 0.2% yield strength decreases, stays relatively the same, or increases--the proportional limit generally decreases when hydrogen concentration increases.

A workable model based on the above theories of hydrogen embrittlement has been proposed to explain stress corrosion of titanium[40] and the conclusion that the model was basically correct for crack propagation was reached by Owen et al.[30] The model is based on the production of hydrogen which--during the corrosion of titanium--is adsorbed and eventually absorbed into the lattice near the crack tip. It is partially based on Otsuka's[13] report that hydrogen is always absorbed when titanium is corroded in an acidic environment. The hydride responsible for stress-corrosion embrittlement is said to be the strain-induced (slow-strain rate) hydride. The hydride is thought to precipitate along active slip planes at the crack front. These hydrides are then thought to cause the slip planes to become inoperative and this in turn limits the plastic relaxation. Since slip is restricted, the plastic zone is thought to be very small--a condition promoting brittle fracture. Because of the velocity of the stress-corrosion crack this model depends on a discontinuous crack propagation where the crack can for a short distance outrun the hydrogen-containing lattice before crack blunting occurs. This condition is sometimes referred to as the "long-range effect."

The long-range effect has been examined by Spurrier and Scully[41] and found to be due to absorbed hydrogen which causes the initial fracture mode to penetrate the width of the grain and penetrate into adjacent grains if the misorientation is not too large. The long-range effect is due to a process referred to as low energy tearing (low energy relative to that required to tear dimples) and is said to be recognized fractographically as cleavage-like patterns, striations, and regions of planar slip. J. C Scully has long been an advocate of hydrogen as the important element in the stress-corrosion cracking of titanium, as witnessed by some of his papers.[42-44] but this is the first paper that seemingly questions the role of hydrides. Reference is made to the possibility that hydrogen absorbed at the crack tip may result in striations caused by the interaction of plastic deformation on more than one slip system. This could then result in the production of cleavage-like river patterns originating from a plastic deformation process.

FRACTURE OF METALS

The language used by those engaged in fractography is confusing to say the least. Brittle fracture has been described by numerous surface fracture patterns whose distinction is rather ambiguous. These include cleavage, quasi-cleavage, river-pattern, transgranular striations, near classic cleavage, and nonclassic cleavage.[45] The distinction seems to be how much or how little plastic deformation has occurred. Recent work has indicated that plasticity is an important feature of practically all fracture, even in the field of stress corrosion. Colangelo and Ferguson[46] showed that the path of the primary stress corrosion crack in a high-strength steel (4340) followed the shear bands within the plastic zone at the crack tip.

The two basic modes of fracture are categorized as (1) pore formation and coalescence, and (2) plastic instabilities in the direction of pure shear.

Pore formation--sometimes known as cavitation--is nucleated at some discontinuity in the matrix (inclusions, precipitates, grain boundaries, etc.). These pores then increase by further plastic deformation and when the loading is halted the pores stop growing. This is the concept of pure ductile fracture. As the load is increased the ligaments between the pores reduce in size like tiny tensile specimens until rupture or 100% reduction occurs. The stress state of the system is an important factor in the final shape of these pores, as has been shown by the work performed by Beachem.[47]

Plastic instability in pure shear directions, defined as the localization of plastic flow leading to highly concentrated strain, has been the subject of intensive studies by Spretnak, one of the authors of this paper. Clear evidence of this phenomenon leading to fracture has been given by Hayden and Floreen.[48] This phenomenon is not to be confused with the geometric instability which is the typical necking

experienced in tensile tests. A comparison of the mathematical models of these instabilities is presented by Chakrabarti.[8] The localization defined as plastic instability has been shown[6,7,8] to take place along characteristics determined by continuum plasticity theories. These are directions of pure shear (zero extensional strain) and in plane strain conditions (maximum shear stress directions). This instability or discontinuity in tangential velocity is based on the material reaching the ideally plastic state in which the stress cannot be raised above the flow stress. Mathematically the ideal plastic state occurs when

$$d\sigma/d\epsilon = 0 \quad \text{and} \quad d\sigma_{ij}d\epsilon_{ij} = 0 . \tag{1}$$

The latter expression shows that over a finite strain value no work is accomplished. The equation predicting this instability phenomenon can be shown to be

$$d\sigma = \left(\frac{\partial\sigma}{\partial\epsilon}\right)d\epsilon + \left(\frac{\partial\sigma}{\partial\dot{\epsilon}}\right)d\dot{\epsilon} + \left(\frac{\partial\sigma}{\partial T}\right)dT \leq 0 . \tag{2}$$

Thus, the condition is dependent on the strain, strain rate, and change of stress by adiabatic heating.

Plastic instability failures normally occur as three distinct types. The first type occurs as highly localized plastic flow with the thickness of the instability band being smaller than any second-phase particles in the matrix (the fracture surface would be very flat and generally particle free). This type is referred to in the literature as a quasi-cleavage fracture, and is supported by Chang[5] who observed plastically deformed metal just below the quasi-cleavage fracture surface. Thus, the fracture was not caused by metal reaching its theoretical cohesive strength and cleaving.

When the plane of instability flow is thicker than second-phase particles there is a tendency toward pore formation at those particles within the plane of instability and coalescence of these pores occurs. This is designated as the second type of instability controlled flow.

The third type may not actually be instability controlled although it may be instability flow limiting. It occurs when diffuse deformation produces pores which are then connected by instability flow. Thus, the instability limits the total deformation possible when 100% reduction of ligaments between pores has occurred.

Since plain strain conditions can exist at notches and flaws in material, the localization of plastic flow is believed to be basic for the development of crack instability. Thus, fracture of the material occurs by either localization (for those materials having low resistance

to plastic instability) or by decohesion due to pore formation and coalescence (for those materials having high resistance to plastic instability and which are interrupted by this latter process before localization of flow can occur). The instability condition is thus basic to the understanding of "brittle" fracture where brittle fracture is defined as unstable crack propagation. It is based on the exhaustion of strain hardening and the obtaining of a state of dynamic ideal plasticity in a very localized region. This plasticized state and its relationship to fracture in metals is described by Spretnak.[51] It is an important condition in both ductile and so-called brittle materials. And since stress-corrosion cracking, except for those conditions where total reliance upon anodic dissolution has been proven, adheres to the fundamental fracture modes these fracture modes are important to the understanding of stress-corrosion cracking.

Recht[52] postulated that titanium and its alloys should be particularly susceptible to localized plastic shear and showed this in his machining experiments. Work by Ernst and Spretnak[8] showed that the susceptibility of titanium alloys was between those AISI 4340 alloy steel having 1228.9 MN/m^2 tensile strength and AISI 4340 having 1498.2 MN/m^2 tensile strength. They also showed that the strength of the instability was very great compared to AISI 4340. In other words fracture occurred immediately after the instability appeared. Their work further demonstrated that instability formation is favored by high strain rates. Chakrabarti[53] showed that the lower the strain-hardening capacity and the strain-rate sensitivity of the material (4340) the lower the strain to the onset of shearing instability and the strain to failure. Because of the high strain-hardening exponent for titanium it is expected that strains to the onset of instability and failure will be relatively high.

EXPERIMENTAL PROCEDURES

Two titanium alloys, supplied by Reactive Metals, Inc., were used for this study. Chemical analyses of the alloys are given in Table IV. Since the alloys were treated in different manners with respect to specimen design and preparation and since they behaved differently experimentally, the two alloys will be handled separately in the description of this study.

ALLOY Ti-5Al-2.5Sn

The alloy used for the initial tests was Ti-5Al-2.5Sn of the ELI (extra-low interstitial) designation. Extra low interstitial was selected in order to obtain an all alpha microstructure (commercial Ti-5Al-2.5Sn contains a small amount of beta phase).

Table IV - Chemical Analysis of As-Received Titanium Sheet

	Ti-5Al-2.5Sn (wt %)	Ti-8Al-1Mo-1V* (wt %)
Aluminum	5.0	7.85
Tin	2.5	--
Iron	0.04	0.13
Oxygen	0.091	0.08
Nitrogen	0.012	0.008
Carbon	0.01	0.02
Vanadium	0.02	1.05
Molybdenum	< 0.01	1.1
Manganese	0.03	--
Copper	< 0.01	--
Hydrogen	--	0.01

*This is the same sheet material as used in Section I, Table I.

The material was originally stocked as 5.08 mm plate. It was then hot-rolled by RMI and "conditioned" (etched) to a thickness of 0.76 mm. The individual specimens were then wet ground in a fixture to 0.66 mm through 600-grit silicon carbide metallographic paper. Specimens were cut from the sheet such that the longitudinal axis of the tensile specimen was parallel to the rolling direction of the sheet. Final grinding was also performed such that the final cutting direction was parallel to the longitudinal axis. Thus, no transverse marks were found on the specimens. The specimens were milled to the dimensions shown in Fig. 4 to provide a width-to-thickness ratio of 25:1 (in bending this has been shown to be the critical ratio necessary for a plane strain state of stress). Also, work by Chakarbarti[8] has shown that curves relating strain to onset of instability and to failure started to flatten out at width/thickness ratios greater than about 25:1.

This experiment was concerned with finding the effect of hydrogen concentration on plastic instability formations and was designed such that pore formation and its interruption of this instability phenomenon would not occur. Thus, phase interfaces like α-β, where pore formation is enhanced, were eliminated by using the ELI material. Hydrogen was charged at high temperature as a gas to obtain hydrogen homogeneity.

Initially all specimens were vacuum annealed to obtain a low reference hydrogen level. The vacuum anneal cycle was $3\frac{1}{2}$-4 hr at 1083 K followed by a furnace cool in vacuum. The vacuum obtained was 0.8-1.0 x 10^{-7} mmHg. The level of hydrogen obtained after this treatment was checked by Leco Technical Service Laboratory, St. Joseph, Michigan. Analysis showed an average hydrogen content of 10.5 ppm. This compares well with values obtained by others using a similar thermal treatment.[53]

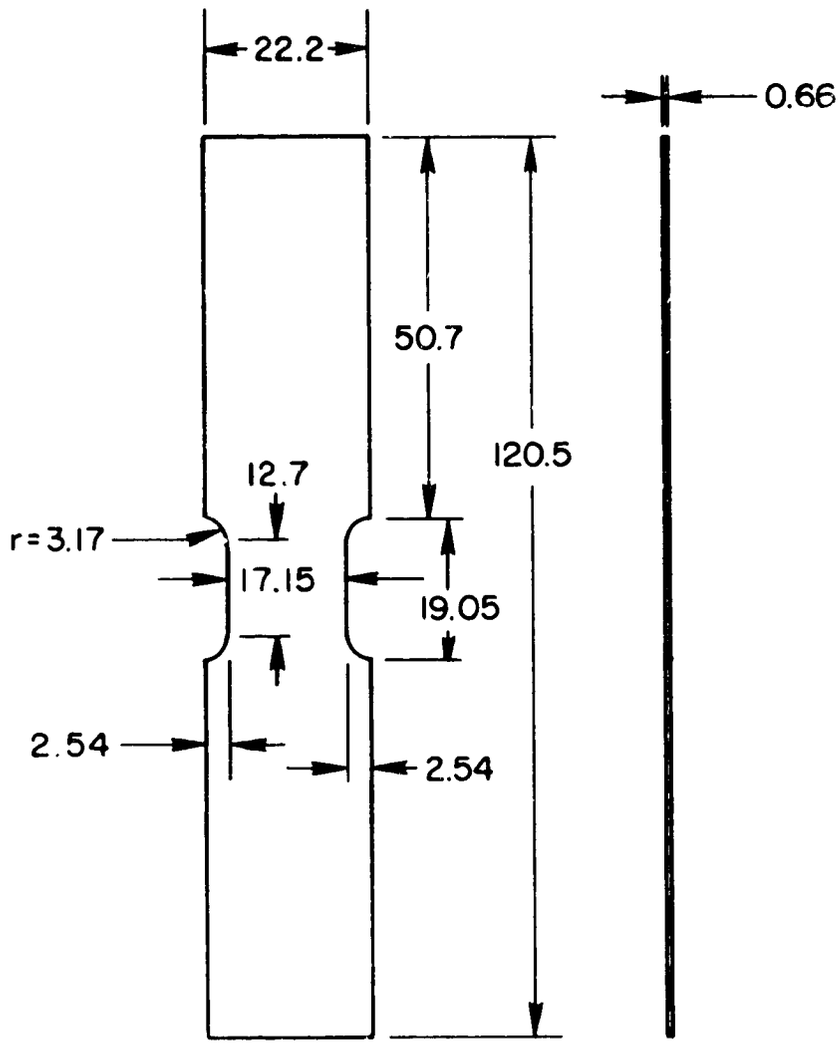

Fig. 4 - Sheet tensile specimen for Ti-5Al-2.5Sn

The hydrogenation procedures were similar to those used by Trzeciak.[54] A diagram of the equipment used in the present study is shown in Fig. 5. A very-slow-leak valve allowed maximum efficiency in the cold trap between the gas source and the specimens and a capsule whose volume had been premeasured was filled to a specific pressure depending on the amount of gas which was desired to diffuse into the titanium sample. (The appendix contains a typical calculation used to give a particular concentration of hydrogen.) The capsule was then sealed off and heat treated in a box furnace. Heat treatment was 1093 K for 20 minutes followed by a furnace cool to 953 K for a total furnace time of $2\frac{1}{2}$ hours. The sample was rapidly cooled from 953 K.

This charging procedure is based on the fact that titanium is a very good "getter" of hydrogen and will quickly absorb the gas available in the capsule (to the equilibrium vapor pressure of approximately 10^{-9} mmHg at room temperature). The concentrations of hydrogen used in this study were such that at the homogenizing temperature the hydride was not stable, as shown in work by Lenning.[53] Thus, except for the highest concentrations, the hydrogen absorption depended on a titanium-hydrogen interaction but not on hydride formation. Lenning[53] showed that hydrogen concentration throughout a specimen charged in this manner was uniform.

Predetermined levels of hydrogen were 10, 80, 150, and 500 ppm. The actual content was determined using a hydrogen analysing apparatus--based on a gas chromatograph sensing system--developed in this laboratory. The operation of this equipment is described by Gloz.[55] A brief summary (below) of the apparatus will give the reader an appreciation for the potential of this procedure.

Basically the system consists of an induction coil furnace to heat a small pre-weighed specimen of the metal and thus drive off the hydrogen. The specimen is located in a tubing system which has been evacuated. The same diffusion pump used for evacuation is used to pump the hydrogen, driven off by heating of the specimen, into a particular area of the system. This hydrogen is then transferred by a mercury pump to a collection station previously purged with nitrogen where volumes can be measured. A syringe is then used to transfer a given amount of the hydrogen and nitrogen gas mixture to the gas chromatograph where the hydrogen concentration is graphically plotted. A hydrogen gas standard is used to check the gas chromatograph, and National Bureau of Standards Ti-H samples are used to check the collecting system during any set of runs. As an example of the accuracy of the system, the samples reported by Leco to contain 10.5 ppm hydrogen were also analyzed with this gas chromatograph method and found to contain 9.7 ppm hydrogen. Table V gives results of further analyses performed on charged specimens.

After charging the specimens were marked (printed) with a grid pattern. Thus, by following the grid distortion, the strains at a given load could be calculated. The grid printing procedure was outlined in the work by Chakabarti[8] and a modified reproduction is given below.

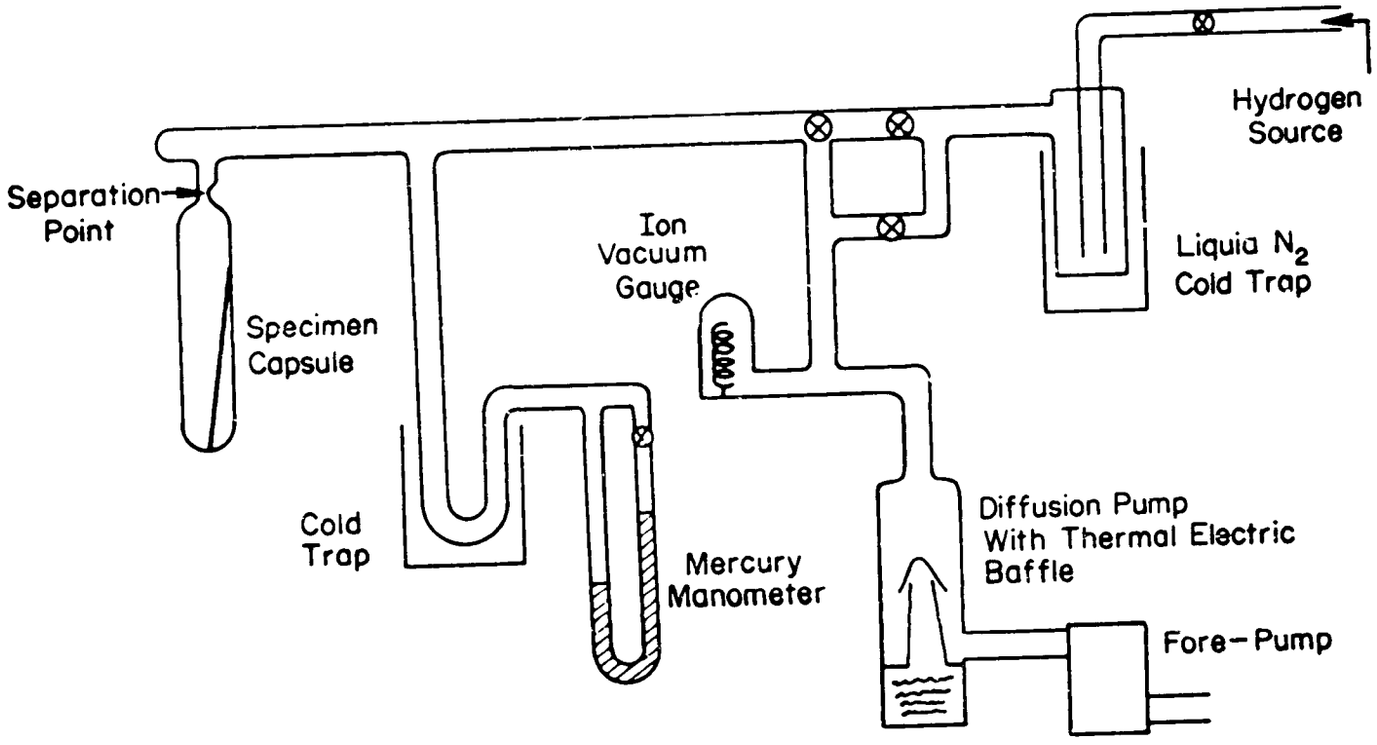

Fig. 5. - Diagram of hydrogenating system

Table V - Hydrogen Concentration of Selected Specimens

Specimen	Calculated Hydrogen (ppm)	Actual Measured Hydrogen (ppm)
1 - Test Strip (vacuum annealed)	10	9.5
2 - Tensile Specimen (vacuum annealed)	10	12.5
3 - Test Strip (hydrogen charged)	125	123
4 - Test Strip (hydrogen charged)	250	265
5 - Tensile Specimen (hydrogen charged)	150	154

(1) The printing surface is thoroughly cleaned and degreased using acetone.

(2) A thin uniform layer of coating solution is applied to the surface to be printed by wiping with a soft, solution-saturated tissue. (The coating solution consists of a 50-50 mixture of Kodak Photo Resist and Kodak Photo Resist Thinner.)

(3) The coating is allowed to air dry (in the dark) for at least 45 minutes.

(4) The coated specimen is then exposed to ultraviolet light for 3 to $3\frac{1}{2}$ minutes. (It is very important that good contact exist between the grid negative and the sample--weights may be necessary to optimize the contact.) Another important step is to keep the lamps as cool as possible. Heat locally was extremely concentrated and a fan was used for cooling.

(5) The specimen is then dipped in Kodak Photo Resist Developer for 2 minutes followed by Kodak Photo Resist Black Dye for 15 seconds.

(6) The specimen is then rinsed in slowly running water for about 5 minutes.

(7) The specimen is then air or force dried at 363 K for about 5 minutes.

The grid pattern produced is very distinct and the particular negative used in this experiment gave square grids of 9 lines/cm over the gage length of the specimen. The prepared specimens were then stored in liquid nitrogen until the time they were tested.

Specimens were tested with an Instron tensile testing machine at room temperature using a crosshead speed of 0.2 cm/minute. In the gage length used this produced a strain rate of 0.1575 min^{-1}. The specimens were mounted in grips and alignment was kept as perfect as possible. Poor alignment would have been visible during the testing since deformation bands were visible on the specimens. Work prior to the actual testing, using strain gages mounted to the sheet specimens, showed that all gages were reading within 1% of each other and thus bending was minimal.

The load was recorded on a X-Y plotter with one parameter being the time function. Distortion of the grids with load was recorded by a 35 mm Nikon camera mounted a small distance from the specimen surface. The corresponding load was marked on the X-Y chart each time the camera shutter was released.

Calculations of true stress versus true strain were made using measurements taken from the grid deformation. (The film negatives were enlarged approximately ten times, which resulted in an actual grid size enlargement of about 7X.) Using spring-loaded dividers and a scale divided into increments of 0.254 mm, the length and width measurements of the grid were obtained. From these true strain could be obtained, since it is the natural logarithm of the instantaneous length divided by the original length ($\epsilon = \ln L/Lo$).

This relationship is true up to the point of necking but at that point accuracy decreases. The amount of error is small if the necking is small and the only way of obtaining a true value would be to use $\epsilon = \ln Ao/A$. This would mean that a way of measuring instantaneous thickness as well as width would be needed. For the Ti-5Al-2.5Sn alloy the necking was greater than for the Ti-8Al-1Mo-1V alloy. As will be shown in the Discussion, the latter alloy had strain values that agreed well with those based on the final area.

From the experiments it was intended that strain parameters measured as above could be related to instability formation or load disruption, and could then be compared at various hydrogen levels.

ALLOY Ti-8Al-1Mo-1V

Figure 6 shows the tensile specimens used for the Ti-8Al-1Mo-1V alloy. This alloy was of a higher strength than the former one and

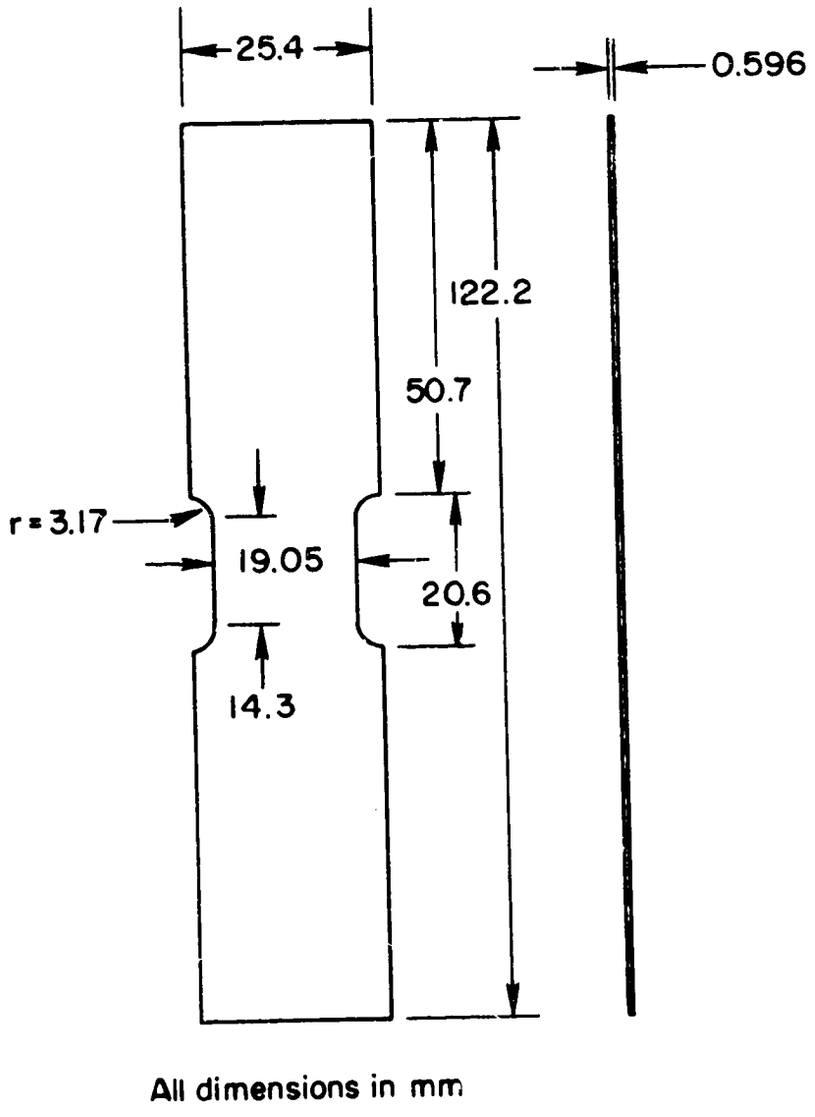

Fig. 6. - Sheet tensile specimen for Ti-8Al-1Mo-1V

specimens were designed to give more constraint with a width-to-thickness ratio of 32:1. The composition of the alloy is given in Table IV. A small percentage of β phase was present as islands in the α phase. The specimens were prepared similarly to the Ti-5Al-2.5Sn except for the thermal treatment which consisted of a vacuum anneal at 1083 K for 4 hours and furnace cool. Specimen capsules were backfilled with hydrogen to obtain levels of 10, 80, and 150 ppm. These levels were chosen because work performed by T. D. Boyd[55] had shown that 200 ppm or more of hydrogen would result in strain-induced hydrogen precipitation. The particular interest in the present study was the effect of interstitial hydrogen and not hydride.

Following hydrogen backfilling of the capsules the specimens were heated at 1083 K for two additional hours. The specimens were next cooled to 923 K, held for one hour, and then part of them were fast-quenched while remaining specimens were furnace-cooled to 873 K for 24 hours and 853 K for 24 hours to duplicate heat treatments used by Boyd et al.[54] This latter treatment was used in order to obtain specimens with the α_2 compound, Ti_3Al. It has been shown that alloys containing this compound are more sensitive to stress corrosion cracking because of the embrittling effect of the compound. The hardness of the specimens was checked to verify compound formation. As in the previous procedures the 10 ppm samples were encapsulated and backfilled with argon so that the thermal cycle on these specimens would be identical to their hydrogen charged counterparts.

The grid pattern was placed on the Ti-8Al-1Mo-1V alloy specimens using a different technique than that for the Ti-5Al-2.5Sn specimens. A ballpoint pen was attached to a vernier height gage having scale increments of 0.025 inch (0.634 mm). The specimens were mounted to precision-ground blocks and the grid lines were drawn on the specimens one line at a time.

RESULTS

Ti-5Al-2.5Sn ALLOY

The mechanical properties of the vacuum-annealed Ti-5Al-2.5Sn specimens were 667 MN/m^2 0.2% offset yield strength, 715 MN/m^2 tensile strength, and 24% elongation. These values compared well with the minimum values specified in company brochures which were 695 MN/m^2 tensile strength, 626 MN/m^2 yield strength, and 10% elongation. Figure 7 shows the grain structure obtained, the grain size being 290×10^{-4} mm. Table VI contains the tabulated results of the 0. cm/min crosshead speed test. The instantaneous area was calculated assuming the volume remains constant and thus

Table VI - Ti-5Al-2.5Sn Alloy: True Stress and True Strain Data for a Strain Rate of 0.1575 Min^{-1}

Photo	Measured Width (cm)	Measured Length (cm)	True Strain ($\ell n L/Lo$)	Instantaneous Area $(mm)^2$	Load (kg)	True Stress (MN/m^2)
10 ppm hydrogen; original measured, width-8.38 cm, length-10.29 cm (Photo 3)						
5	8.46	10.21	.009	11.21	740	651.9
8	8.56	10.06	.021	11.10	802	713.8
12	8.86	9.75	.055	10.70	820	757.6
14	9.06	9.49	.079	10.47	821	772.8
16	9.42	9.07	.117	10.08	808	790.9
18	9.7	8.84	.146	9.77	790	798.6
19	9.86	8.58	.161	9.64	780	797.9
20	9.96	8.5	.172	9.53	770	797.9
21	10.3	8.36	.180	9.46	752	785.3
22*	10.11	8.30	.187		690	
23	10.21	8.20	.197			
24	10.39	8.00	.215			
25	10.95	7.57	.267			
80 ppm hydrogen; original measured, width-14.53 cm, length 11.78 cm (Photo 1)						
2	14.5	11.96	.015	10.74	826	760
4	14.3	12.24	.038	10.49	852	801
6	13.94	12.49	.059	10.30	860	825
7	13.76	12.63	.069	10.19	860	833
9	13.34	13.00	.098	10.02	860	848
10	13.13	13.18	.112	9.77	852	862
11	12.95	13.31	.121	9.67	843	861
13	12.42	13.77	.155	9.34	832	879
14	12.03	14.05	.175	9.15	812	876
15	11.84	14.22	.188	9.06	800	873
16	11.63	14.45	.204	8.89	787	874
17	11.41	14.6	.214	8.82	780	874
18	11.09	14.88	.233	8.63	762	872
19	10.85	15.08	.247	8.53	749	867
150 ppm hydrogen; original measured, width-14.59 cm, length-11.86 cm (Photo 21)						
22	14.53	12.01	.013	11.42	875	755
23	14.35	12.17	.025	11.28	895	784
[illegible]	13.66	12.52	.054	10.97	903	813
26	13.36	12.80	.076	10.73	903	831
27	13.03	13.08	.098	10.49	897	844
29	12.65	13.44	.125	10.20	882	853
30	12.32	13.69	.143	10.02	870	858
31	12.04	13.94	.162	9.85	855	858
32	11.81	14.15	.176	9.72	845	860
33	11.51	14.40	.194	9.53	830	861
34	11.28	14.61	.208	9.38	820	863
35	10.79	15.01	.235	9.13	787	851
36			.247			842
500 ppm hydrogen: original measured, width-12.67 cm, length-10.29 cm (Photo 1)						
2	12.49	10.29		11.32	870	758.2
3	12.42	10.31	.002	11.27	932	816.6
4	12.29	10.49	.019	11.12	967	859.0
5	12.14	10.64	.034	10.92	971	877.1
6	11.94	10.77	.046	10.82	975	890.3
7	11.86	10.87	.055	10.71	976	900.7
8	11.63	11.13	.078	10.47	977	920.9
9	11.35	11.35	.099	10.24	978	943.1
10	11.10	11.66	.125	9.97	977	967.7

*Appearance of first crack

$$l'w't' = l_o w_o t_o \tag{3}$$

and

$$t' = \frac{l_o w_o t_o}{l'w'} , \tag{4}$$

where t' is the instantaneous thickness.

The instantaneous area (A_i) is then equal to t' x w'.

Figures 8 and 9 show the results of plotting true stress versus true strain. These results illustrate that the true stress reached a maximum value and did so at a strain greater than the maximum load point. Chakrabarti[8] showed this maximum true stress value to be the onset of the instability meeting the condition

$$d\sigma = \left(\frac{\partial \sigma}{\partial \varepsilon}\right) d\varepsilon + \left(\frac{\partial \sigma}{\partial \dot{\varepsilon}}\right) d\dot{\varepsilon} + \left(\frac{\partial \sigma}{\partial T}\right) dT \leq 0 . \tag{5}$$

Ernst[57] showed that the plastic instability in titanium alloys under a torsional state of stress was very strong. In other words, the strain at onset of instability minus the strain at failure ($\varepsilon_{ins} - \varepsilon_f$) was very small. This is observed to be true in the present experiments. From the graphs it can be seen that failure occurred very soon after the true stress maximum. Synthesis of the data obtained from the graphs is shown in Table VII. No values are given for disruption strain in the 10 ppm hydrogen sample because there was no real disruption stage. The crack appeared at the edge and grew slowly along the deformation band; most of the growth was in this stable manner. Therefore, at the given strain rate, instability fracture in the specimen was not manifested.

Of particular concern to this study was the effect of the interstitial hydrogen. Lenning[58] had shown that the hydrogen solubility in a Ti-5Al alloy was approximately 200 to 300 ppm. The data in Figs. 8 and 9 of the present work indicate that between 150 and 500 ppm hydrogen were sufficient to cause spontaneous hydride precipitation. The photomicrograph (Fig. 10) shows hydride precipitate in a sample containing 500 ppm hydrogen. The hydride is mostly grain boundary oriented, although a few hydride spikes can be seen in the grains. It would be expected that as the alloy content increased or as the supersaturation of hydrogen increased, more and more of the hydrides would precipitate on particular habit planes in the titanium crystal. These planes have been indexed by a number of investigators.[6,35-40] This spontaneous hydride precipitation resulted in a definite decrease in the ductility of the material. The strain to failure was determined to be lower than those of the less concentrated samples.

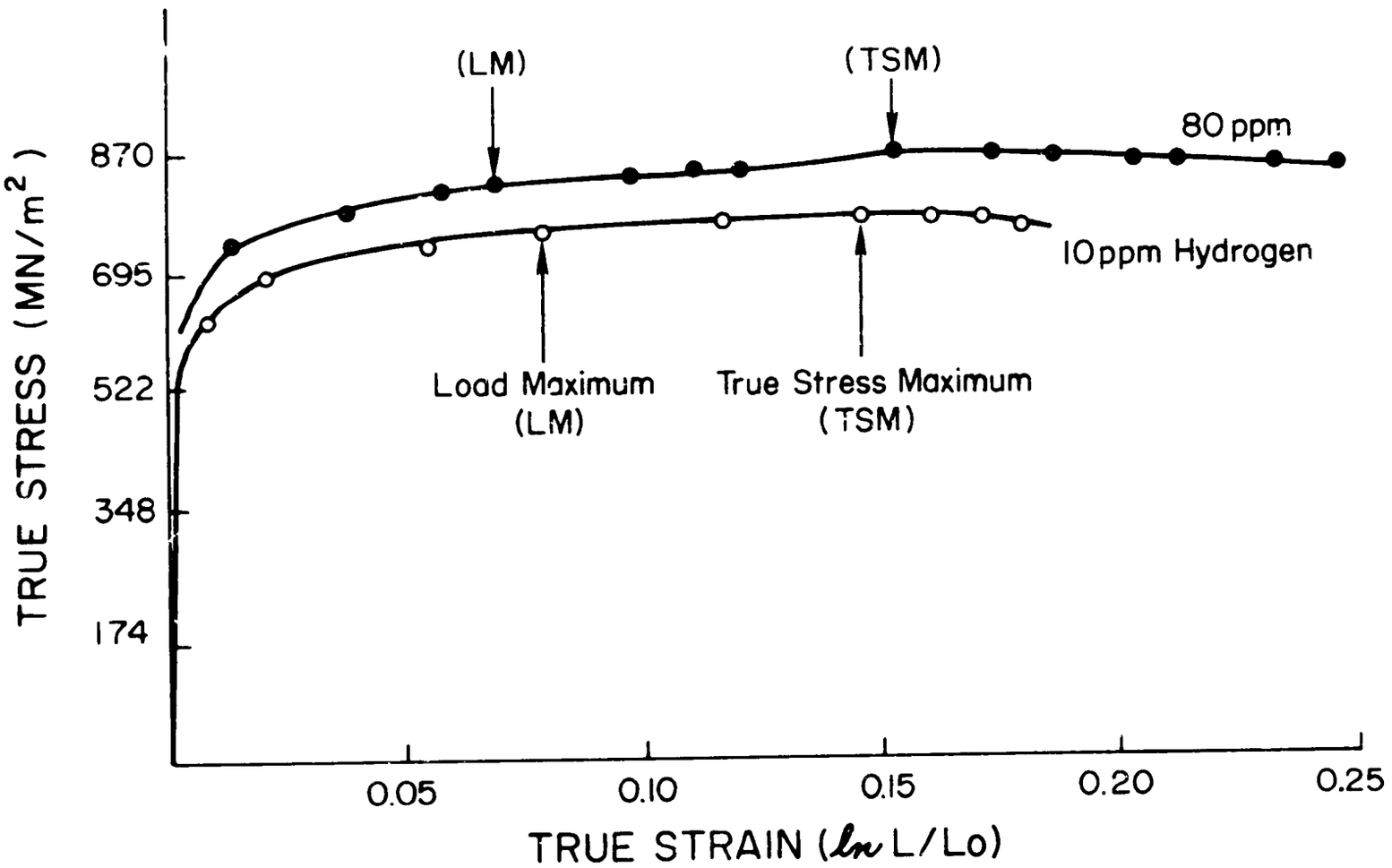

Fig. 8 - True stress vs true strain for Ti-5Al-2.5Sn with strain rate 0.1575 min^{-1}

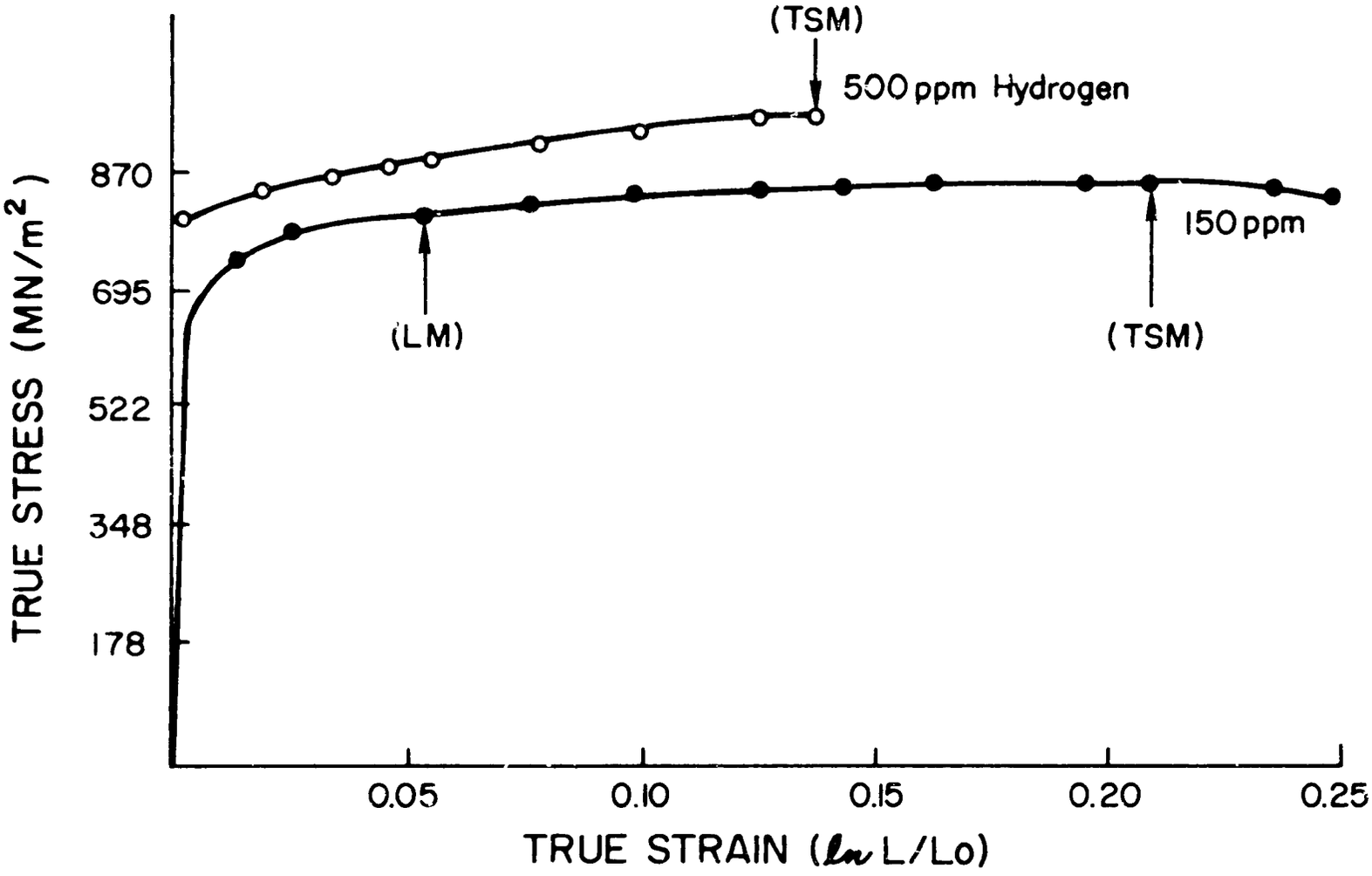

Fig. 9 - True stress vs true strain for Ti-5Al-2.5Sn with strain rate 0.1575 min^{-1}

Table VII - Strain Parameters for Ti-5Al-2.5Sn Alloy as Affected by Hydrogen Concentration

Crosshead Speed 0.2 cm/min; Strain Rate 0.1575 min^{-1}

	Hydrogen Concentration (ppm)			
	10	50	150	500
Strain at d^{-1} 0	.14	.155	.208	.137
Strain at Disruption	--	.247	.247	.137
True Stress at Disruption (kg/mm^2)	--	864	843	968

Fig. 10 - Hydrides present in the Ti-5Al-2.5Sn alloy containing 500 ppm hydrogen 500X

Examination of the fracture patterns of the specimens showed a variety of results. Figure 11 shows a sample of one of these. Although it appeared as though some of the specimens initiated fracture from the edge, initiation occurred primarily in the center.

Ti-8Al-1Mo-1V ALLOY

The Ti-8Al-1Mo-1V specimens had a tensile strength of 1012 MN/m^2 and a yield strength of 9[illegible]3 MN/m^2. Figure 12 shows the grain structure of the specimens after vacuum annealing. The α grain size was measured to be 145 x 10^{-4} mm. As can be seen, islands of β phase exist at the α grain boundaries. Table VIII gives the deformation measurements taken on some of the specimens tested. As can be seen from Figs. 13 and 14 the tests once again show a true stress maximum. The important strain parameters from these tests were recorded and are shown in Table IX.

The fracture pattern was quite different than in previous tests. The specimens showed definite mixed fracture modes, a combination of plane stress and plane strain. The plane strain mode is denoted by a horizontal crack as predicted when $\sigma_2 = \frac{1}{2}\sigma_1$, and it is evident that the higher hydrogen concentration resulted in a higher percentage of the plane strain mode. This can be seen in the fractures shown in Figs. 15 and 16. The angles of plane stress fracture were much easier to measure than in previous tests. The concentrated shear fractures or instability fractures were at angles less than 36° as was expected from the large width-to-thickness ratio. Thus, in the center $\sigma_2 = \frac{1}{2}\sigma_1$, and at the edges [illegible] became smaller because of less constraint.

Another group of specimens tested were those which had been aged to produce the α_2 compound Ti_3Al. This compound has been shown to affect the fracture toughness of the titanium alloys.[59] Investigators have shown[56] that the precipitation of this compound has a small effect on the tensile or yield strength of the material. The data gathered in the present experiments revealed a significant increase in tensile strength and a decrease in ductility. The tensile strength of an unhydrogenated aged specimen was 1090 MN/m^2 compared with the 1012 MN/m^2 for an unaged specimen.

There was little noticeable difference in the hardness of the specimens as recorded by Knopp hardness measurements. The hardness of the unaged material was 410 KHN and the aged material was 448 KHN.

Table X gives the strain parameters for the aged specimens, as determined from the measured values recorded in Table VIII. No true stress maximum was observed and all the specimens, regardless of hydrogen content, showed mostly a plane strain mode of fracture. Figure 17 shows two of the broken specimens. The specimen containing 80 ppm H_2 broke prematurely at a very low strain value. This fracture was directly related to a score mark on the surface and although the results are included in the table below, they will be excluded from further discussion.

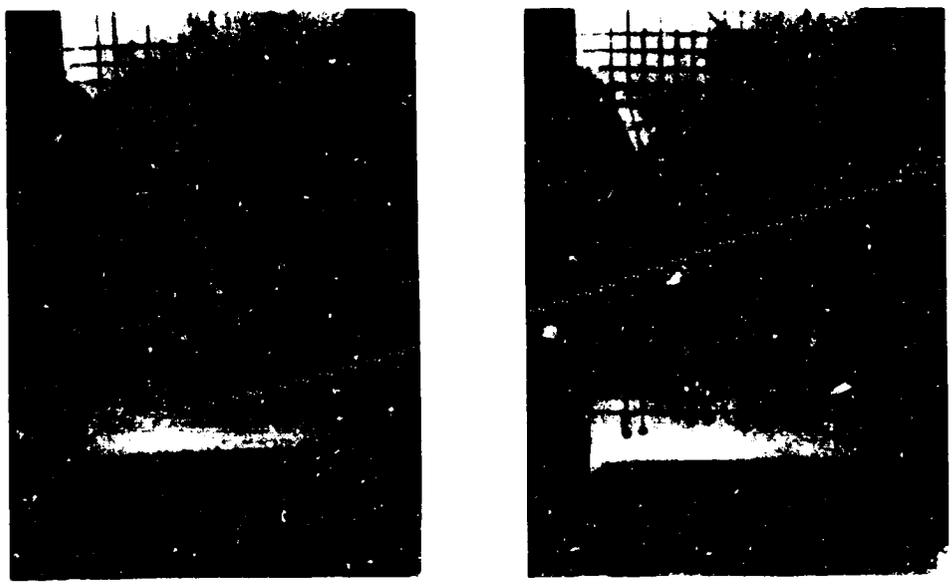

Fig. 11 - Fracture events for Ti-5Al-2.5Sn with 80 ppm hydrogen at 0.15% min^{-1} strain rate

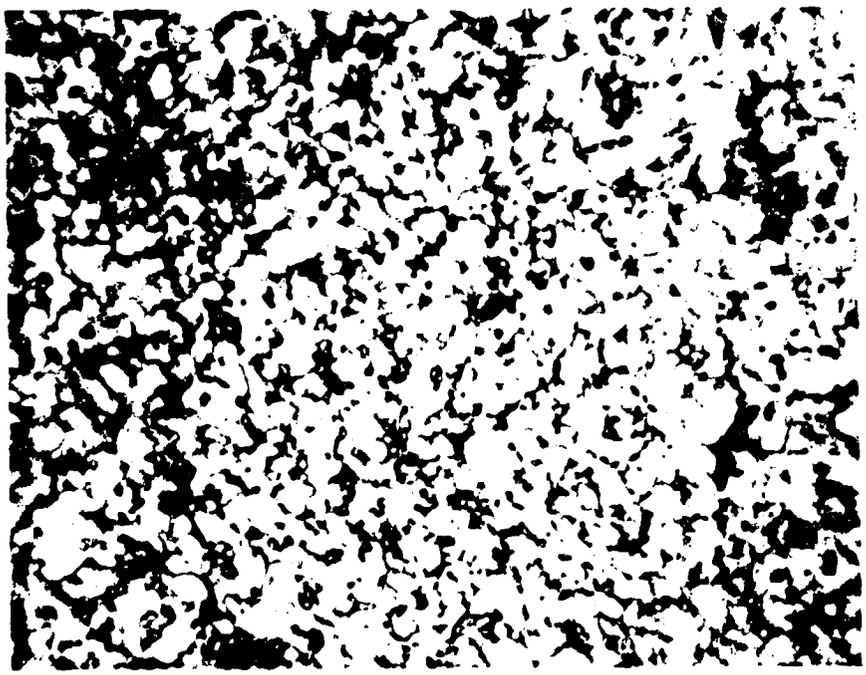

Fig. 12 - Vacuum annealed Ti-5Al-1Mo-1 alloy showing fine α grain size with islands of β phase 500X

Table VIII - Ti-8Al-1Mo-1V Alloy: True Stress and True Strain Data for a Strain Rate of 0.140 Min^{-1}

Photo	Measured Width (cm)	Measured Length (cm)	True Strain (ℓn L/Lo)	Instantaneous Area $(mm)^2$	Load (kg)	True Stress (MN/m^2)
80 ppm hydrogen; original measured, width-14.71 cm, length-10.62 cm (Photo 14)						
16	14.50	10.99	.035	10.75	1099	1008.4
17	14.33	11.25	.058	10.49	1114	1047.4
18	14.17	11.48	.078	10.31	1124	1075.9
19	14.02	11.61	.089	10.19	1129	1092.5
20	13.94	11.73	.100	10.07	1129	1105.7
21	13.84	11.81	.106	10.00	1130	1114.8
22	13.72	11.99	.121	9.86	1134	1134.9
24	13.64	12.12	.132	9.75	1136	1148.8
25	13.26	12.62	.173	9.36	1136	1196.8
26	13.18	12.72	.181	9.28	1134	1205.1
27	13.03	12.83	.189	9.22	1129	1207.9
28	12.95	12.95	.199	9.13	1114	1203.7
29	12.85	13.05	.207	9.06	1106	1203.7
150 ppm hydrogen; original measured, width-14.66 cm, length-10.74 cm (Photo 1)						
3	14.3	11.17	.039	10.92	1144	1034.2
4	14.1	11.48	.066	10.65	1158	1073.1
5	13.99	11.63	.079	10.50	1160	1089.8
6	13.87	11.74	.097	10.32	1162	1109.9
7	13.72	11.99	.110	10.17	1170	1134.2
8	13.61	12.14	.122	10.05	1170	1148.1
9	13.46	12.37	.141	9.88	1170	1168.3
10	13.26	12.63	.161	9.67	1160	1182.9
11	13.06	12.85	.179	9.50	1156	1199.6
12	12.85	13.06	.195	9.36	1142	1203.0
13	12.80	13.16	.202	9.28	1140	1211.4
14	12.75	13.29	.206	9.25	1124	1198.2
10 ppm hydrogen; original measured, width-14.96 cm, length-11.02 cm (Photo 1)						
4	14.94	11.18	.014	11.22	1228	1081
5	14.83	11.48	.041	10.92	1228	1109
6	14.68	11.76	.065	10.68	1240	1147
7	14.55	12.05	.084	10.46	1248	1179
8	14.35	12.29	.105	10.24	1256	1210
9	14.15	12.54	.129	10.00	1258	1242
10	13.77	12.98	.163	9.67	1256	1282
11	13.49	13.28	.186	9.46	1256	1309
150 ppm hydrogen; original measured, width-14.48 cm, length-10.74 cm (Photo 17)						
20	14.43	10.92	.016	11.18	1260	----
23	14.27	11.17	.039	10.93	1260	----
26	14.09	11.43	.062	10.70	1268	----
28	13.97	11.63	.079	10.49	1270	----
30	13.79	11.81	.095	10.35	1274	----
32	13.66	12.04	.114	10.12	1278	----
33	13.56	12.12	.120	10.07	1282	----
34	13.49	12.32	.137	9.91	1284	----
35	10.9	12.42	.145	9.83	1284	----

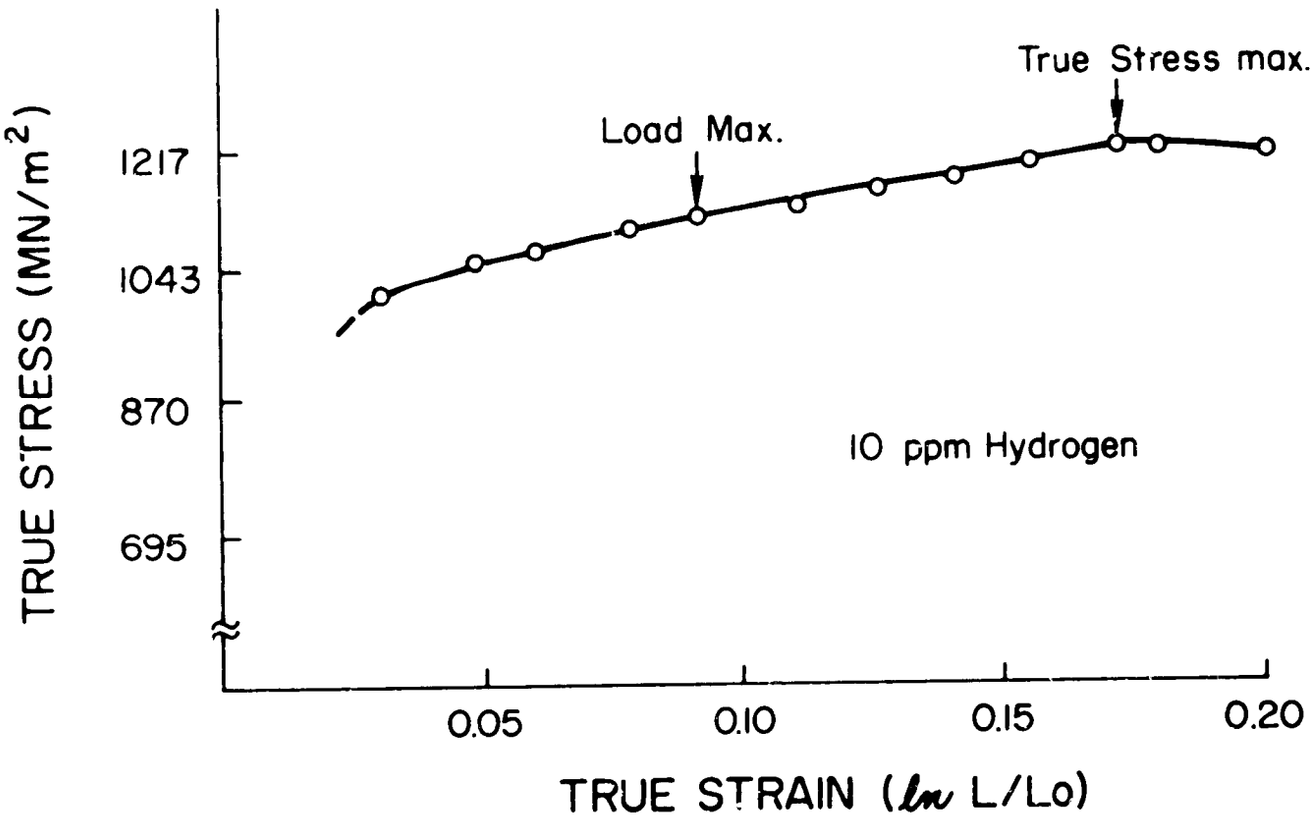

Fig. 13 - True stress vs true strain for Ti-8Al-1Mo-1V with strain rate 0.14 min^{-1}

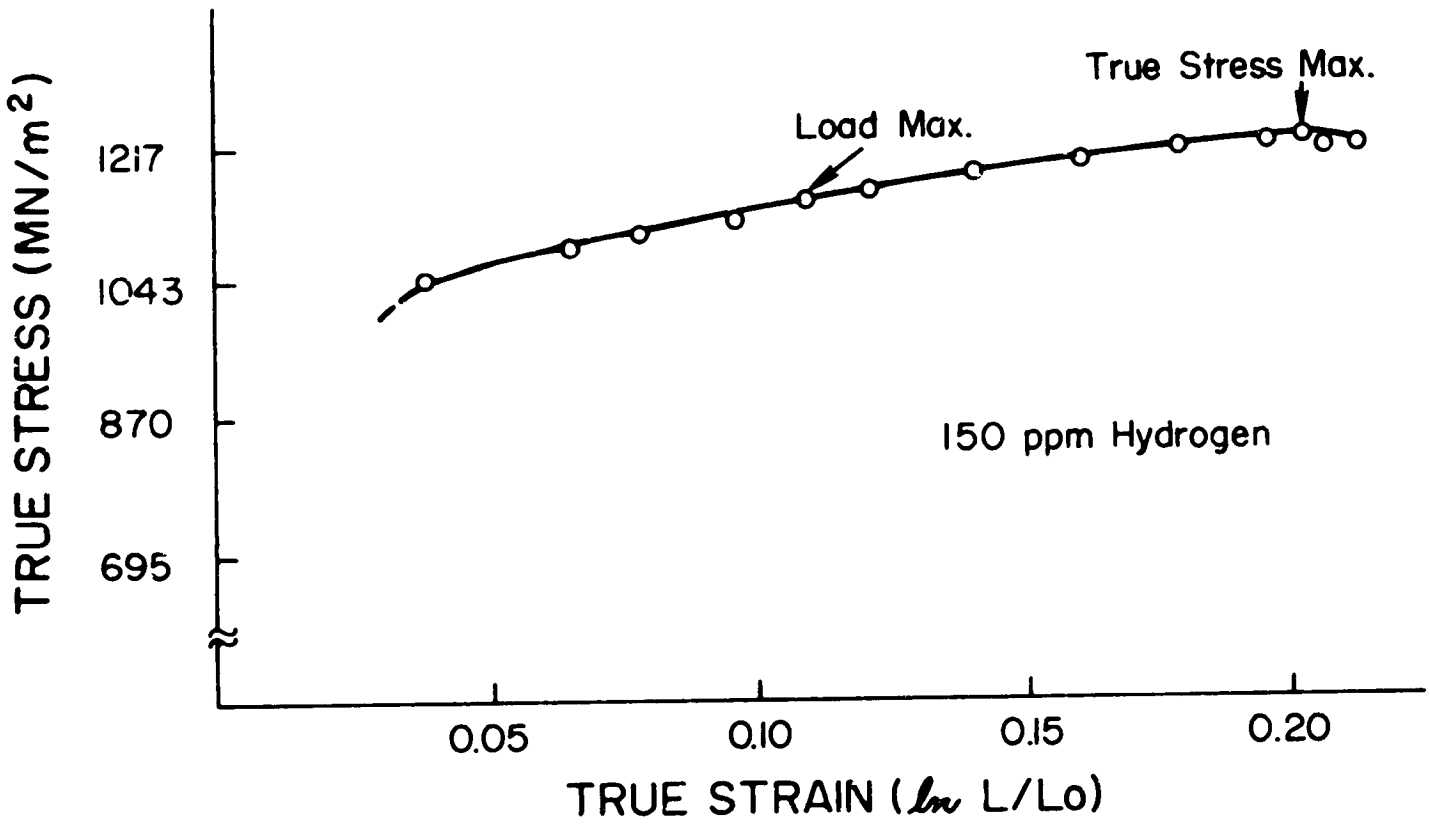

Fig. 14 - True stress vs true strain for Ti-8Al-1Mo-1V with strain rate 0.14 min^{-1}

Table IX - Strain Parameters as Affected by Hydrogen Concentration Ti-8Al-1Mo-1V Alloy

Crosshead Speed 0.2 cm/min; Strain Rate 0.140 min^{-1}

	Hydrogen Concentration (ppm)		
	10	80	150
Strain at $d\sigma = 0$	.171	.189	.202
Strain at Disruption	.199	.216	.212
True Stress at Disruption (MN/m^2)	1194	1201	1199

Table X - Strain Parameters for Ti-8Al-1Mo-1V Aged to Produce Ti_3Al Compound

Strain Rate 0.14 min^{-1}

	Hydrogen Concentration (ppm)		
	10	80	150
Strain at Disruption	.186	.065	.145
True Stress at Disruption (MN/m^2)	1310	1123	1292

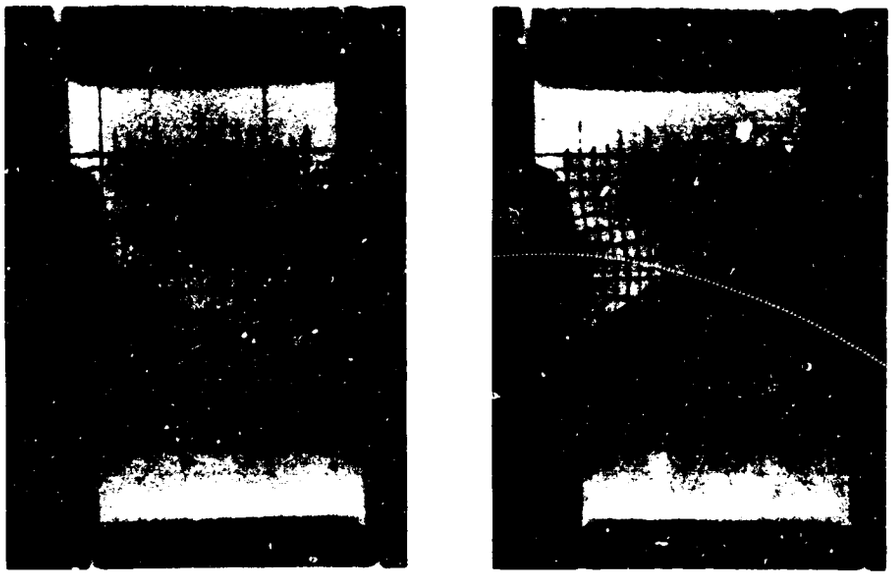

10 ppm hydrogen 80 ppm hydrogen

Fig. 15 - Fractures of Ti-8Al-1Mo-1V at 0.14 min^{-1} strain rate

150 ppm hydrogen

Fig. 1[illegible] - Fractures of Ti-8Al-1Mo-1V at 0.14 min^{-1} strain rate

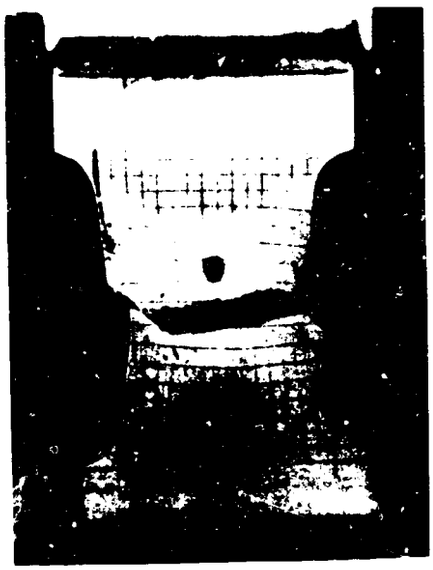

To determine if texturing might play a part in the fracture phenomenon, samples were made having the tensile axis both 45° to the rolling direction and transverse to the rolling direction. The samples contained 10 and 150 ppm of hydrogen. The strain parameters found are shown in Table XI (the capsule containing the transverse bar at 10 ppm broke in the furnace so no data were obtained for the 10 ppm specimen).

Table XI. Strain Parameters for Ti-8Al-1Mo-1V as Affected by the Rolling Direction

	10 ppm Hydrogen			150 ppm Hydrogen		
	Trans.	45°	Long.	Trans.	45°	Long.
Strain at $d\sigma = 0$	-	.203	.192	.167	.202	.222
Strain at Disruption	-	.213	.216	.209	.246	.246
Stress at Disruption (MN/m^2)	-	1089	1180	1205	1164	1263

DISCUSSION

Ti-5Al-2.5Sn ALLOY

As can be seen from Figs. 8 and 9, the flow stress increased with the addition of hydrogen. This would be in agreement with data reported by many observers. The strain at the maximum true stress or at the onset of instabilities increased with increasing hydrogen except for the highest hydrogen level. This would seem to indicate that the hydrogen was hindering the onset of instabilities. This is opposite to what might have been predicted if hydrogen had acted as a "plasticizer" in titanium. If this had been the case, hydrogen would have caused instability onset at lesser strain values. This could be predicted from the fact that the instability failures depend on the plastic character of the material.

If the material were made more plastic, it might be expected to strain harden to the point of exhaustion sooner and at this point become ideally plastic and fail along characteristics in an unstable manner. It has been shown that in low interstitial titanium one slip plane is active (10$\bar{1}$1); but in higher interstitial titanium (O and N being the interstitial elements) all three slip planes are nearly

equally favored.[60] It was thought that the effect of hydrogen at interstitial sites in the titanium lattice was to expand the lattice in directions such that more slip planes could be activated. This does not appear to be the case and no known literature is available to show how interstitial hydrogen affects the resolved shear stress.

A log-log plot of the flow stress data for the 0.1575 min^{-1} strain rate specimens is shown in Fig. 18. The curves reveal no real trend as to the effect of hydrogen on the strain hardening exponent.

One thing that is evident is that the greater the hydrogen concentration, the less tolerance the material has for the instability (Fig. 19). Thus, the higher the hydrogen the sooner failure occurs after the instability onset or the smaller is the value for strain at $d\sigma = 0$ minus strain at disruption.

A typical fracture sequence for center crack initiation is diagrammed in Fig. 20. "A" shows the initial stages of straining and "B" represents the deformation bands which initiate at certain points in the plastic deformation region of the stress-strain curve. These bands were originally at an angle of approximately 36° with the horizontal. From theories of Kobayashi[61] this would indicate that the stress state in the specimen was uniaxial. This means that there is no σ_2 initially. Kobayashi developed formulas for determining slip line directions for the plane stress condition. When a uniform state of stress is assumed these formulas become

$$\theta = \pm\left(\frac{\pi}{4} + \frac{\psi}{2}\right), \tag{6}$$

where θ is the angle between the slip lines and the principal stress direction (σ_1), and

$$\sin \psi = \frac{1}{3}\,\frac{\sigma_1 + \sigma_2}{\sigma_1 - \sigma_2}. \tag{7}$$

This predicts that when $\sigma_2 = 0$, $\theta = 54° 44'$ and when $\sigma_2/\sigma_1 = -\frac{1}{3}$, $\theta = 90°$. The formation of the bands in the present study was associated with either the start of plastic deformation or the maximum load point, and definitely not associated with the true stress maximum. The instability formation, which may have occurred at the true stress maximum, was within these deformation bands.

Stage "C" shows the deformation band widening and at stage "D" a running crack occurred which covered about one-half the specimen width. After this crack was arrested the continuance of loading caused a slow tearing until final edge shear resulted in complete separation. An

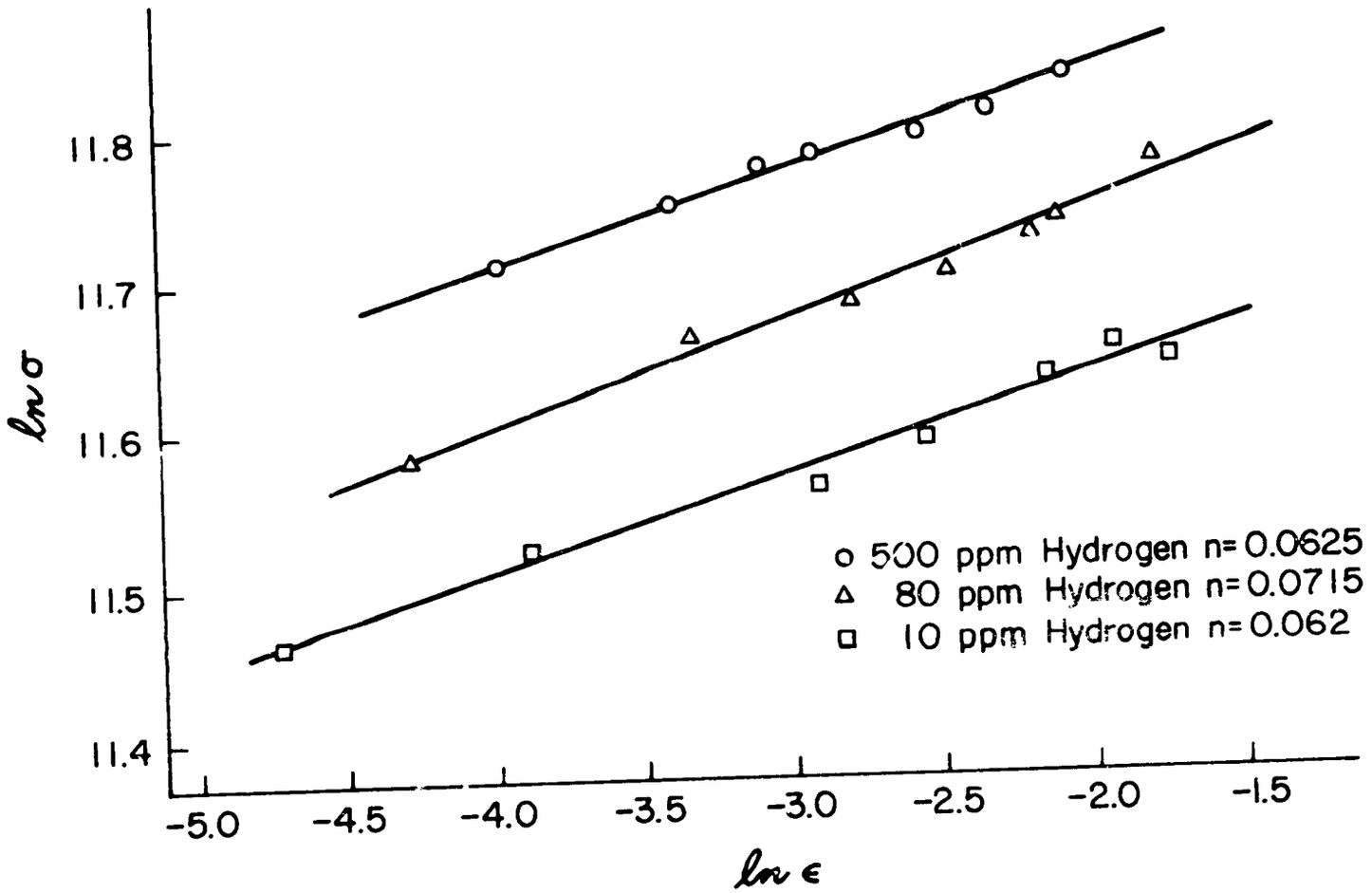

Fig. 18 - Log true stress vs log true strain for Ti-5Al-2.5Sn

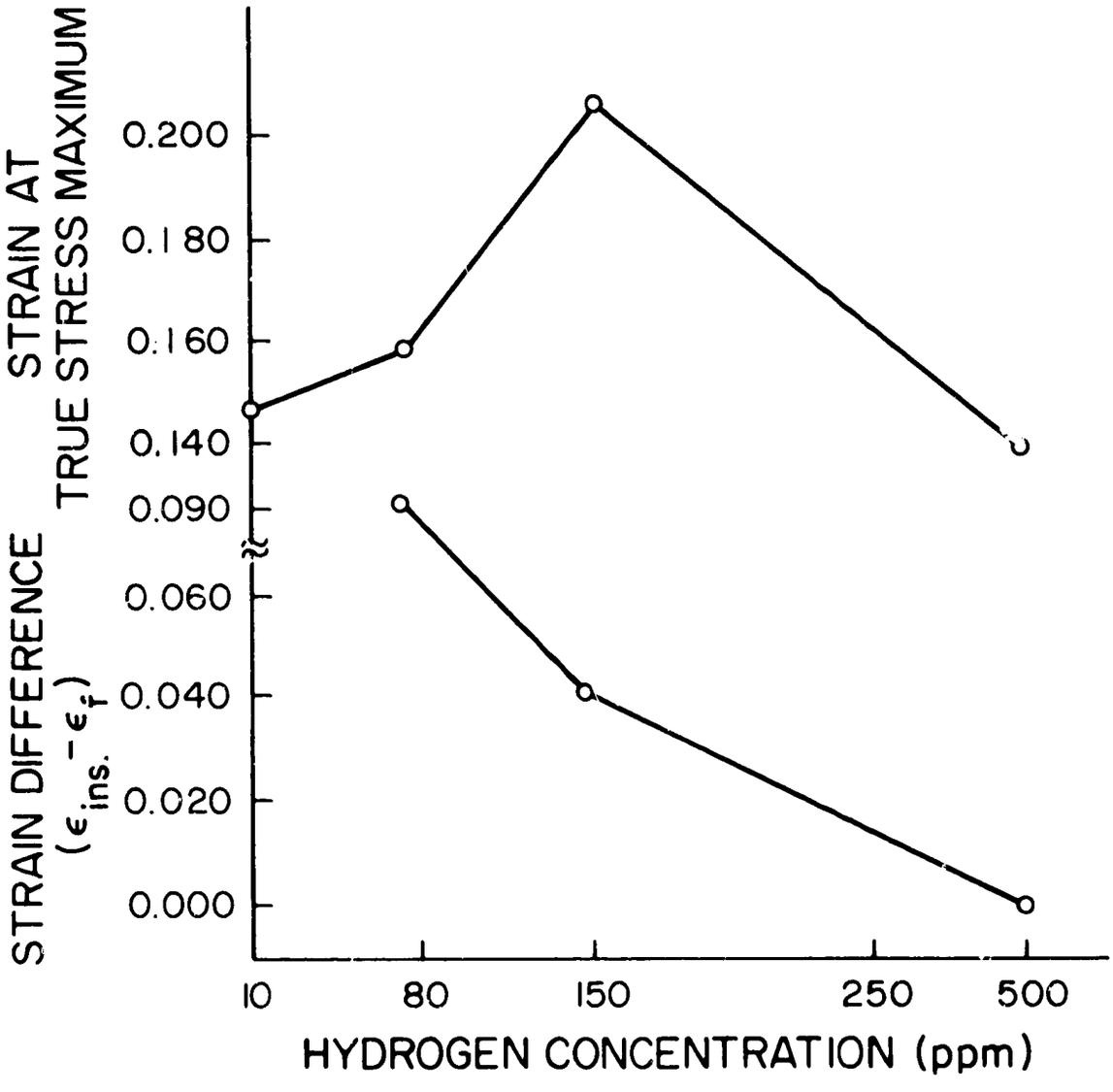

Fig. 19 - Strain parameters for Ti-5Al-2.5Sn with strain rate 0.1575 min^{-1}

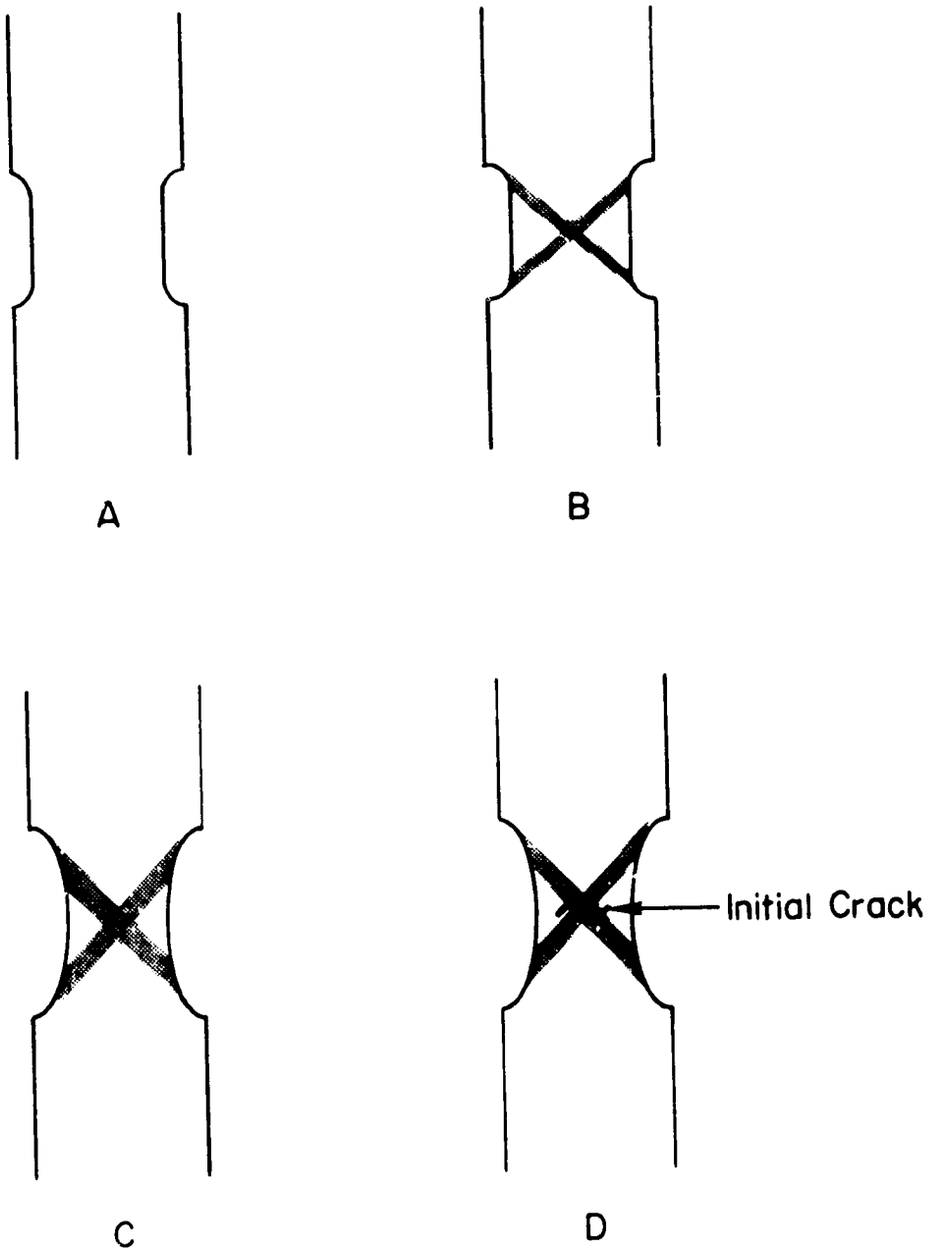

Fig. 20 - Typical fracture pattern for separation at the center of a tensile specimen

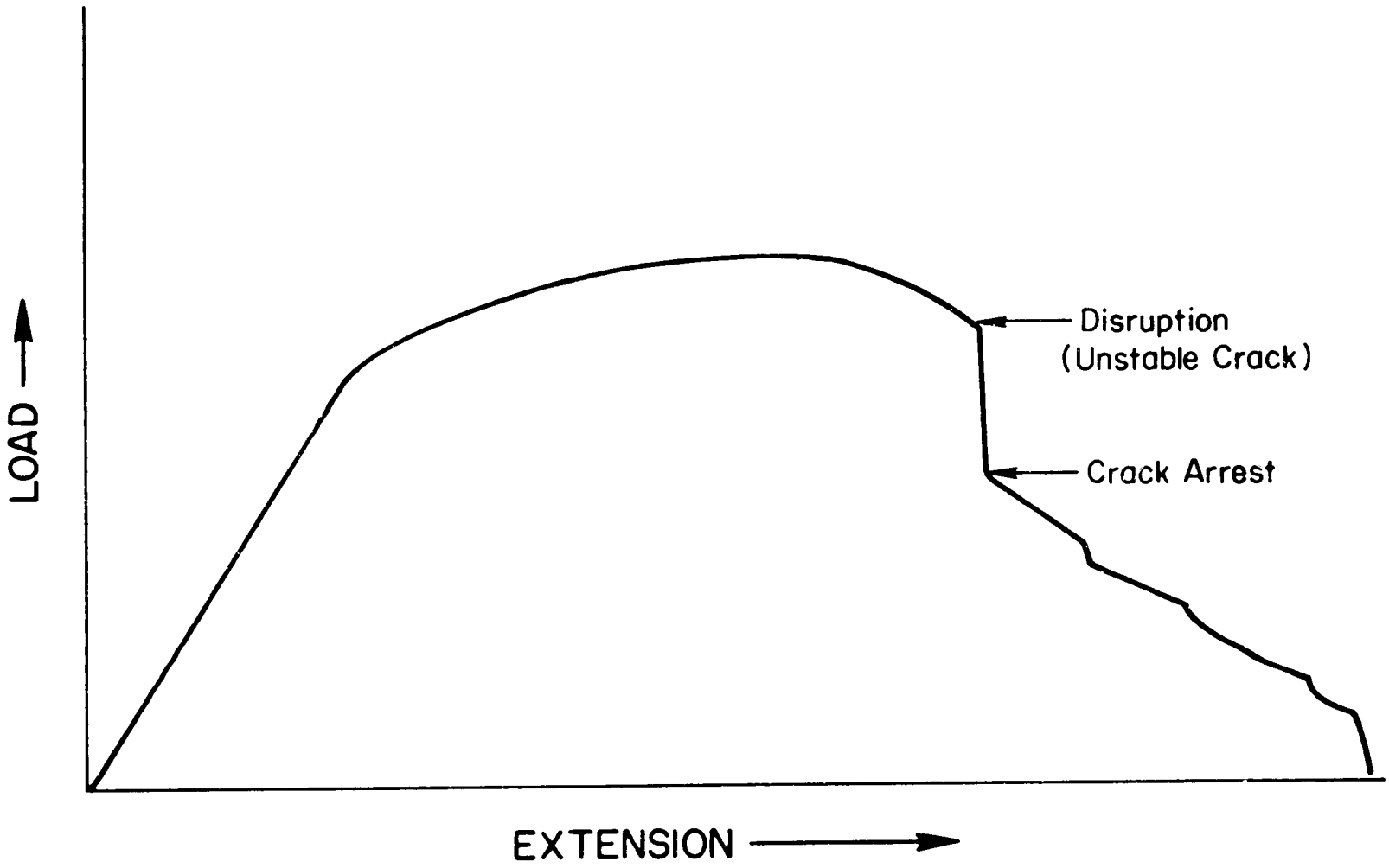

Fig. 21 - Typical load-extension curve for Fig. 22 fracture

example of the load vs extension plot corresponding to this failure is shown in Fig. 21. The disruption stage can be seen in each of the load curves at the first crack appearance.

Parker[62] has shown a detailed diagram of fracture (in a ductile material) which was identical to the behavior in this experiment. He explained that the stepped pattern in the high shear stress regions at the central part of the specimen consisted of steps making angles of 45° or less with the specimen axis. While it is not easy to accurately measure these short steps, they appear never to be more than 40° in this experiment. Therefore, these angles do not necessarily support the argument that the fractures occur on planes of maximum shear stress.

When the failed specimen sections were mounted and polished it became immediately obvious that pore formation was occurring. The greatest concentration of pores was found in the central part of the specimen where triaxial stresses were greatest. This triaxial state of stress enhances pore formation. Pore formation and coalescence is a common failure mode and it had been the intention of these experimental methods to inhibit this type of failure mode.

It is believed that pores which formed and grew in this material became the initiation sites for the plastic instability mode of failure. Thus, failure was due to the third type of instability flow as described in the literature review. Load disruption did occur in each test with the formation of an unstable crack. This crack was not at angles of maximum shear stress but more nearly along angles determined by plasticity theory. The pores provided the stress gradient and free surface necessary for instability formation. The crack propagated through the area of highest shear stress (smallest cross-section due to necking) but was arrested in the area of lower shear stress. From that point the specimens failed because of a slow tear (pore formation and coalescence) until final shear at the edges occurred.

Metallographic examination of the pores showed that they were associated with grain boundaries and may well have been enhanced by possible hydrogen partitioning in the boundaries. They were definitely associated with grain boundary particles and, although it was not proven that these were oxides, it is suspected that they are oxides since this material as in any commercially available titanium contained about 0.1% oxygen content by weight. Figure 22 shows the particles and the voids they caused.

Ti-8Al-1Mo-1V ALLOY

In the Ti-8Al-1Mo-1V alloy it is evident, as with the first alloy discussed, that the strain at the true stress maximum increases as hydrogen concentration increases. Likewise, the tolerance for the instabilities decreases with increased hydrogen concentration, as shown in Fig. 23. Thus, once the instability forms in the 150 ppm hydrogen

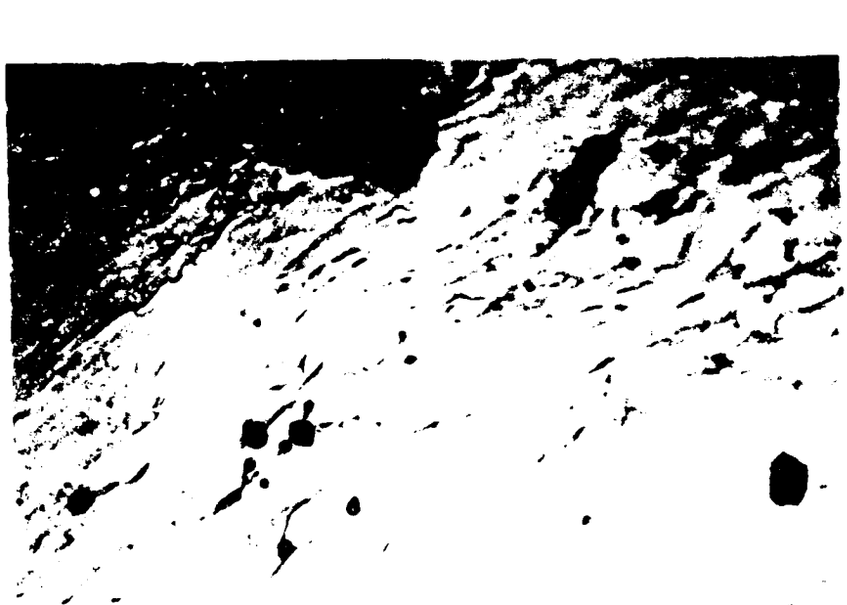

Note: Possible oxide particles can be seen in lower left quadrant. The large black area at top is the edge of the fracture.

Fig. 22 - Void formation in a Ti-6Al-4V specimen related to particles in the grain boundaries. 500 X

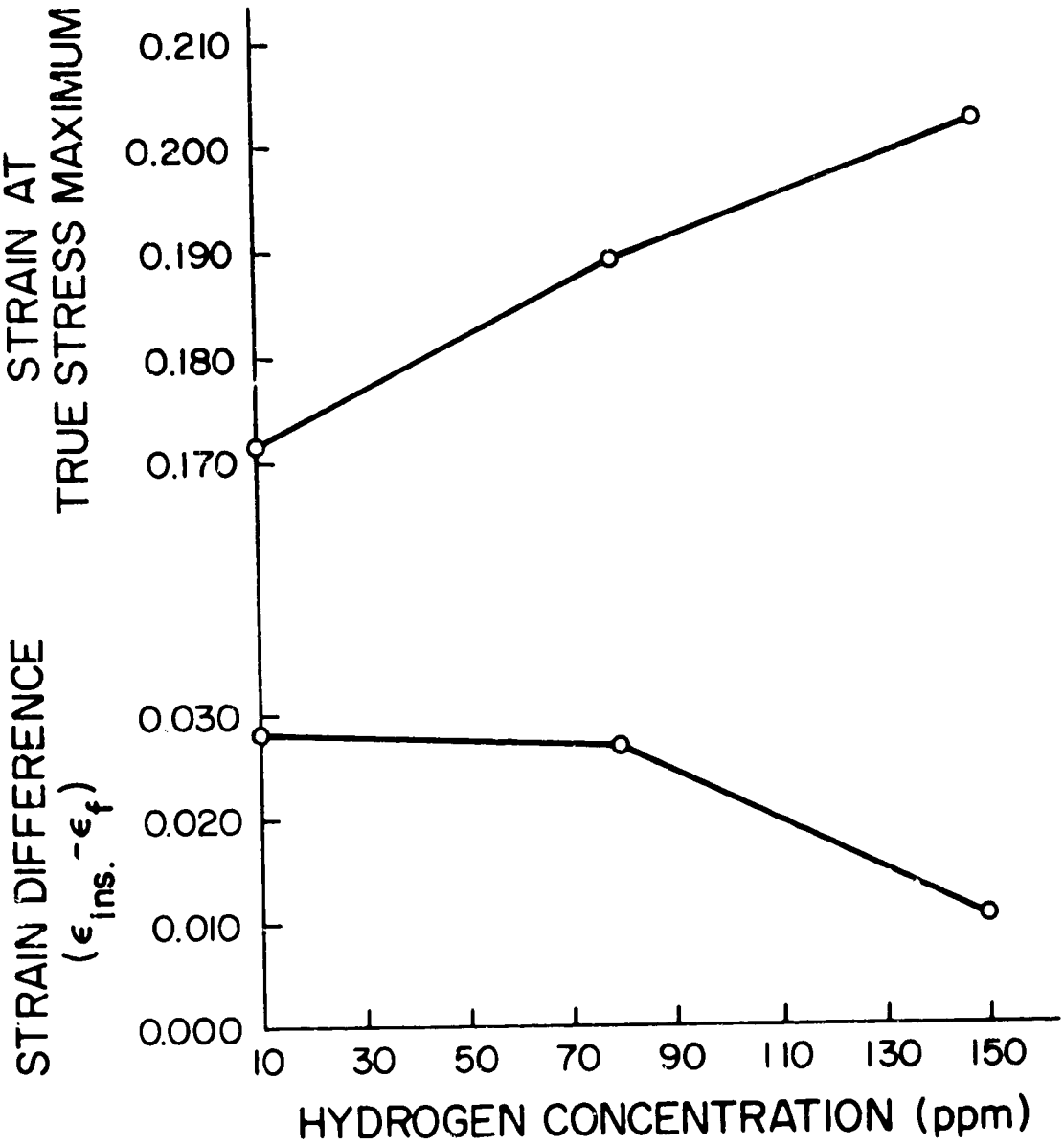

Fig. 23 - Strain parameters for Ti-8Al-1Mo-1V

specimen, failure occurs sooner than in the 10 ppm specimen. Not as evident as before are changes in the flow stress, which appears to change very little with increasing hydrogen.

To determine how accurate the strain data were using ε_n L/Lo, the final strain was compared to that calculated strain using the final measured width and thickness (ε_n Ao/A). The results were very good, as shown in Table XII.

Table XII - Comparison of Final Strain Using ε_nL/Lo and ε_nAo/A

Specimen	Original Area (mm^2)	Final Area (mm^2)	Final Strain (ε_n Ao/A)	Final Strain (ε_nL/Lo)
Ti-8-1-1 10 ppm hydrogen	11.41	9.32	.202	.199
Ti-8-1-1 80 ppm hydrogen	11.41	9.15	.221	.216

The tensile sheet specimens were originally designed in an attempt to produce both a plane stress and a plane strain state of stress. Torsional specimens, which have been used successfully for several years to show instability formation, have at their surface this same state of stress (plane strain and plane stress). In the tensile specimens the plane strain state exists when $\sigma_2 = \frac{1}{2}\sigma_1$. This can be shown by looking at the equation for width strain in the plastic deformation region of the flow curve. The equation is

$$\varepsilon_3 = \frac{1}{P}(\sigma_2 - \nu\sigma_1), \tag{8}$$

where P is the plastic modulus and, in plasticity, ν (Poisson's ratio) is $\frac{1}{2}$. Thus, $\varepsilon_3 = 0$ when $\sigma_2 = \frac{1}{2}\sigma_1$. The plane strain state results in the coincidence of directions of pure shear and maximum shear stress, both in the direction of σ_1. Thus, a horizontal fracture results.

It is apparent from Figs. 15 and 16 that as the hydrogen concentration increased the specimens showed greater degrees of plane strain fracture. These horizontal fractures were slanted from front to back whereas the remaining inclined fractures were not. Slant fractures in failure analysis are often incorrectly determined to be ductile fracture shear lips. This familiar slant fracture was determined in this study to be the plane strain mode.

Table XIII shows the angle between the inclined fracture and the horizontal axis, and it can be seen that, in general, the existence of hydrogen caused a decrease in the angle. It is not understood why the angle did not continue to decrease gradually between 80 and 150 ppm hydrogen. Others[8] have shown a minimum angle of about 28° before complete horizontal fracture occurred, and it appeared as the same type of a phenomenon as is related to this alloy. It seems that a gradual decrease in the angle or a sudden decrease (as in this case) depends on which flow condition (Tresca or von Mises) the material follows.

Table XIII - Angle of Instability Formation

Hydrogen Concentration (ppm)	Angle Between Fracture Plane & Horizontal Axis (°)
10	33-34
80	32
150	32

No real explanation can be made as yet to explain the increased total strain resulting from hydrogen concentration increases. Boyd et al.,[56] using tensile sheet specimens, showed that the presence of even enough hydrogen to produce strain-induced hydrides (> 200 ppm) does not affect the ductility of Ti-8Al-1Mo-1V. Actually the ductility increased with higher hydrogen concentration regardless of the strain rate used (they used 3/min and 3 x 10^{-4}/min strain rates). Only when spontaneous hydrides were precipitated did ductility decrease. These data agree fairly well with those generated in this report. Total strain and reduction in area data for the Ti-8Al-1Mo-1V used in the present experiment are shown in Table XIV.

Table XIV - Ti-8Al-1Mo-1V Ductility Data

Hydrogen Content (ppm)	10	80	150
Total Strain at Disruption	.199	.216	.212
Reduction in Area (%)	17.3	20.0	19.0

Schwartsberg[54] has shown drastic effects of slow strain rates on reduction of area properties in some titanium alloys (Ti-140A). His data indicated a drop in reduction area from 60 to 12% for testing speed change from 2.54 cm/min to 0.0127 cm/min in an alloy (α-β) containing 500 ppm hydrogen. Yet Lenning's data[58] for α-titanium alloy showed an increase in reduction in area. Thus, both the amount of β phase and the strain rate seem to be significant.

An attempt was made to obtain samples for transmission microscopy but for the most part the attempt was futile. A very small area of one 150 ppm hydrogen sample was examinable and no strain-induced hydrides were found: but in general it is not possible to say whether or not strain-induced hydrides existed in the lower hydrogen concentrations.

From examination of the flow curves in Figs. 13 and 14 it is seen that hydrogen has no noticeable effect on the strain hardening coefficient of Ti-8Al-1Mo-1V alloy. Boyd et al.[57] had shown a strain-hardening effect, but his hydrogen concentrations were considerably higher than those used in this study.

Comparison of the aged and unaged Ti-8Al-1Mo-1V alloy revealed that the aging treatment resulted in a significant increase in strength and a decrease in ductility. Figure 24 shows the strain-hardening exponents for the 10 ppm hydrogen samples. The aged specimen has a lower strain-hardening exponent than does the unaged specimen. Chakrabarti[5] has shown that instability formation is easier the lower the strain-hardening exponent. Chakrabarti's work was on 4340 steel and may not be applicable to other material systems. Since no true stress maximum was obtained for the aged specimens in the present study, it is not possible to determine the effect of the strain-hardening exponent on instability formation. The only speculation that can be made is that if the aged specimens failed because of instability formation, they did so at a lower strain than the unaged specimens and they possessed no tolerance for the instabilities.

Examination of scanning electron microscope (SEM) fractographs in Figs. 25 and 26 show that much of the fracture was related to pore formation. Optical metallography showed very few pores near the fracture. One can notice in Fig. 25 that there are many flat areas connecting the pores. It is felt that the fracture of this material must follow the second type of instability controlled failure. This takes place when the plane of instability flow is thicker than the second-phase particles (in this case, β phase) and causes pore nucleation. This was quite evident in the microsample observed from the Ti-8Al-1Mo-1V specimen having 150 ppm hydrogen. The photomicrograph for this structure was not clear but a schematic is shown in Fig. 27. A very sharply defined deformation band was found at the small tip on either side of which there was very little or no deformation. In this deformed band were very small pores (much larger in the schematic than in reality) which had been elongated. These pores are believed to have been created by the instability flow.

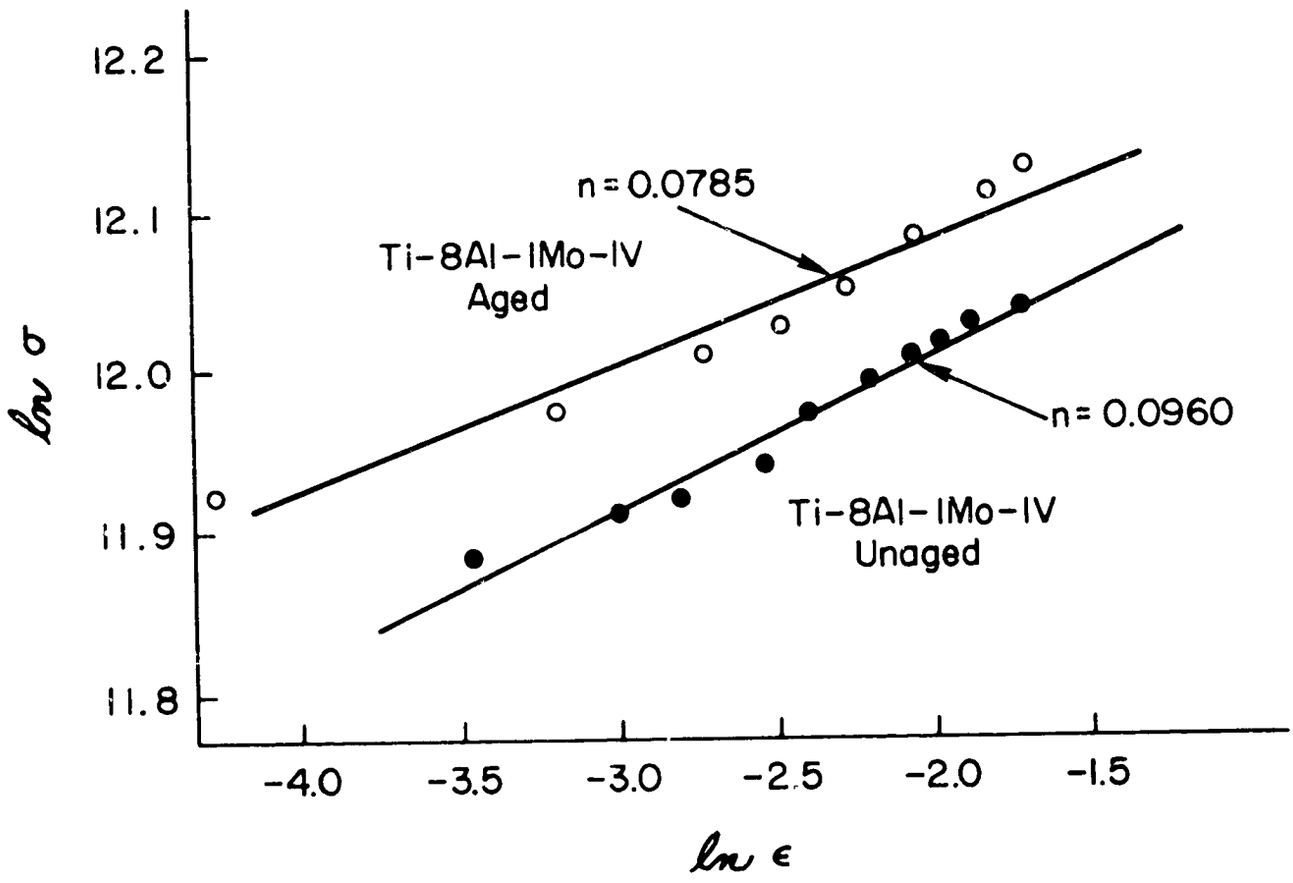

Fig. 24 - Log true stress vs log true strain

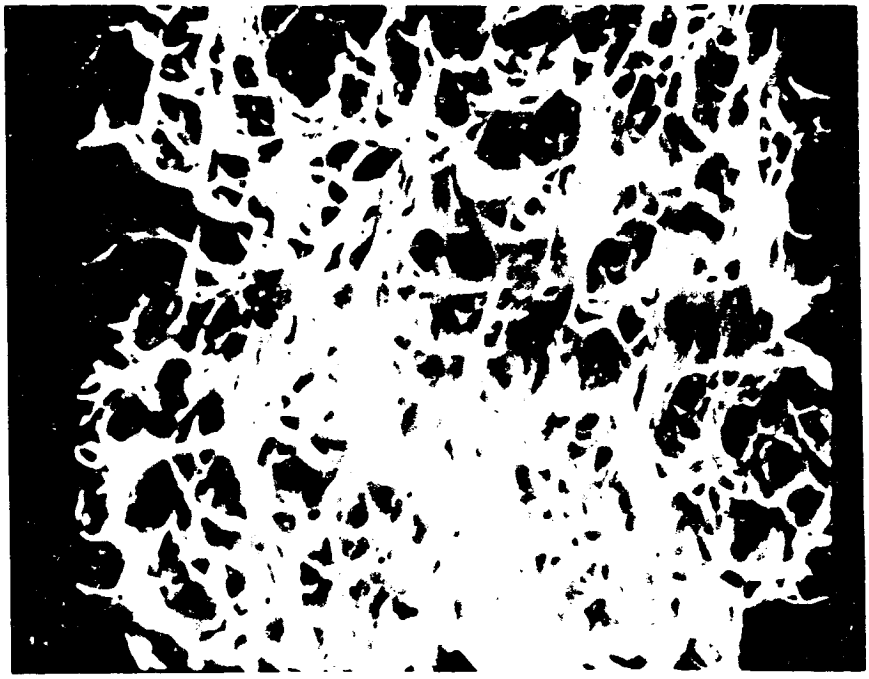

Fig. 2[illegible] - Fracture surface of unaged Ti-8Al-1Mo-1V specimen containing 10 ppm hydrogen
SEM 1000X

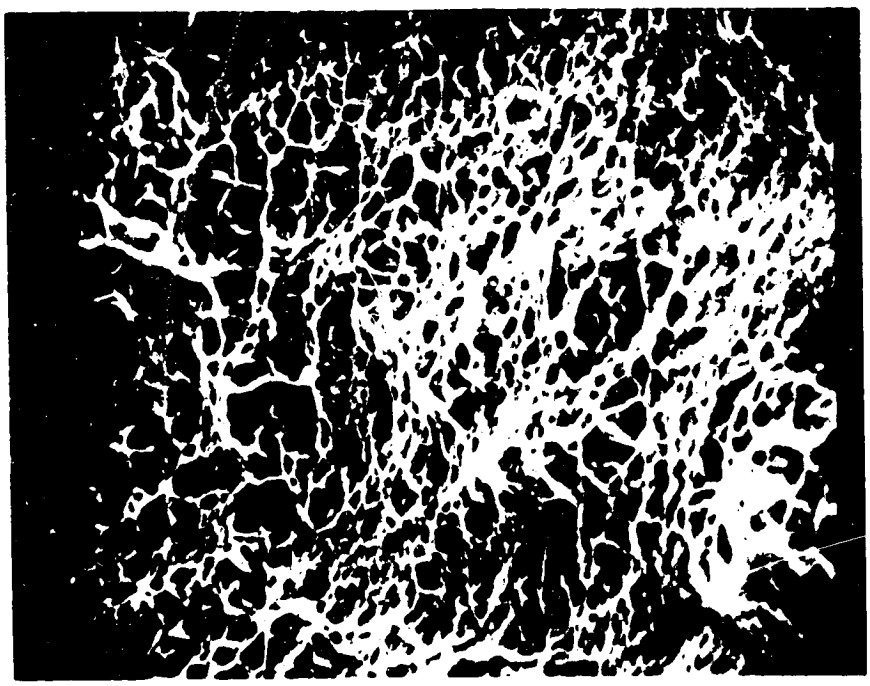

[illegible] - Fracture surface of aged Ti-8Al-1Mo-1V specimen containing 10 ppm hydrogen
SEM 1000X

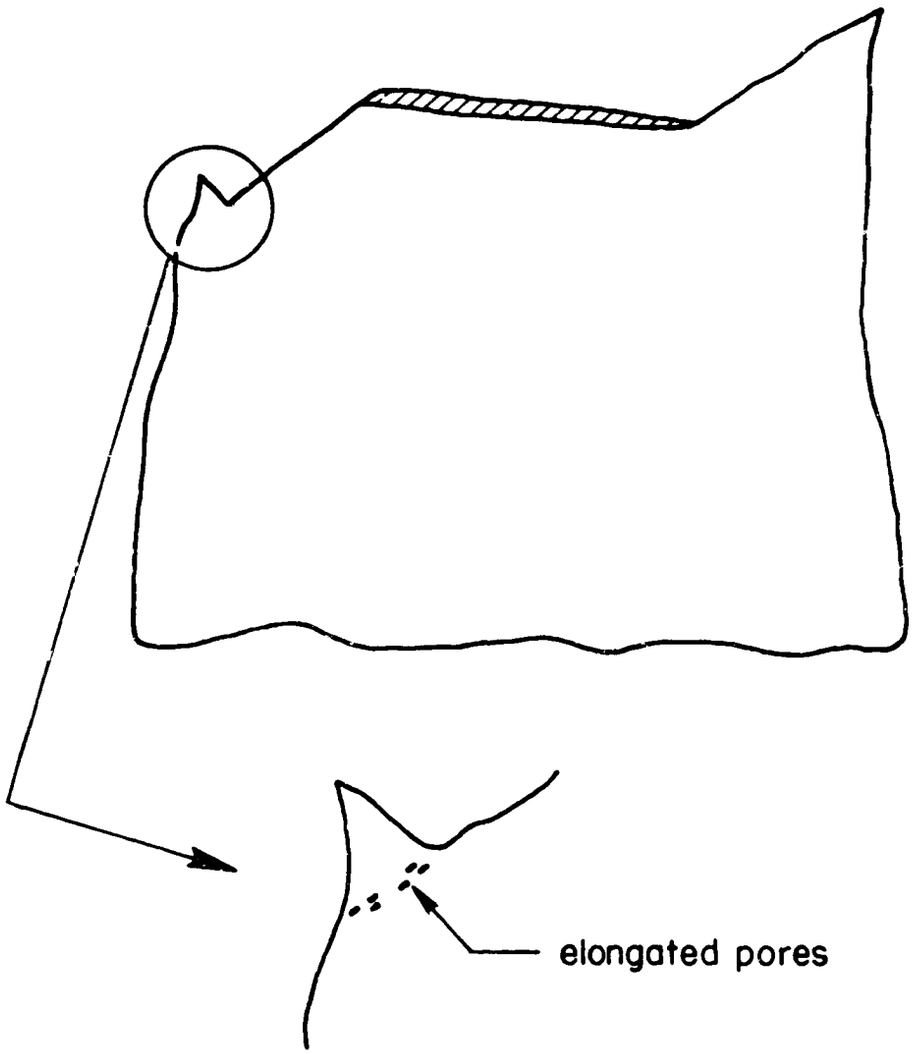

Fig. 27 - Schematic of Fig. 28A showing thick instability flow band and the pores nucleated in it

The fractograph in Fig. 26 shows a finer structure than in Fig. 25, but both specimens showed a consistent structure over their entire surface whether on the horizontal or inclined part of the fracture. It is therefore apparent that the first crack initiated was unstable across the entire width. This can also be evidenced from the load-extension diagram which showed only one load disruption which lowered the load instantaneously to zero with no arrests.

The results of testing specimens taken in directions other than the rolling direction showed that the same phenomena occurred. Table XI indicates that the higher hydrogen concentration produced higher disruption strains. There was some indication that less strain occurred when the specimen axis was transverse to the rolling direction. Fractures were similar to those found in the first tests and angles of separation were about 33°.

The effect of hydrogen on the strain rate sensitivity was investigated. Specimens having 10 and 150 ppm hydrogen were tested, with each test starting at a strain rate of 0.14 min^{-1}, and at approximately 0.03 strain the strain rate was changed to 1.4 min^{-1}. The load increased from 1176 to 1204 kg for the 10 ppm hydrogen specimen, and from 1256 to 1300 kg for the 150 ppm specimen. The strains used were much lower than the strain for necking so that necking caused no inaccuracies. The strain rate sensitivity "m" could be calculated from the relationship

$$m = \frac{\partial \ln \sigma_2/\sigma_1}{\partial \ln \epsilon_2/\epsilon_1} . \qquad (9)$$

The results gave a value of m = .0099 for 10 ppm hydrogen and m = 0.0145 for 150 ppm hydrogen. Thus, increasing the hydrogen concentration from 10 to 150 ppm resulted in a 46% increase in the strain rate sensitivity exponent.

This observation furnishes a rationale for stabilization of the α-Ti alloys against the shearing instability. According to the necessary condition for onset of this type of instability

$$d\sigma = \left(\frac{\partial \sigma}{\partial \epsilon}\right) d\epsilon + \left(\frac{\partial \sigma}{\partial \dot{\epsilon}}\right) d\dot{\epsilon} + \left(\frac{\partial \sigma}{\partial T}\right) dT = 0 . \qquad (10)$$

Increasing strain hardening and increasing strain rate sensitivity will increase the strain at instability, whereas increasing the adiabatic heating contribution to the flow stress will decrease this strain. The tensile data indicate no significant effect of hydrogen on strain hardening capacity. The constant specimen geometry and rate of straining furnishes no expectancy of a change in the adiabatic heating. Therefore, it must be concluded that hydrogen increases the strain to instability through the effect on strain rate sensitivity.

It is not known exactly how interstitial hydrogen affects the slip system in titanium. If it behaves as other interstitials (oxygen or nitrogen) it might be expected to increase the number of slip planes. Thus, dislocation movement might be made easier, leading to easier dislocation interaction, the result being increased strain hardening. As the dislocation density increases the periodicity of the atoms decreases.[54] Therefore, when the strain hardening is exhausted the atoms can flow over each other in directions dictated by continuum plasticity theories, and are not necessarily confined to movement in crystallographic directions. In this high degree of disorder hydrogen might be expected to aid flow and to cause it to occur sooner. Thus, the localization of flow would occur at a lower strain rate with hydrogen present.

On the other hand if hydrogen hindered the dislocation movement, it would cause the titanium to have less strain-hardening capacity, resulting in faster exhaustion of strain hardening and a lower strain for plastic instability formation.

From this study, it appears that hydrogen does affect the plasticity of the titanium alloys used. The result being to increase the total strain as hydrogen concentration is increased. When the hydrogen concentration reaches that necessary for spontaneous hydride precipitation the total strain decreases. The material is first affected while it is deforming as a crystallographic solid. Hydrogen seems to prolong uniform deformation and prevent the unstable straining associated with very localized cross section fluctuations. Thus, in Figs. 13 and 14 the maximum load point (usually associated with the diffuse necking phenomena) occurs at a higher strain with increased hydrogen.

Hydrogen forestalls localization of plastic flow into narrow deformation bands, but allows or forces it to occur over a wider area. The resulting instability flow initiates at higher rather than lower strains. Once localization and instability flow do occur, hydrogen aids the instability flow causing instability fracture to occur sooner with increased hydrogen concentration. This suggests that anything which helps to localize plastic flow in the presence of a high hydrogen concentration will aid in instability formation. Therefore, notches and hydride precipitates would tend to localize the plasticity and cause instability flow. The introduction of the γ compound could lower the diffuse ductility to the point where localization occurs faster and there is no tolerance for the instability.

The occurrence of ever-increasing amounts of plane strain mode with increasing hydrogen content, as shown in Figs. 15 and 16, may be explained by the interaction of the deformation regions. If hydrogen increased overall slip, as observed, then it might be expected that σ_2 would rise over a wider distance as σ_1 increased. It turned out that the interaction of the deformation bands was directly related to the amount of plane strain mode present, as shown schematically in Fig. 28. "A" shows a narrow interaction region and a small plane strain fracture; "B" and "C" show increasing interaction regions and larger plane strain fractures.

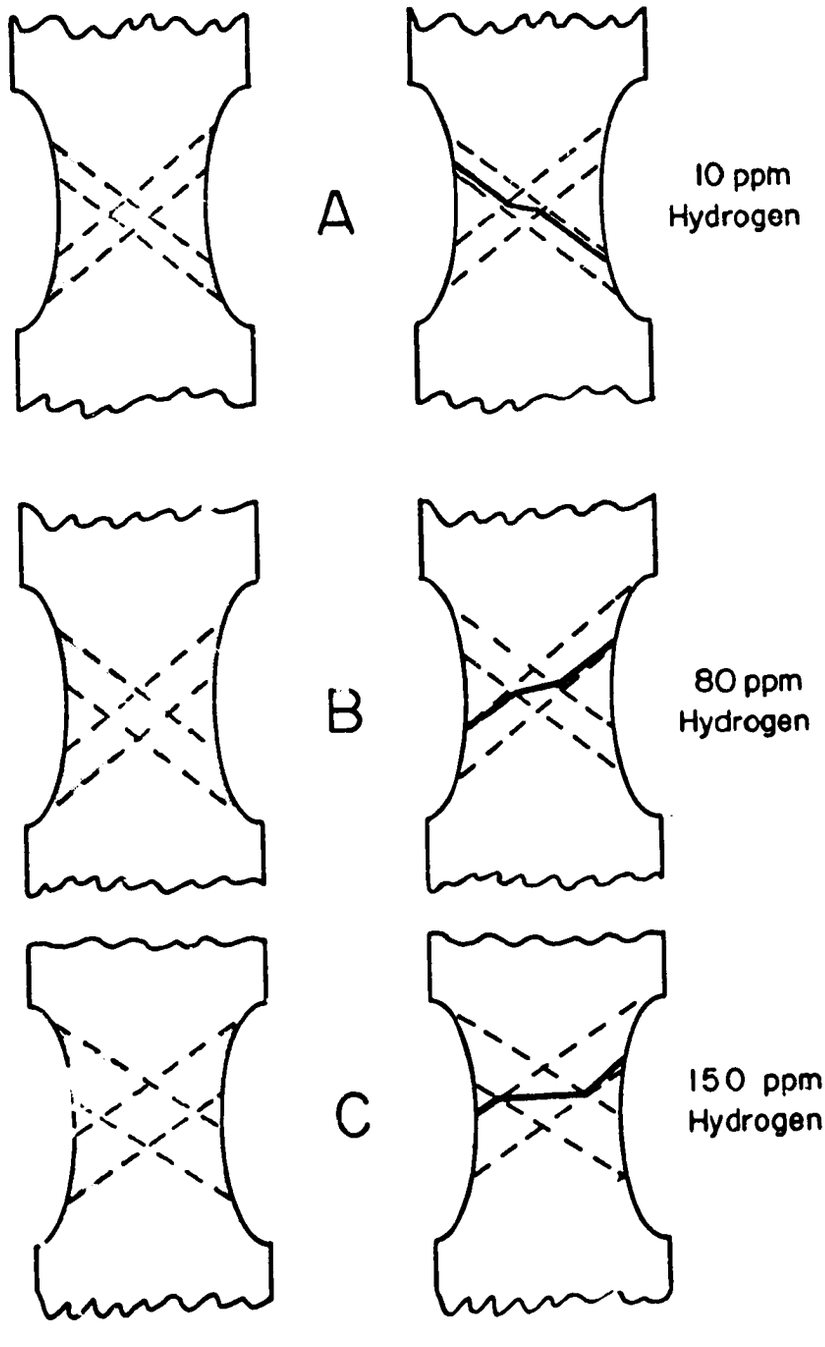

Fig. 28 - Schematic of the interaction of major deformation bands and the fracture pattern produced

Relative to the stress corrosion of titanium the phenomenon of instability flow could predict that there is a critical strain at the notch at which unstable flow occurs. The hydrogen absorbed into the lattice at this notch root would increase the plasticity of the material and cause instability flow to occur sooner than if the environment produced no hydrogen.

CONCLUSIONS

The effects of hydrogen concentration on the critical strain at which plastic instability along pure shear directions occurs was determined for titanium alloys Ti-8Al-1Mo-1V and Ti-5Al-2.5Sn.

In most cases the effect of hydrogen, in concentrations less than those necessary for spontaneous hydride precipitation, was to increase the strain necessary for any given event (instability formation or instability failure). The increase in strain instability is attributed to the increase of strain rate sensitivity with increasing hydrogen content.

The titanium alloys used showed a decreasing tolerance for instability, once it forms, with increasing hydrogen concentration; or, in other terms, hydrogen increases the magnitude of the instability.

The strain-hardening exponent for the titanium alloys used, particularly the Ti-8Al-1Mo-1V, was not significantly affected by different hydrogen concentrations. The strain rate sensitivity seemed to be increased by increased hydrogen concentration.

The presence of the spontaneous hydrides or the Ti_3Al compound lowered the total strain to fracture and the strain necessary for instability formation.

Results of the tests performed on the Ti-8Al-1Mo-1V alloy indicated that an instability flow mechanism was controlling the fracture. The second type of instability control is thought to be operative.

Hydrogen increased the amount of plane strain mode fracture in the Ti-8Al-1Mo-1V material.

Failure of the Ti-5Al-2.5Sn alloy appeared to be caused by instability flow connecting large pores in the specimen.

The Ti-5Al-2.5Sn (ELI) alloy, regardless of its single-phase matrix, is not a good material to work with using the sheet tensile specimen. The ductility and toughness are too great to allow thorough examination of instability flow.

III. THE EFFECTS OF HYDROGEN ON SLIP AND TWINNING IN TITANIUM SINGLE CRYSTALS

INTRODUCTION

Titanium technology has advanced rapidly since 1937 when W. J. Kroll first produced several hundred grams of ductile titanium. Through the years, mainly due to reduced cost in production, titanium has gradually been accepted as a structural material. Obvious advantages of titanium are strength-to-weight ratio and excellent corrosion resistance. The biggest consumer of titanium is the aerospace industry where it is used in jet engines and aircraft structures, and the second biggest consumer is the chemical industry where the use of titanium in some corrosive environments is more resistant than stainless steel. Titanium has its share of problems. One of the most serious is contamination by various interstitial elements, such as oxygen, hydrogen, nitrogen and carbon. Also, titanium is a very reactive metal and its oxide, hydride, nitride and carbide are all stable at room temperature. It is probably the strong bonding with these interstitial elements that causes the high-strength sensitivity of titanium to very small amounts of interstitials. Contamination, except for hydrogen, is usually not a problem at room temperature.

Hydrogen is readily absorbed by titanium in almost all hydrogen-containing environments. There are two reasons for this high hydrogen absorption. First, hydrogen exists in just about every environment and is, therefore, readily available (for example, hydrogen can form as a reaction product when titanium metal or its salts react with water). Second, the size of the hydrogen atom or ion is extremely small so that adsorption and diffusion rates can be appreciable at room temperature.

Most metals are subject to hydrogen embrittlement--titanium is no exception. The presence of hydrogen severely reduces ductility in titanium. A high concentration of hydrogen was found at stress corrosion crack tips of titanium alloys and, therefore, it was thought to be the culprit for stress corrosion cracking. Lower fatigue endurance was also noticed for titanium in hydrogen gas as compared to tests in air. There is no doubt that hydrogen is detrimental to mechanical properties, but there is little agreement among scientists concerning the mechanism by which metals are embrittled. A theory, advocating that brittle hydride is responsible for all hydrogen embrittlement in titanium and titanium alloys, has been offered. However, the fact that many metals do not form hydride, and yet are severely embrittled by the presence of hydrogen, strongly contradicts the hydride theory.

All metals deform by slip, twinning and/or phase transformation. The majority of the metals are deformed by slip and twinning, while phase transformation induced deformation is relatively unimportant.

When slip and twinning become inoperative the material becomes embrittled since necessary dimensional changes can not be accommodated by plastic deformation--cracks form and brittle failure is initiated. A study of the effects of hydrogen on basic deformation processes is necessary to clarify the hydrogen embrittlement mechanism. It is with this fact in mind that research on the effects of hydrogen on slip and twinning of titanium was started. Results of this research are presented and discussed, and a new model of transgranular stress corrosion cracking in alpha titanium is presented.

CRYSTALLOGRAPHY OF TITANIUM

Pure titanium is an allotropic metal. At 1158 K it changes from a BCC structure to an HCP structure which is commonly referred to as the alpha phase. Alpha phase has a c/a ratio of 1.587 with a = 2.95 Å and c = 4.68 Å. The calculation of angles between planes and plane spacings can be done, using the concept of reciprocal lattice, through the following equations:

For plane $(h_1k_1m_1\ell_1)$ where $m_1 = -(h_1 + k_1)$, the plane spacing d_1 is

$$d_1 = \left[\frac{1}{h_1^2 + h_1k_1 + k_1^2 + 3/4\ (a^2/c^2)\ell_1^2}\right]^{1/2} \tag{11}$$

and the angle between planes $(h_1k_1m_1\ell_1)$ and $(h_2k_2m_2\ell_2)$ is

$$\theta = \cos^{-1}\left[\frac{h_1h_2 + k_1k_2 + 1/2\ (h_1k_2 + h_2k_1) + \frac{(3/4)\ (a^2/c^2)\ell_1\ell_2}{[h_2 + h_2k_2 + k_2^2 + 3/4\ (a^2/c^2)\ell_2^2]^{1/2}}}{[h_1^2 + h_1k_1 + k_1^2 + 3/4\ (a^2/c^2)\ell_1^2]^{1/2}}\right] \tag{12}$$

One must be careful when using three- or four-index systems in expressing planes and directions in hexagonal crystals. Both three- and four-index systems are used in describing planes, and they are interchangeable. Plane (h,k,ℓ) in the three-index system would simply be plane $(h,k,-k-h,\ell)$ in the four-index system. Directions, however, are not interchangeable. Directions $[h,k,m,\ell]$ in the four-index system would be $[h-m,k-m,\ell]$ in the three-index system. Moreover, direction $[h,k,m,\ell]$ is not perpendicular to plane (h,k,m,ℓ) unless it is a direction in, or normal to, the basal plane. Angles between directions $[h_1k_1\ell_1]$ and $[h_2k_2\ell_2]$ can be calculated by:

$$\theta = \cos^{-1}\left[\frac{h_1h_2 - 1/2\ (h_1k_2 + h_2k_1) + k_1k_2 + \ell_1\ell_2(c^2/a^2)}{[h_1^2 - h_1k_1 + k_1^2 + \ell_1^2(c^2/a^2)]^{1/2}[h_2^2 - h_2k_2 + k_2^2 + \ell_2^2(c^2/a^2)]^{1/2}}\right] \tag{13}$$

The above equations are very useful when analyzing Laue patterns and transmission electronmicroscope diffraction patterns. It is obvious from these equations that plane spacings and angles between planes are functions of the c/a ratios. Nolder et al.,[64] using the above equations, tabulated the plane spacings and angles between planes of hexagonal crystals. The relative reciprocal lattice vectors, which equal the inverse of the plane spacings, are shown in Table XV. It is clear from Table XV that below the ideal c/a ratio the {100} plane has the highest spacing, {002} has the second highest, and {101} has the third highest. The areas per atom for {100}, {002}, and {101} planes are $1/0.794a^2$, $1/0.866a^2$, and $1/0.903a^2$, respectively. The nature of {100} and {101} planes are particularly interesting in that they are corrugated planes as shown in Fig. 29. As a matter of fact, they share part of their planes. The shortest lattice vector in titanium is $1/3\langle 11\bar{2}0\rangle$.

There are two possible interstitial sites in titanium: octahedral and tetrahedral sites. The octahedral and tetrahedral sites shown in Fig. 29 occupy (1/3,2/3,1/4) and (2/3,1/3,3/4) positions, respectively. Based on the hard ball model, the octahedral site will accommodate an interstitial atom of radius 0.59 Å, and the tetrahedral site will accommodate an atom of radius 0.315 Å.

Interstitial elements have been found to have an important effect on the c/a ratio of pure titanium. Finley et al.[104] found that nitrogen, oxygen and carbon increase both the c and the a parameters, and also the c/a ratio. The effects of oxygen and nitrogen were quite similar, whereas the effect of carbon stood out alone. For example, 0.35 atomic percent of oxygen or nitrogen expanded the c parameter from 4.6835 Å to 4.6860 Å and had little effect on the a parameter, whereas 0.35 atomic percent of carbon expanded the c parameter from 4.6835 Å to 4.688 Å and the a parameter from 2.9505 Å to 2.9507 Å. Carbon apparently had expanded both the c and a parameters much more than oxygen and nitrogen. Based on the hard ball model, one would automatically assume that carbon must have a greater influence on the yield stress of titanium, but experimental results indicated that the opposite is true.

The effects of hydrogen on the lattice parameter of pure titanium is not known. Based on the small size of the hydrogen atom and on very limited hydrogen solubility, one would assume a limited effect of hydrogen on the lattice parameter.[105]

Titanium-aluminum alloys are particularly important because aluminum is used commonly in commercial titanium alloys as an alpha stabilizer, and it changes the properties of titanium in many ways. Titanium-aluminum alloys have smaller c and a vectors than pure titanium. There are limited data in the literature concerning the crystallography of titanium-aluminum alloys. However, from the data on slip in titanium-aluminum alloys, it appears that these alloys have c/a ratios similar to pure titanium.

Table XV - Relative Reciprocal Lattice Spacing for Hexagonal Close-Packed Lattices

h	k	ℓ	c/a ratios												
			1.00	1.20	1.40	1.55	1.60	1.65	1.80	1.85	1.90	2.0	2.20	2.40	2.60
0	0	0	0.	0.	0.	0.	0.	0.	0.	0.	0.	0.	0.	0.	0.
0	1	0	1.000	1.000	1.000	1.000	1.000	1.000	1.000	1.000	1.000	1.000	1.000	1.000	1.000
0	0	2	1.732	1.443	1.237	1.117	1.083	1.050	0.962	0.936	0.912	0.866	0.787	0.722	0.666
0	1	1	1.323	1.233	1.176	1.146	1.137	1.129	1.110	1.104	1.099	1.090	1.075	1.063	1.054
0	1	2	2.000	1.756	1.591	1.500	1.474	1.450	1.388	1.370	1.353	1.323	1.273	1.233	1.202
1	1	0	1.732	1.732	1.732	1.732	1.732	1.732	1.732	1.732	1.732	1.732	1.732	1.732	1.732
0	1	3	2.784	2.385	2.108	1.952	1.907	1.865	1.756	1.724	1.694	1.639	1.547	1.474	1.414
0	2	0	2.000	2.000	2.000	2.000	2.000	2.000	2.000	2.000	2.000	2.000	2.000	2.000	2.000
1	1	2	2.449	2.255	2.129	2.061	2.043	2.025	1.981	1.969	1.957	1.936	1.903	1.876	1.856
0	2	1	2.179	2.126	2.093	2.077	2.072	2.068	2.057	2.054	2.051	2.046	2.038	2.032	2.028
0	0	4	3.464	2.887	2.474	2.235	2.165	2.099	1.925	1.872	1.823	1.732	1.575	1.443	1.332
0	2	2	2.646	2.466	2.352	2.291	2.274	2.259	2.219	2.208	2.198	2.179	2.149	2.126	2.108
0	1	4	3.606	3.055	2.669	2.448	2.385	2.325	2.169	2.123	2.079	2.000	1.865	1.756	1.666
0	2	3	3.279	2.947	2.728	2.610	2.576	2.545	2.466	2.444	2.423	2.385	2.323	2.274	2.236
1	2	0	2.646	2.646	2.646	2.646	2.646	2.646	2.646	2.646	2.646	2.646	2.646	2.646	2.646

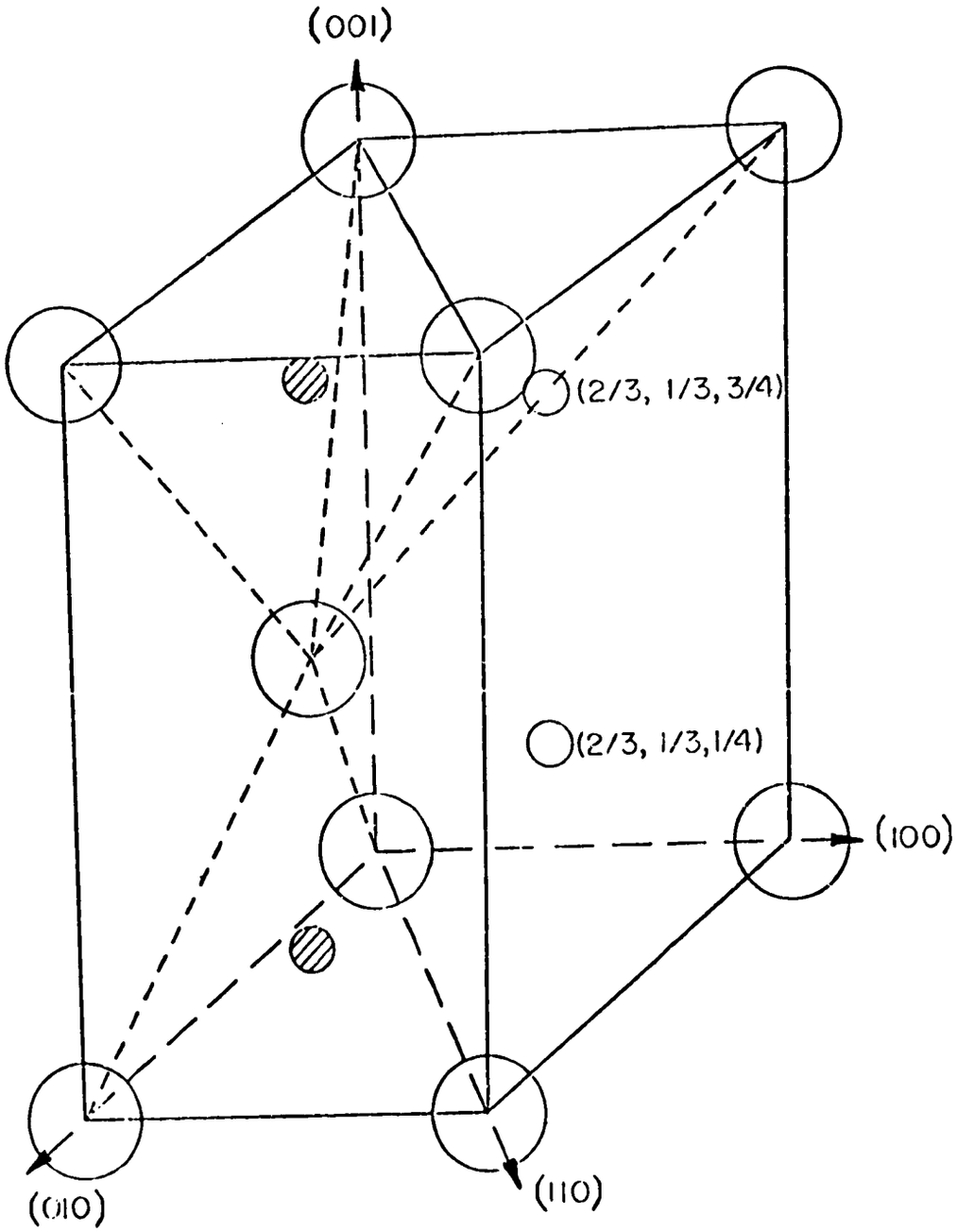

TITANIUM CRYSTAL STRUCTURE

Fig. 29 - The lattice structure of pure titanium. Open small circle is octahedral site. Crossed small circle is tetrahedral site.

SLIP SYSTEMS

There are three slip systems in titanium:

$$\{10\bar{1}0\}1/3\langle 11\bar{2}0\rangle$$

$$\{10\bar{1}1\}1/3\langle 11\bar{2}0\rangle$$

$$\{0001\}1/3\langle 11\bar{2}0\rangle$$

From plane spacings presented previously it is not surprising to see that these are the slip planes. Planes $\{10\bar{1}0\}$ have the largest spacing, $\{0001\}$ the second largest, and $\{10\bar{1}1\}$ the third. One would expect $\{10\bar{1}0\}$ to have the lowest critical resolved shear stress, $\{0001\}$ the second, $\{10\bar{1}1\}$ the third, but it turns out that $\{10\bar{1}1\}$ planes generally have a lower critical resolved shear stress than do the $\{0001\}$ planes. Churchman[85] used two groups of specimens in his determination of the critical resolved shear stress in pure titanium single crystals. Group I (Vickers hardness 90) had a combined oxygen and nitrogen content of approximately 0.01 wt% while Group II (Vickers hardness 170) had a combined oxygen and nitrogen content of approximately 0.1 wt%. His results showed critical resolved shear stresses of 90.06, 97.02, and 106.82 MN/m^2 for planes $\{10\bar{1}0\}$, $\{10\bar{1}1\}$ and $\{0001\}$, respectively. For Group I crystals, the $\{10\bar{1}0\}$ planes were the principal slip system with a minimum value of critical resolved shear stress of 13.72 MN/m^2. Only one $\{0001\}$ slip was observed with a critical resolved shear stress of 61.74 MN/m^2. One can clearly see that $\{10\bar{1}0\}$ slip is most favorable, but decreasingly so as the oxygen and nitrogen content increased. The ratio of critical resolved shear stress between $\{10\bar{1}0\}$ and $\{0001\}$ planes decreases from 1:1.86 to 1:3 as the combined oxygen and nitrogen contents decreased from 0.1 wt% to 0.01 wt%. The critical resolved shear stress for these three slip systems were also determined by other researchers, whose results are tabulated in Table XVI.

These data show that the critical resolved shear stress is sensitive to interstitial concentration and that the discrepancies among researchers are due mainly to impurity levels of the titanium. The Vickers hardness number of pure titanium is also sensitive to the interstitial content. Jaffee et al.[86] plotted the Vickers hardness vs. the combined oxygen and nitrogen content, and the resulting curve has been used as an indication of interstitial concentration.

William and Eppelsheimer[87] published an analysis of the preferred orientation texture of titanium in which they predicted that slip should occur on $\{10\bar{1}1\}$, $\{10\bar{1}0\}$ and $\{0001\}$ planes, together with twinning on $\{10\bar{1}2\}$ and $\{11\bar{2}2\}$ planes in order to account for the textures. From their analysis they concluded that the $\{10\bar{1}1\}$ plane would be the principal slip system, while the critical resolved shear stress for $\{0001\}$ slip would be 1.1 times that of the $\{10\bar{1}1\}$ slip, and $\{10\bar{1}0\}$ slip would be 1.02 times that of $\{0001\}$ slip. Churchman's results did not agree quantitatively with their predictions. Churchman[85] proposed that the

Table XVI - Slip Systems

Ref.	(O+N)*(ppm)	H (ppm)	Slip Plane	CRSS, MN/m^2
140	580	150	$10\bar{1}0$	49
140	930	120	$10\bar{1}0$	44.1
140	980	110	$10\bar{1}0$	49
140	1600	80	$10\bar{1}0$	114.6
140	1800	80	$10\bar{1}0$	63.7
140	580	150	0001	106.8
140	1400	160	0001	128.38
140	1700	40	0001	132.3
65	1000	10	$10\bar{1}0$	90.06
65	1000	10	$10\bar{1}1$	97.02
65	1000	10	0001	106.82
65	100	10	$10\bar{1}0$	13.7
65	100	10	0001	61.74
141	75	< 0.1	$10\bar{1}0$	19.6
141	79	< 0.1	0001	83.3

*The content from ref. 140 is oxygen content only

discrepancies were due to the different amount of deformation and the differences in operating the slip system between single crystal and polycrystal titanium. William's prediction was based upon the preferred orientation texture of heavily deformed polycrystalline titanium. A complex stress state of a crystal in a polycrystalline material could have favored $\{10\bar{1}1\}$ slip. A further factor involved is that the work hardening rate on $\{10\bar{1}1\}$ slip could be smaller than $\{10\bar{1}0\}$ slip, and after a certain amount of deformation, $\{10\bar{1}1\}$ slip has a lower critical resolved shear stress than $\{10\bar{1}0\}$ slip.

The sensitivity of mechanical properties of pure titanium to interstitial contents could be explained because titanium forms a strong bond with these interstitial elements, but the actual mechanism which accounts for the different sensitivities among the three slip phases is not known. Churchman[65] attempted to explain the different sensitivities using dislocation theory as follows: Oxygen and nitrogen are believed to be in octahedral sites of pure titanium because their sizes are just about the size of a octahedral site. As shown in Fig. 29, these sites are (2/3,1/3,1/4) and (2/3,1/3,3/4) in the pure titanium lattice. The positions of these sites are such that atoms occupying the sites are not coplanar with either the {0001} or the $\{10\bar{1}0\}$ layers and, therefore, provide obstacles to the movement of adjacent layers. On the other hand, 50 percent of the atoms on these sites are coplanar with the $\{10\bar{1}1\}$ planes and, therefore, provide no obstacles to $\{10\bar{1}1\}$ slip. Churchman postulated that dislocations dissociated as partial dislocations of the Burgers vector $1/3\langle 10\bar{1}0\rangle$ on the basal plane as shown in Fig. 30. The atoms shown represent the basal plane. Repeated layers of atoms occupy A and B sites alternately. The C sites are octahedral sites. If C sites are occupied by interstitial atoms, then the dissociation would be prevented. Therefore, dislocations must move as a perfect dislocation rather than the easier moving partial dislocations. Based on the foregoing arguments, one would expect that the interstitial atoms on octahedral sites would have different degrees of effect on the critical resolved shear stress of $\{10\bar{1}0\}$, {0001} and $\{10\bar{1}0\}$ slips. Interstitial atoms occupying tetrahedral sites will not be coplanar with any of the slip planes, and therefore, provide obstacles to all three slip planes.

The slip systems of titanium-aluminum alloys have been observed by several researchers. Blackburn[68] used annealed Ti-8Al-1V-1Mo alloys, Ti-9Al alloys, and pure titanium which were tensile tested at room temperature. After testing, thin foils of these materials were made for observation by transmission electronmicroscopy. Slip has found to be primarily on $\{10\bar{1}0\}$ planes, but {0001} and $\{10\bar{1}1\}$ slip systems were also observed to some extent. The dislocation arrangements in titanium and the Ti-9Al alloy were quite different. These arrangements will be discussed later in this section. The slip systems in Ti-Al alloys were quite similar to pure titanium, suggesting that the c/a ratio of Ti-Al alloys should be close to pure titanium.

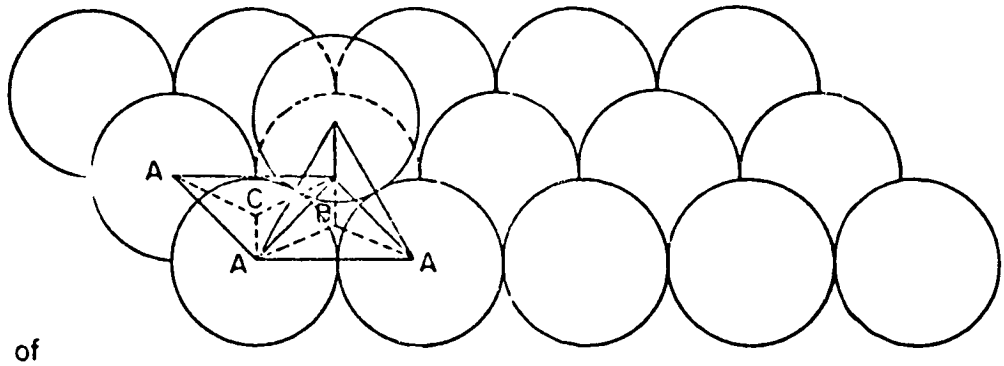

Position of
Octahedral Site C in
Basal Plane

Possible BurgersVectors
in Hexagonal Lattice

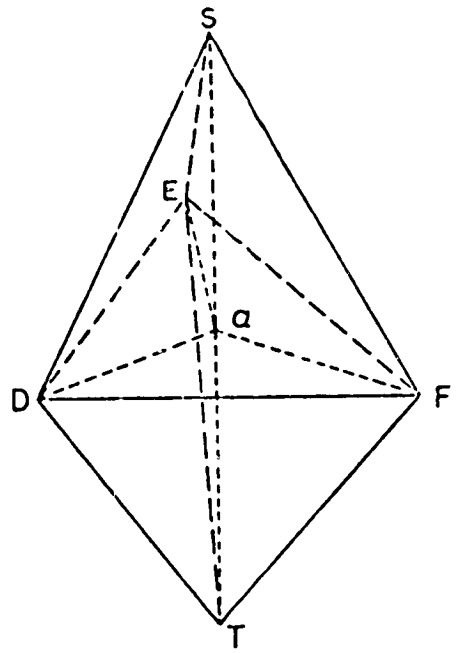

Fig. 30 - Atom arrangement on the basal plane and the position of the octahedral site. The lower diagram shows the Burgers vectors in pure titanium.

The dominant slip system in a single crystal is determined by two factors: (1) critical resolved shear stress and, (2) orientation relationship of the loading axis to the slip system. The orientation relationship of the loading axis to the slip system is usually expressed by the Schmid Factor. As shown in Fig. 31, the Schmid Factor is defined as cos α cos β. The shear stress in the slip direction on the slip plane (σ_{xy}) is related to the loading stress by the equation: $\sigma_{xy} = \sigma \cos \alpha \cos \beta$.

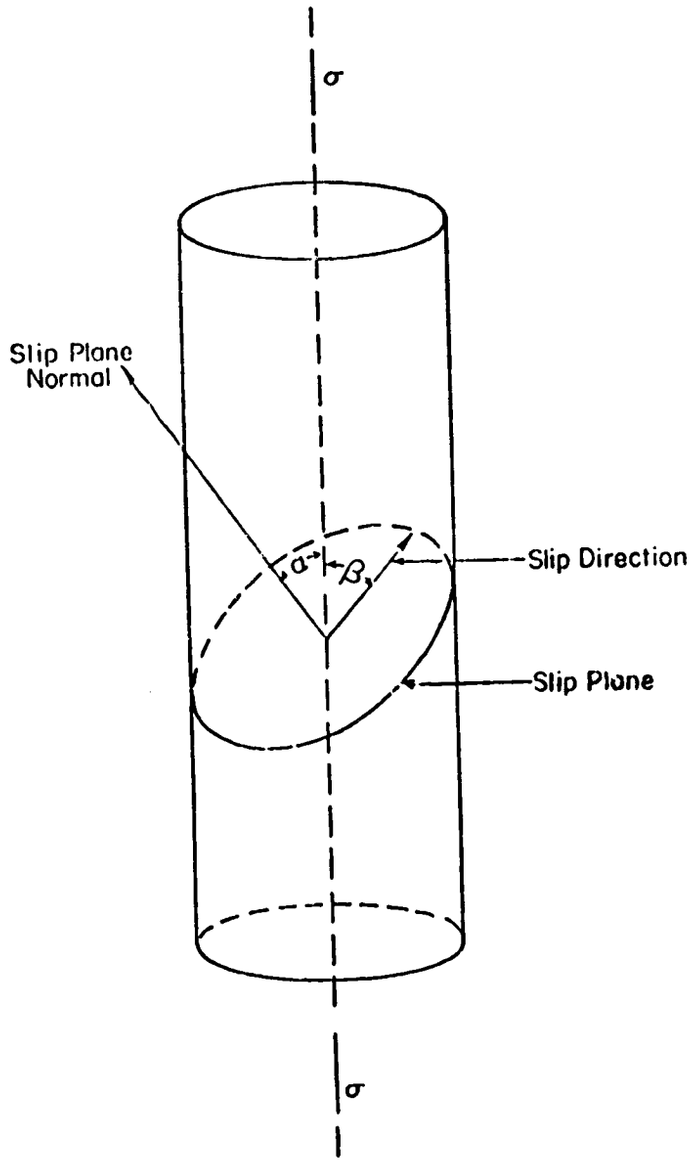

Fig. 31 - The relationship of the tensile axis to the slip plane normal and the slip direction.

Shechtman and Brandon[69] plotted equi-Schmid factor lines on a stereographic projection of titanium. They are shown in Fig. 32. Based on Fig. 32, the dominant slip system of a single crystal can be determined. With the knowledge of slip plane rotation under the conditions of single slip and multislip, and with the use of Fig. 32, the cold work texture of titanium can be predicted.[67,69]

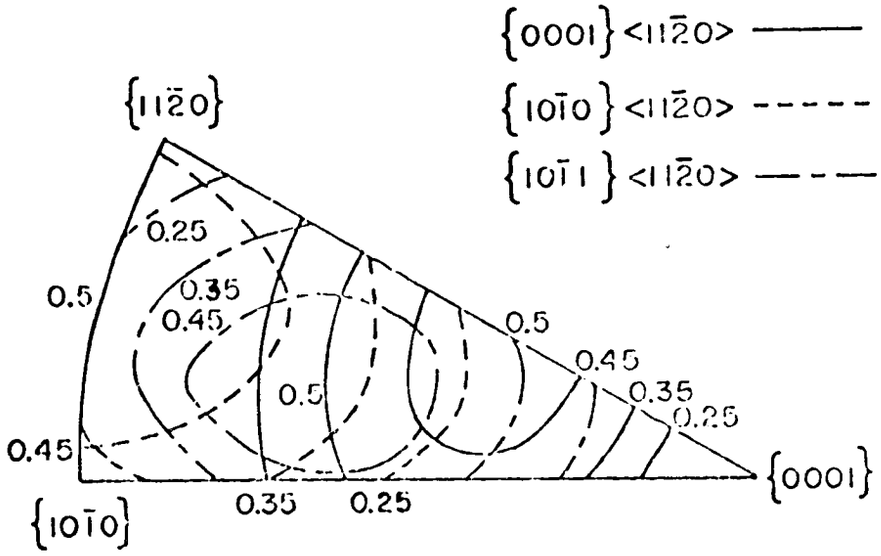

Fig. 32 - Equi-Schmid factor lines for the three slip systems projected on the stereographic triangle of pure titanium.

To achieve an arbitrary strain in a single crystal, according to von Mises' principle, requires five independent slip systems. If not enough independent slip systems are present, other forms of deformation such as grain boundary sliding, twinning, phase transformation and fracture must occur. In general, each independent slip direction can produce, at most, two independent slip systems. In titanium $\{10\bar{1}0\}1/3\langle 11\bar{2}0\rangle$ has three slip systems, $\{10\bar{1}1\}1/3\langle 11\bar{2}0\rangle$ has six slip systems, and $\{0001\}1/3\langle 11\bar{2}0\rangle$ has three slip systems. All of these slip systems have $\langle 11\bar{2}0\rangle$ slip directions, but only two of the three are independent. Therefore, there are only four independent slip systems out of 12 distinct slip systems. More specifically, with all the slip directions in basal planes, it is not possible to produce a normal component of strain in the $\langle 0001\rangle$ direction. It is clear now that either mechanical twinning or the (c + a) type of slip must be present when a crystal is deformed arbitrarily.

TWINNING

Twinning is a necessary mechanism, during plastic deformation of titanium. Six different twinning systems have been observed by researchers.[70-73] They are listed in Table XVII. Twinning is defined by four vectors;[74] (1) K_1 twin plane, (2) η_1 twin shear direction, (3) K_2 second undistorted plane, and (4) η_2 intersection of K_2 with plane of shear. They are shown in Fig. 33.

There are three kinds of twinning:

(a) K_1 is a rational plane and η_1 a rational direction,

(b) K_2 is a rational plane and η_2 a rational direction,

(c) K_1, K_2 are rational planes and η_1, η_2 are rational directions.

Table XVII - Twinning Systems

K_1	K_2	η_1	η_2	Twin Shear
$10\bar{1}2$	$\bar{1}012$	$\bar{1}011$	$10\bar{1}1$	0.174
$11\bar{2}1$	0001	$\bar{1}\bar{1}26$	$11\bar{2}0$	0.63
$11\bar{2}2$	$11\bar{2}\bar{2}$	$11\bar{2}\bar{3}$	$11\bar{2}3$	0.22
$11\bar{2}3$	--	--	--	--
$11\bar{2}4$	--	$22\bar{4}3$	--	0.22
$10\bar{1}1$	$\bar{1}013$	$\bar{1}012$	$30\bar{3}2$	0.104

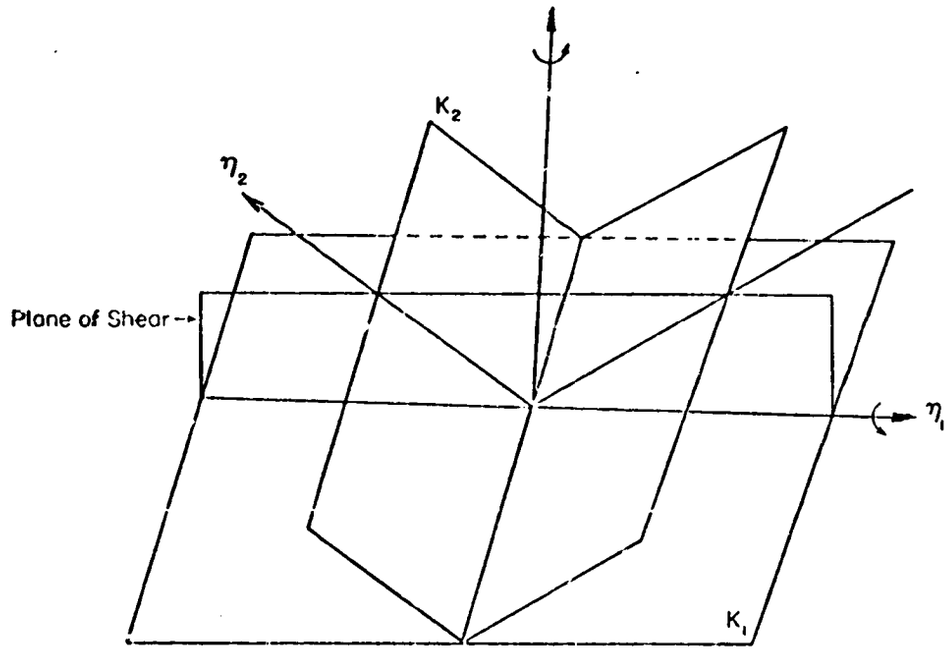

K_1 Twin Plane
η_1 Twin Shear Direction
K_2 Second Undistorted Plane
η_2 Intersection of K_2 and Plane of Shear

Fig. 33 - Definition of the twinning vectors.

In a twin of the first kind, the lattice in the sheared section is related to that in the unsheared section by a rotation of 180° about the normal to K_1. The corresponding 180° rotation in a twin of the second kind is about η_1 as an axis. In a compound twin, the third kind, both types of rotation result in the same final orientation. Most of the twinning in metals are of the third kind since high symmetry exists in most metal lattices. A sketch of a $\{10\bar{1}2\}$ twin (third kind) is presented in Fig. 34.

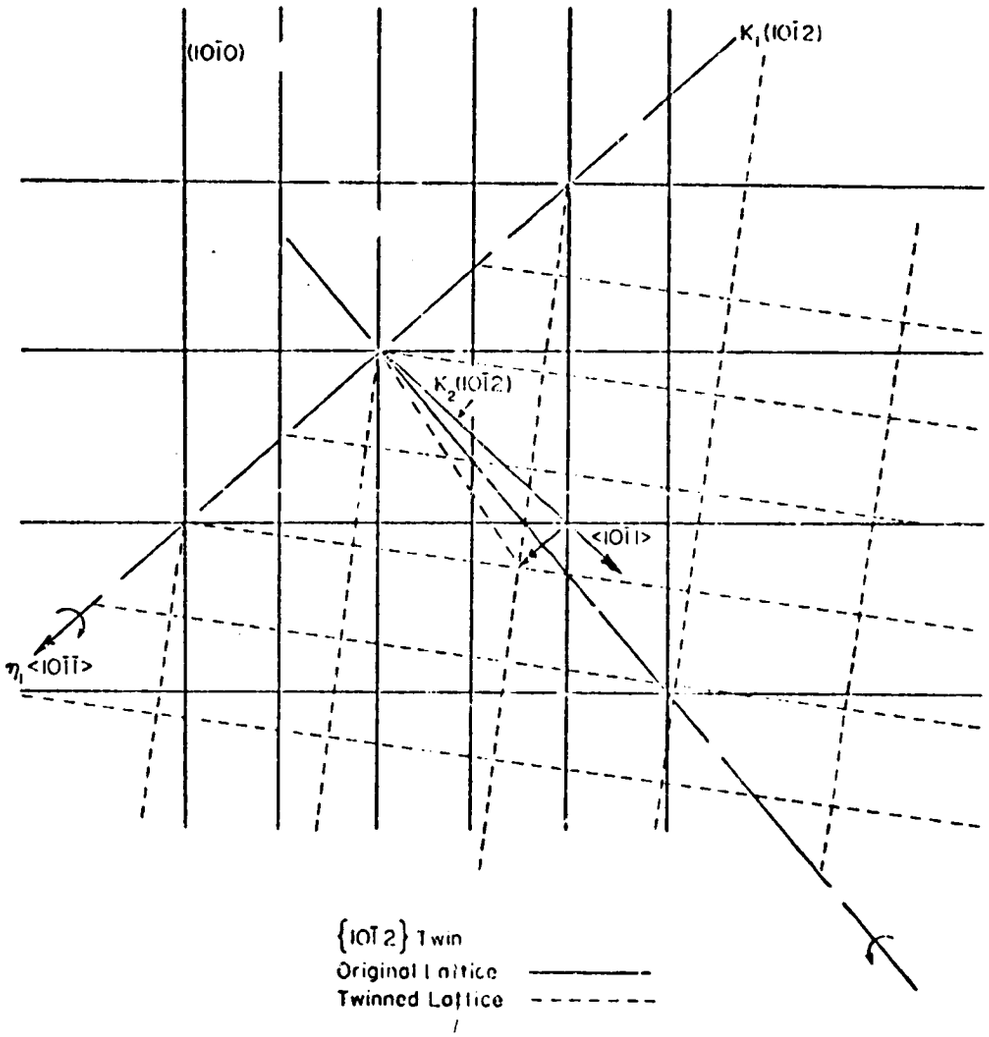

Fig. 34 - The relationship between the {10$\bar{1}$2} twin and the parent crystal.

Schmid and Boss have derived an expression for the theoretical tensile strain due to the transformation of a single crystal into a twin:

$$\epsilon_t = (1 + 2S \sin x \cdot \cos \lambda + S^2 \sin^2 x)^{1/2} - 1 \qquad (14)$$

ϵ_t is the tensile strain due to twinning, S is the twinning shear strain, λ the angle between the tensile stress axis and the twinning shear direction, and x the angle between the twinning plane normal and the tensile axis. If the loading axis of a crystal is known, Eq. (14) can be used to predict possible twinning. For example, if we compress a crystal normal to the (0001) plane and use the data in Table XVII, ϵ_t will be:

$$\epsilon_t = (1 + 2S \sin x \cos \lambda + S^2 \sin^2 x)^{1/2} - 1 \qquad (15)$$

for $\{10\bar{1}2\}\langle 10\bar{1}\bar{1}\rangle$ twinning in titanium,

$$S = 0.18$$
$$s = 42.73^\circ$$
$$\lambda = 47.27^\circ$$
$$\epsilon_t = 0.087$$

By examining Fig. 34, it is clear that the $\{10\bar{1}2\}$ twin will not occur when compressed. Unlike slip, twinning is polar; for a single crystal, the twinning system which operates under tension will not operate under compression if the same loading axis is maintained.

Basically, twinning involves two processes, initiation of the twin and growth of the twin. Like any nucleation and growth process, the initiation stage is always a barrier for the process. Considerable evidence exists to conclude that twin initiation is a heterogeneous process, initiation occurs at free surfaces, stress concentrations, grain boundaries and precipitates. Homogeneous nucleation of the twin has never been reported. Even with the help of heterogeneous nucleation, nucleation of the twin still requires a higher stress than for twin growth. This can be proven easily by examining the stress-strain curve of a crystal deformed by twinning as shown in Fig. 35; along with twin nucleation there is a big load drop followed by twin growth at a much lower stress.

To understand the phenomenon of twin nucleation and growth one has to look at the mechanism more closely. It is generally accepted that a twin is formed by twin dislocation glide on the twin plane. These dislocations are located at the twin-parent crystal interface. As they move into the parent crystal twin growth results. Twin dislocations are quite complicated and they not only provide the shear strain observed, but they are also associated with atom shuffling involved in the twinning process. The energy used in the initiation of a twin involves two terms: (1) energy of formation of the twin dislocation and, (2) a surface energy term. It is of the order of 0.05G for homogeneous nucleation and 0.02G at a surface step, where G is the shear modulus. The energy involved in the growth of a twin also has two terms: (1) a surface energy term and, (2) energy for gliding of the twin dislocation. The twin surface increment per unit volume is much less in twin growth than in twin initiation. Thus, the surface energy term becomes less important as twin growth progresses. Gliding of twin dislocations requires much less energy in comparison with the nucleation of these twin dislocations. From the above one can explain why twin nucleation requires a higher stress than does twin growth.

Simple shear, such as illustrated in Fig. 34, referred to here to show the orientation relationship between the parent and the twin

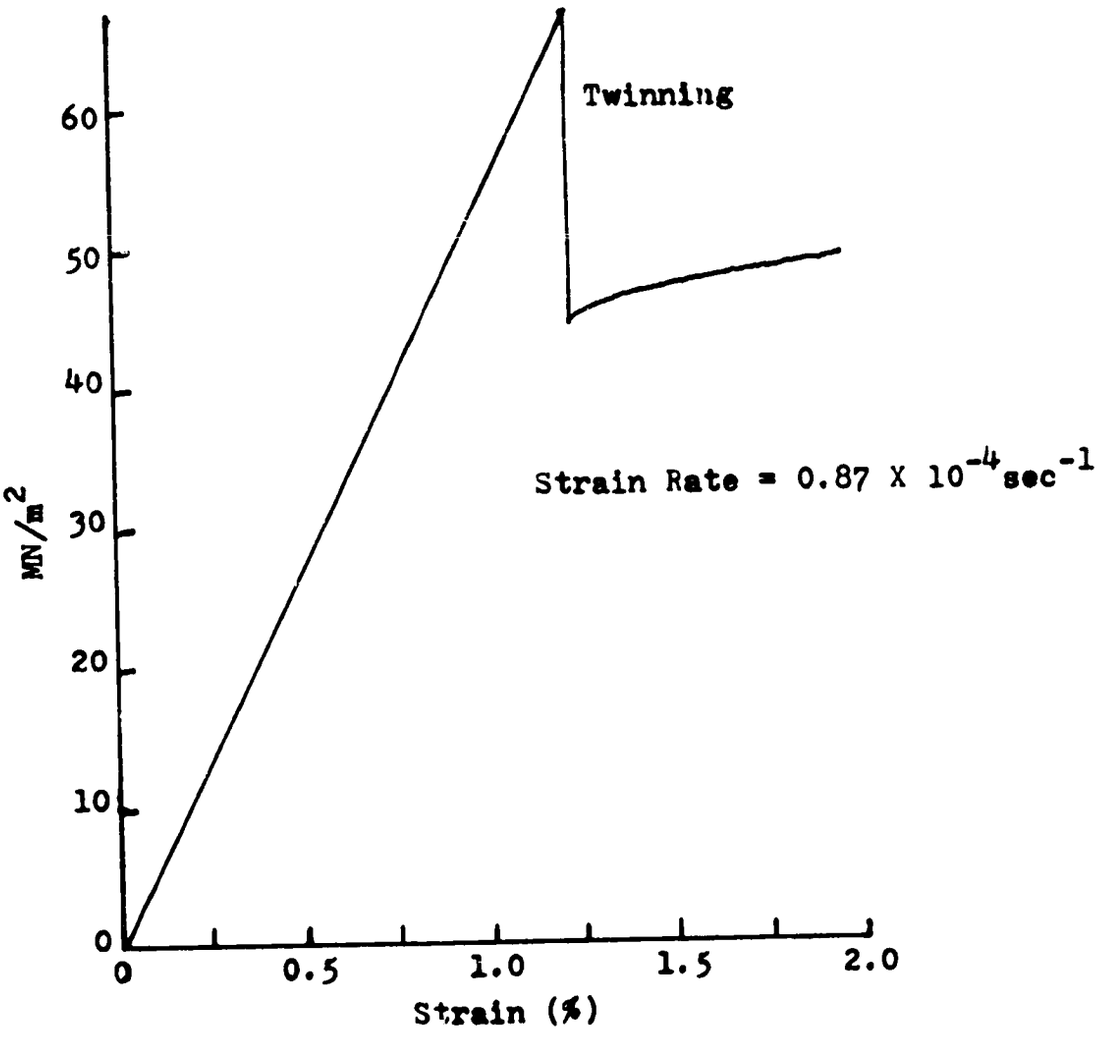

Fig. 35 - Stress-strain curve of a pure titanium single crystal compressed normal to the basal plane (ref. 121).

structures, can not move all of the atoms from the parent structure to correct positions in the twin structure. Atom shuffling must also occur to account for the twin structure, and this shuffling is believed to be associated with twin dislocations. Crocker and Bevis[70] showed the probable atomic shuffling for $\{10\bar{1}2\}$, $\{11\bar{2}1\}$, $\{11\bar{2}2\}$ and $\{11\bar{2}4\}$ twins.

Twinning in iron alloyed with 25 atomic percent beryllium was studied extensively by Bolling and Richman.[75-77] In this alloy, below 295 K, the critical resolved shear stress for twinning is lower than that for gross slip. Therefore, mechanical deformation is achieved primarily by repeated formation of mechanical twins. In their compression test they observed that both the yield stress and the work hardening rate increased with temperature and decreased with increasing strain rate. This result is the opposite of that observed for deformation by slip.

Paton and Backofen[72] compressed pure titanium single crystals normal to their basal plane over the temperature range 273-1073 K. As was shown above, none of the slip systems in titanium is capable of producing strain normal to the basal plane and, therefore, twinning must occur in order to absorb this compression strain. The twins observed upon compressing normal to the basal plane below 673 K were all $\{11\bar{2}2\}$ twins. A load drop accompanying the $\{11\bar{2}2\}$ twin initiation was always followed by $\{11\bar{2}2\}$ twin growth at a lower stress. The stress at which twin initiation occurred increased with temperature. Above 673 K several things changed. First, the twinning mode changed from the $\{11\bar{2}2\}$ twin to the $\{10\bar{1}1\}$ twin. Second, the c + a type of dislocation becomes an important mechanism of plastic deformation. Third, the load drop which accompanied the $\{11\bar{2}2\}$ twin initiation was not observed with $\{10\bar{1}1\}$ twin initiation. Paton and Backofen felt that the transition from $\{11\bar{2}2\}$ twinning to $\{10\bar{1}1\}$ twinning resulted from the stress for nucleation of $\{11\bar{2}2\}$ twins continuing to rise with temperature until it exceeded the stress for $\{10\bar{1}1\}$ twinning. Above 673 K the yield stress decreased with increasing temperature. This meant that twin nucleation no longer controlled the yield stress and nucleation stress was less than or equal to the stress for twin growth, and also explained the disappearance of the load drop above 673 K.

The positive temperature dependence and the negative strain rate dependence are also supported by other research on mechanical twinning. It is generally agreed that twins nucleate at stress concentrations, but at higher temperature or slower strain rates, where slip is easier, stress concentration such as at intersecting dislocations or at dislocations arrested at obstacles will not form as easily; consequently a higher apply stress is needed for twin nucleation. If plastic deformation is achieved by repeated twin formation, the same argument can be applied to explain how the work hardening rate increases with temperature and decreases with increasing strain rate.

The volume fraction of twins for the same amount of deformation in the same material varies with grain size. For example, Orava, Stone and Conrad[73] failed to find any twinning in fine-grained commercial

purity titanium tested at 77 K. Subsequently, Jones and Conrad[79] reported that twinning was not evident even in the necked part of a fine-grained titanium specimen deformed at 4.2 K. On the other hand, twinning was reported by other researchers[80,81] as an important plastic deformation mechanism for titanium single crystals.

Since mechanical twins are polar, twins favorable in compression will not nucleate under tension. Therefore, when twinning is an important deformation mechanism, the mechanical properties under compression are quite different from those under tension. For example, extruded magnesium rod has its basal plane parallel to the rod axis. A compressive stress applied nearly parallel to the basal plane favors $\{10\bar{1}2\}$ twinning, whereas a similarly directed tensile stress can not induce this twin. As a consequence, the stress-strain curves obtained by compressing and extending an extruded magnesium rod along its axis are very different.[82] For the same reason, texture hardening or softening becomes very important when mechanical twinning is an important part of the deformation process.

There is evidence[83] that a critical resolved shear stress exists for twinning as in slip. Thompson and Millard,[84] using a piezoelectric method, accurately measured the critical shear stress of twin nucleation for cadmium single crystals. The results indicated a critical resolved shear stress of 1.35 MN/m^2 ± 0.03 MN/m^2 at room temperature.

THE TITANIUM-HYDROGEN SYSTEM

Titanium is commonly referred to as an exothermic occluder with respect to hydrogen. This means that under isobaric conditions, the amount of hydrogen absorbed by titanium decreases with temperature.[85,86] This is shown in Fig. 36 along the beta and beta+1 atmosphere-hydrogen boundary and the gamma and gamma+1 atmosphere-hydrogen boundary.

The entire titanium-hydrogen phase diagram is shown in Fig. 36, where γ is the hydride phase. As can be seen from this diagram, hydrogen stabilizes the β phase down to 600 K at approximately 44 at.% hydrogen, which is the eutectoid composition. It is for this reason that hydrogen is referred to as a β stabilizer.

The solubility of hydrogen in the β phase at the eutectoid temperature is about five times that in the α phase. If we extrapolate the β and $\beta+\gamma$ boundary to room temperature, the solubility is approximately 18 at.% hydrogen. On the other hand, the low temperature portion of α and $\alpha+\gamma$ boundary was studied carefully by Lenning, Craighead and Jaffee,[87] and the solubility of hydrogen in the α phase at room temperature was determined to be 0.1 at.%. It is quite obvious that the β phase has a much higher hydrogen solubility than the α phase even at room temperature. More recent work by Mackay and Tiner[88] using electron microautoradiograph has also shown that, in Ti-8Al-1Mo-1V, hydrogen is concentrated in the β phase and along the α-β boundary. The ratio of hydrogen in the β phase to hydrogen in α phase was about 20 to 1 for Ti-8Al-1Mo-1V containing 40 ppm of hydrogen.

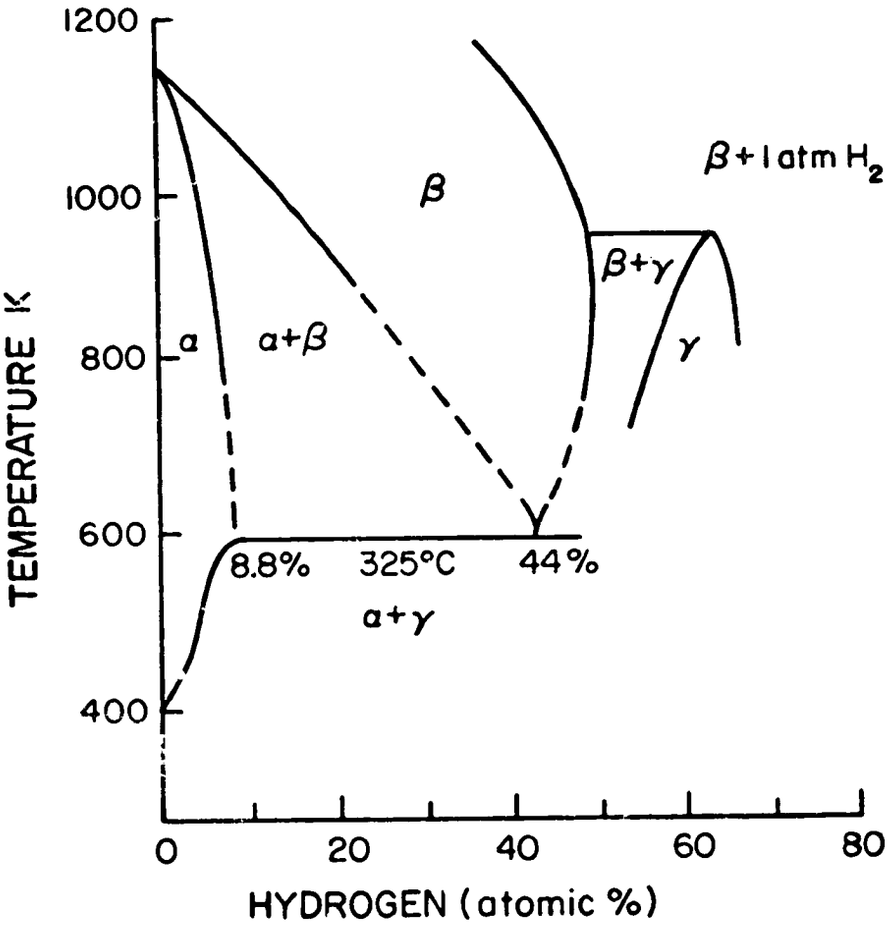

Fig. 36 - Titanium-hydrogen phase diagram (ref. 94).

Alloying elements change the hydrogen solubility markedly. Beta stabilizers, such as iron, vanadium, and molybdenum, stabilize the β phase at room temperature and, in turn, increase hydrogen solubility. Alpha stabilizers are aluminum, nitrogen and oxygen. Aluminum increases the hydrogen solubility in α titanium markedly at room temperature.[89] Paton, Hickman and Leslie[9] showed that at room temperature, hydrogen solubility was 21 ppm for pure titanium and the solubility increased to 250 ppm for Ti-10 at.% aluminum. In addition to the increase in hydrogen solubility they noticed that hydride nucleated and grew with difficulty in Ti-10 at.% aluminum. This finding supported the earlier claim by Boyd[91] that aluminum suppressed hydride precipitation. They explained that, along with hydride precipitation, there was a volume expansion, and that this expansion had to be taken up by the matrix through elastic and plastic work. The high strength of the titanium-aluminum alloy made elastic and plastic work more difficult, consequently a higher supersaturation was needed for nucleation and growth of the hydride phase.

The influence of oxygen and nitrogen on the solubility of hydrogen in pure titanium at temperatures below the eutectic point was investigated by Lenning, Spretnak and Jaffee.[92] To construct the solubility curve, they hydrogenated specimens were annealed at 673 K for 64 hours, cooled to the required temperature, held at this temperature for 24 hours, and then water quenched. These data show that neither oxygen nor nitrogen has an appreciable influence on the solubility of hydrogen in titanium at room temperature. However, above 651 K both of these elements increase somewhat the solubility of hydrogen in titanium.

Hydrogen present in titanium is in a state of dynamic equilibrium between the ionized atom or proton and hydrogen atoms in the interstitial site. There are two types of interstitial sites in titanium. As was mentioned before, octahedral sites could accommodate atoms of radius 0.59 Å and tetrahedral sites could accommodate atoms of radius 0.315 Å. Since the hydrogen atom has a radius of 0.41 Å, the majority of interstitial hydrogen atoms will occupy octahedral sites. Additions of aluminum decrease both the c and the a parameters of the hexagonal titanium lattice, consequently octahedral sites will be slightly smaller than 0.59 Å. A better fit of hydrogen atoms in octahedral sites will result and this could be the reason why aluminum increases the hydrogen solubility of the α phase. Beta phase has a tetrahedral hole of 0.44 Å radius in which hydrogen could fit very well. This is generally believed to be the reason why hydrogen solubility in the β phase is so much higher than in the α phase.

THE HYDRIDE PHASE

The γ phase, as previously mentioned, is the hydride phase and does not have a fixed composition. It exists over the range of TiH to $TiH_{1.99}$,[33-35] and several different crystal structures have been reported. In 1931, Hagg[33] determined, by x-ray diffraction, that the hydride phase had a FCC lattice with a = 4.397 Å at 50 at.% to a = 4.460 Å at 62.4 at.% hydrogen. Yakel,[35] using neutron diffraction, determined that hydride had a BCT (body-centered-tetragonal) lattice with a = 3.12 Å and c = 4.18 Å. Sidhu[36] reported that as the composition approached TiH_2, the FCC structure distorted into a FCT (face-centered-tetragonal) structure which was the same as BCT, depending on how the lattice was chosen. Yakel also reported that, as the temperature was increased above 310 K, the FCT structure changed to the FCC structure. A recent communication by Barraclough and Beevers[37] showed that at least three hydride phases existed in the zirconium-hydrogen system: FCT ($c/a > 1$) γ-phase existed up to $ZrH_{1.60}$, FCC δ-phase existed over $ZrH_{1.6}$ to $ZrH_{1.7}$ and ϵ-phase with FCT ($c/a < 1$) structure existed over $ZrH_{1.75}$ to ZrH_2. A similar arrangement of titanium-hydride could exist.

The orientation relationships between the α phase and the γ phase in Ti-8Al-1V-1Mo were determined by Boyd.[91] The hydrides observed were

all indexed as a FCC structure with a = 4.40 Å. Three different orientation relationships were found:

(1) $\{0001\}_\alpha \parallel \{001\}_\gamma$, $\langle 12\bar{1}0\rangle_\alpha \parallel \langle 110\rangle_\gamma$

(2) $\{0001\}_\alpha \parallel \{112\}_\gamma$, $\langle 12\bar{1}0\rangle_\alpha \parallel \langle 110\rangle_\gamma$

(3) $\{0001\}_\alpha \parallel \{110\}_\gamma$, $\langle 12\bar{1}0\rangle_\alpha \parallel \langle 110\rangle_\gamma$

Blackburn[98] and Sanderson and Scully[99] also determined the orientation relationship of titanium hydride. All of the hydrides analyzed by Blackburn had orientation (1), whereas Sanderson and Scully found examples of orientation of both (1) and (2). It was pointed out by Boyd that Blackburn and Scully had introduced hydrogen to their Ti-8Al-1V-1Mo alloy at room temperature by chemical polishing, whereas in Boyd's work the hydrogen was introduced at elevated temperature; therefore, more possible orientation relationships were observed.

The hydride habit planes determined by Boyd were all $\{10\bar{1}0\}$ planes. Liu et al.[98] found that hydride habit plane changed with the c/a ratio of titanium. They showed:

Material	c/a ratio	Habit planes
Ti and Ti-2%V	1.587	$10\bar{1}0$, $10\bar{1}1$
Ti-10%Zr	1.577	$10\bar{1}1$, $11\bar{2}2$
Ti-3%Ta	1.589	$10\bar{1}1$, $11\bar{2}2$, $11\bar{2}1$
Ti-3%Al	1.592	$10\bar{1}1$, $11\bar{2}2$, $10\bar{1}2$

In addition to spontaneous hydride, Boyd[41] observed strain induced hydride in the Ti-8Al-1V-1Mo alloy with as little as 200 ppm of hydrogen. Hydrogen solubility in Ti-8Al-1V-1Mo was determined to be 800 ppm. Over 800 ppm of hydrogen resulted in spontaneous hydride precipitation. As was mentioned earlier aluminum strengthened the titanium matrix, consequently hydride precipitation was suppressed. Therefore, with the help of plastic strain, hydride would precipitate. These strain induced hydrides were found to precipitate in active slip planes.

Hydride also exhibited stress orientation. Louthan[100] determined that hydride precipitation in titanium, supersaturated with hydrogen, occurred on the habit planes oriented most nearly perpendicular to the stress axis, probably a result from the volume expansion accompanying hydride precipitation. Hydride $TiH_{1.3}$ has a density of 3.912 gm/mm^3, compared to the density of pure titanium this is a 13% decrease. Therefore, the most favorable habit planes would be those oriented such that the volume expansion of the plate-like hydride would act to relieve some of the tensile stress in the lattice.[100]

DIFFUSION OF HYDROGEN

Diffusivity of hydrogen in pure titanium has been investigated by several researchers.[101,102] The diffusion coefficients obtained by Wasilewski and Kehl seems to be most accurate. The expressions for the diffusion coefficients are,

$$D_\alpha = 1.8 \times 10^{-2} \exp\left(\frac{-12.380 \pm 680 \text{ cal/mole}}{RT}\right) \quad (16)$$

$$D_\alpha = 1.95 \times 10^{-3} \exp\left(\frac{-6.640 \pm 500 \text{ cal/mole}}{RT}\right) \quad (17)$$

Williams, Koehl and Bartlett[103] showed that a small amount of oxygen in hydrogen gas at atmospheric pressure and room temperature could effectively slow the reaction between hydrogen and titanium. A thin oxide layer which has been known to stop hydrogen absorption probably formed on the surface. Interstitial hydrogen is thought to diffuse to the point of maximum triaxiality such as the tip of a crack or notch. Experimental evidence to support this theory has yet to be found. This is, of course, the basis for many theories which hold that hydrogen is responsible for stress corrosion cracking.

HYDROGEN EMBRITTLEMENT

Hydrogen embrittlement is now accepted as a general phenomenon resulting from the interaction of hydrogen and the metal. Metals are affected by different kinds of hydrogen embrittlement depending on the different characters of their interaction with hydrogen and the different natures of phases formed as the result of this interaction. Numerous researchers have devoted their time in studying and analyzing hydrogen embrittlement.[105-111] A complete and logical classification was presented by Livanov et al.[106] According to their classification there exist two types of hydrogen embrittlement:

(1) Embrittlement originating from sources existing in the metal as a result of high hydrogen content before strain is applied.

(2) Embrittlement originating from sources developing in the metal with increases in hydrogen content in the course of plastic deformation.

The first type of embrittlement increases with increasing strain rate and is an irreversible phenomenon by its nature. It may be due to the following causes:

(a) gas products formed in the metal by reaction of hydrogen with impurities or alloying elements,
(b) molecular hydrogen in voids and cavities under high pressure,
(c) hydride precipitation, and
(d) distortion of the crystal lattice by interstitial hydrogen atoms.

The second type of hydrogen embrittlement is developed in a specific strain rate range. It may be due to:

(a) Precipitation from supersaturated solid solution in respect to the prolonged action of static load or in the process of deformation with low strain rate.
(b) Hydrogen atom transportation by moving dislocations to the tip of piled up dislocations.
(c) Directed diffusion of hydrogen atoms in uneven elastic and thermal stress fields or in electrical fields.

The hydrogen embrittlement of titanium and its alloys is believed to be type (1)(c) and (2)(a). Alpha titanium has very limited hydrogen solubility. Hydride plates are found quite commonly in pure titanium. This hydride phase, although it has some ductility,[113] is a much more brittle phase than the α titanium matrix.

Type (1)(c) embrittlement--impact embrittlement--is found primarily in α titanium. Lenning et al.[32] showed that the presence of hydride was directly related to the loss of impact ductility. The addition of 5 wt% aluminum increased the room temperature hydrogen solubility limit in α titanium to greater than 180 ppm. This increase in hydrogen solubility decreased the sensitivity of the alloy to hydrogen embrittlement down to testing temperature as low as 77 K. Hydrogen in solid solution, in both the titanium-5 wt.% aluminum-0.2 wt.% oxygen and titanium-5 wt.% aluminum alloys, increased the tensile properties mildly but did not decrease the ductility or toughness significantly. Westlake[115] has also shown that zirconium hydride was a brittle phase and that the zirconium matrix saturated with hydrogen appeared to be very ductile. Rylski[114] showed that the presence of hydride in α titanium caused a reduction of both percent elongation and reduction in area of impact tensile tests as shown in Fig. 37. This reduction was much more severe in the presence of a notch.[114] Type (2)(a) embrittlement--slow strain rate embrittlement--was found mostly in α-β titanium alloys. Supersaturation of hydrogen can be achieved by quenching titanium alloys of higher strength levels, such as Ti-5Al, Ti-5Al-2.5Sn, Ti-6Al-4V etc., since the higher strengths of these materials suppress hydride precipitation. When alloys are in a supersaturated state with respect to hydrogen and all of the hydrogen is retained in solution, high strain rate embrittlement was not observed, but low rates of deformation resulted in precipitation of hydrides and low strain rate embrittlement was observed. Embrittlement of the latter kind may be developed under static loading.

In the case where the titanium matrix is supersaturated with hydrogen and some hydride has precipitated, both impact embrittlement and slow strain rate embrittlement will be observed.

Livanov et al.[116] suggested that some titanium alloys could be embrittled by the mechanism of distortion of the crystal lattice by interstitial hydrogen, type (1)(d) and by the mechanism of hydrogen interact with dislocations, type (2)(b).

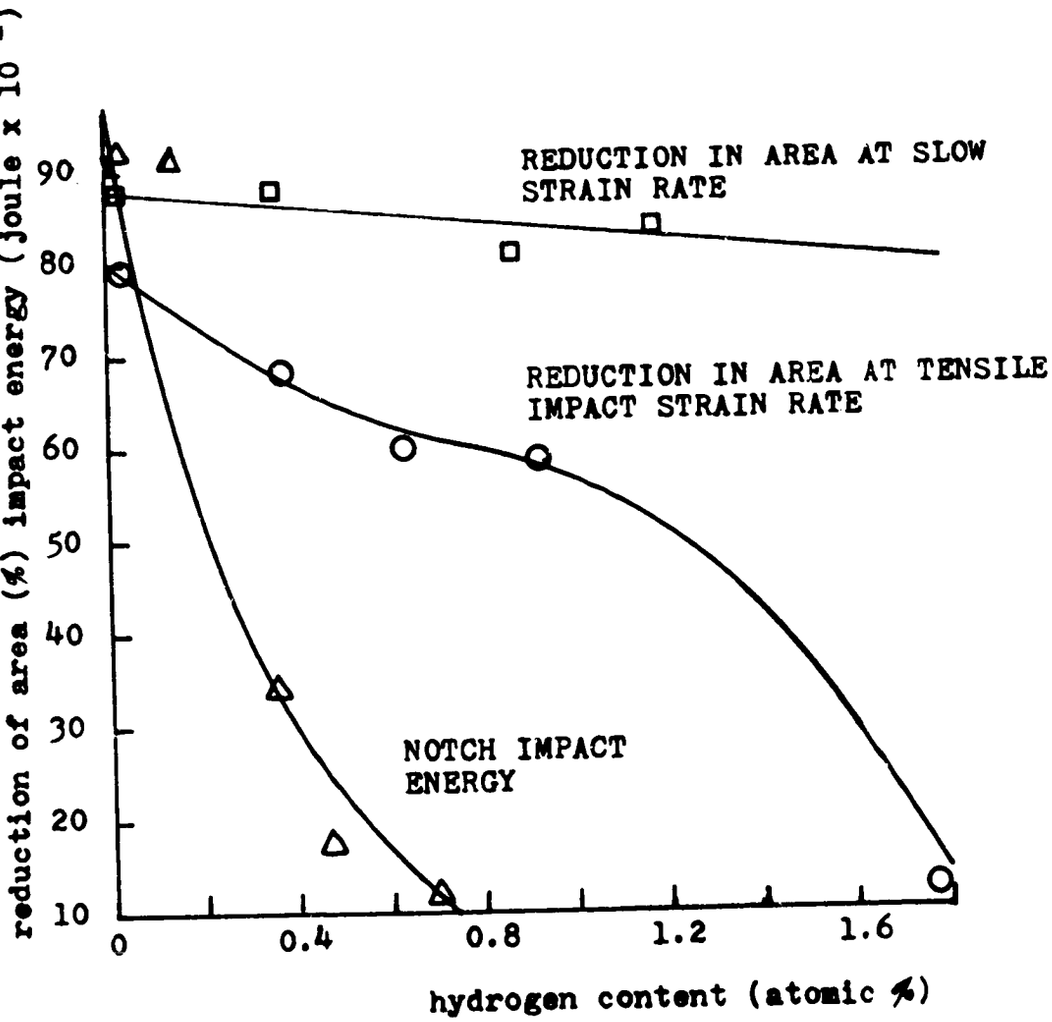

Fig. 37 - The loss of ductility with increasing hydrogen content in pure titanium under different testing conditions (ref. 114)

Evidence of hydride blocking plastic deformation in zirconium was presented by Westlake.[113] Cracks were found in hydride at the point where twins intersected the hydride. These cracks were observed to propagate into the zirconium matrix, but did not propagate catastrophically. Cracks were also found in hydride where slip intersected the hydride. Crystals, which were deformed by slip alone, required considerably more total deformation to initiate cracks in hydride plates. Others have also noticed the importance of twinning. Lenning stated that hydrogen embrittlement became most severe below 373 K, compared with the observed increase in the amount of twinning deformation below this temperature; he suggested that the effect of twinning on embrittlement might be more significant than the effect of slip on embrittlement.

A new model for hydrogen assisted cracking was presented by Beachem.[114] His model suggests that the presence of sufficiently concentrated hydrogen dissolved in the lattice just ahead of the crack tip aids whatever deformation processes the microstructure will permit. This model suggests that instead of hydrogen locking dislocations in place, it unlocks them and allows them to multiply or move at reduced stresses. This new theory does not contradict any hydride embrittlement theory, but it adds a new possible mechanism to titanium hydrogen embrittlement theories. It adds the possibility that hydrogen in solution alone could develop fracture at considerably lower stresses. This is particularly possible for α-β titanium alloys which tolerate considerable hydrogen in solution before hydride precipitation.

STRESS CORROSION CRACKING

An extensive review of stress corrosion cracking of titanium alloys was presented by Owen, Beck and Fontana.[115] Their work will be described later with results of the present study on hydrogen embrittlement as the mechanism for stress corrosion cracking.

Corrosion produced hydrogen has long been suspected as the embrittling species in many stress corrosion systems. However, until recently, there have not been quantitative analytical techniques capable of determining hydrogen concentrations on a microscopic scale. An ion microprobe and a laser microprobe were used for the first time by Gray[116] to measure the concentration of corrosion produced hydrogen on a microscopic scale. Ti-8Al-1V-1Mo alloy specimens with known hydrogen concentrations were subjected to hot salt stress corrosion cracking and then analyzed in stepped intervals below stress corrosion fracture surfaces for hydrogen content. Concentrations of several thousand ppm of hydrogen were measured.

An extensive series of experiments on the stress corrosion cracking of titanium in methonal/HCl environment were performed by Spurrier and Scully.[117] Their experiments consisted of initiating intergranular cracks in a methonal/HCl environment, and then breaking the specimens in air after washing the methonal solution from the crack. Fractographs

of these specimens showed that a narrow intermediate zone existed between the intergranular stress corrosion crack and the high energy dimple fracture region (caused by fracture in air). This intermediate zone consisted of a very narrow zone resembling, in appearance, a cleavage fracture immediately next to the intergranular stress corrosion fracture, and a wider straited region. A series of tests were then performed to show that the intermediate zone was caused by the absorption of an embrittling species from the solution. The embrittling species had diffused in front of the crack tip before being removed from the methonol HCl environment. They stated "The cleavage crack, once initiated in such tests on α-titanium alloys, may propagate outside the zone enriched in hydrogen for purely mechanical reasons until it is arrested by plastic relaxation--a process that results in the appearance of striations." Therefore, it is not necessary for hydrogen to diffuse into the lattice to much greater depth than the immediate depth at the crack tip to cause extensive fracture. This finding explained the discrepancy between the rate of hydrogen diffusion and the observed rate of crack propagation. Their work also clearly showed that an absorbed embrittling element was the cause for transgranular cracking.

A comparison between hydrogen embrittlement cracking and stress corrosion cracking of titanium-aluminum alloys was made by Hochman et al.[13] Orientations of brittle fracture facets were determined for both hydrogen embrittled cracks and stress corroded cracks. All fracture planes determined were found to be oriented within about 12 ± 3° of the basal plane near the $\langle \bar{1}2\bar{1}0 \rangle$ zone. The similarity of hydrogen embrittled fracture and stress corrosion fracture strongly supported the contention that hydrogen played a significant role in the stress corrosion cracking of titanium-aluminum alloys.

DISLOCATIONS IN α-TITANIUM

Figure 30 shows all the possible Burgers vectors in α titanium. The glissile dislocations are:

(A) Perfect dislocations

		Burgers vector	Glide plane
DF	a	$1/3\ 11\bar{2}0\rangle$	$\{0001\}$, $\{10\bar{1}0\}$, $\{10\bar{1}1\}$
ST	c	$\langle 0001 \rangle$	$\{10\bar{1}0\}$
SD/TF	c + a	$1/3\langle 11\bar{2}3\rangle$	$\{10\bar{1}1\}$

(B) Partial dislocations

	Burgers vector	Glide plane
Di	$1/3\langle 10\bar{1}0\rangle$	$\{0001\}$

The c/a ratio of hexagonal metals has a profound effect on dislocation structures. Cadmium (c/a = 1.886) and zinc (c/a = 1.856) have $\{0001\}\ 1/3\langle 11\bar{2}0\rangle$ slip systems as the most frequently observed slip. In these two metals the stacking fault energy on the basal plane was estimated to be less than 30 erg/cm^2.[120] Dislocations of Burgers vector $1/3\langle 11\bar{2}0\rangle$ were observed to dissociate into two partial dislocations with Burgers vector $1/3\langle 10\bar{1}0\rangle$. The two partial dislocations were connected by a stacking fault ribbon. Partial dislocations can not cross slip to other slip planes; therefore, HCP metals with low stacking fault energies will have their dislocations restricted to the basal plane.

Titanium has a c/a ratio of 1.587 and its stacking fault energy was estimated to be 300 erg/cm^2.[68] Cross slip from the basal plane to other slip planes were quite evident for the Ti-9Al alloy.[121] This observation suggests that $1/3\langle 11\bar{2}0\rangle$ dislocations do not dissociate on the basal plane. The fact that extended dislocations have not been found--using transmission electron microscopy--supports this claim.

The most frequently observed dislocations in titanium are $1/3\langle 11\bar{2}0\rangle$ dislocations. Backofen et al.[72] showed that the c + a type of dislocation became more important at temperatures above 673 K. They also showed that the c + a type of dislocation could dissociate into c and a dislocations. At room temperature these c + a dislocations were primarily associated with $\{11\bar{2}2\}$ twinning.

Blackburn[68] compared the dislocation arrangements of commercial purity titanium and Ti-9Al alloys after about 5% strain. An irregular cell structure was observed with an average size of about 0.7 μm for commercial purity titanium. The Ti-9Al alloy exhibits a much more regular dislocation arrangement with the dislocations occurring in well-defined slip planes which were established as $\{10\bar{1}0\}$ by trace analysis. After deformation the Ti-8Al-1Mo-1V alloy had dislocation arrangements similar to the Ti-9Al alloys. It appeared that additions of aluminum to titanium caused the $\{10\bar{1}0\}$ planes to become the preferred slip planes.

EXPERIMENTAL PROCEDURES

MATERIAL PREPARATION

Two purities of titanium were used in this study. High purity titanium single crystals with a Vickers hardness of 88, purchased from Material Research Corporation, were used in part of the work. Single crystals with a Vickers hardness of 120 were prepared in the OSU laboratory from commercial purity titanium.

The single crystal preparation method of Cass, Quinn and Spencer[122] was employed in this investigation. Growth of hexagonal titanium single

crystals is complicated by the α-β transformation at 1153 K on cooling. If the Burgers relationship is obeyed exactly, i.e., $(0001)_\alpha \parallel (110)_\beta$, $[11\bar{2}0]_\alpha \parallel [111]_\beta$, there are 12 variants that may be formed from any β grain. In fact, this relationship was obeyed. Nevertheless, titanium single crystals can be grown from the melt if α polycrystals do not result from the β-α transformation. The method of Cass et al. employed an electron beam zone refiner operated at a relatively rapid scan rate. This arrangement promoted a planar transformation interface by impressing uniaxial heat flow down the rod axis. If multiple variants are not nucleated during the passage of the interface a hexagonal single crystal is obtained.

The starting material was 7.94 mm diameter commercially pure titanium; the chance of success increases with higher purity titanium. Thus, the surface material containing high oxygen and nitrogen content has been removed to yield a bar of 6.35 mm diameter. The entire set-up is shown in Fig. 38. An ac current was used to heat the tungsten filament and a dc voltage of about 2 kV was applied between the filament and the titanium rod. Two rods, separated by 2 mm, were mounted vertically in the scanner. The gap guarded against sideways deflection due to the thermal expansion which occurred, as would be the case for a single length of rod. Growth runs were started at a vacuum of 1.33×10^{-4} N/m (10^{-6} torr). Ultimate pressures obtained during growth were within a factor of 5 or less.

To start a run, the zone was brought slowly to the melting temperature and the power was adjusted until a stable molten zone was established. The tip of the upper rod was melted first so that a concave zone could be produced. The concavity of the molten zone could then be adjusted by manually moving the scanner up or down. Attainment of zone stability was important because subsequent power adjustments made during the pass would affect the β-α transformation, which would, in turn, result in polycrystal formation. When the molten zone was sufficiently stable, the filament was moved upward at about 2.5 cm per hour.

The vacuum system was simply a glass bell jar with an O-ring seal placed on a stainless base plate. The progress could be observed from outside the bell jar. A boundary separating the β and the α phase could be observed. In general, β single crystals resulted from the melt, but α polycrystals often formed after the boundary had passed. This was believed to occur because titanium vapor containing oxygen and nitrogen deposited back onto the surface, forming nuclei for new α crystals. Thus, a cylindrical protective shielding was positioned approximately 4 mm from the rod extending from the melt-β interface to below the α-β interface. The addition of this shielding greatly improved the yield of single crystals.

The required zone stability, which is very important, was not achieved through the use of the single turn tungsten filament. As shown in Fig. 38, the gap existing in the filament often resulted in a curved melt-solid interface. No single crystals formed under this

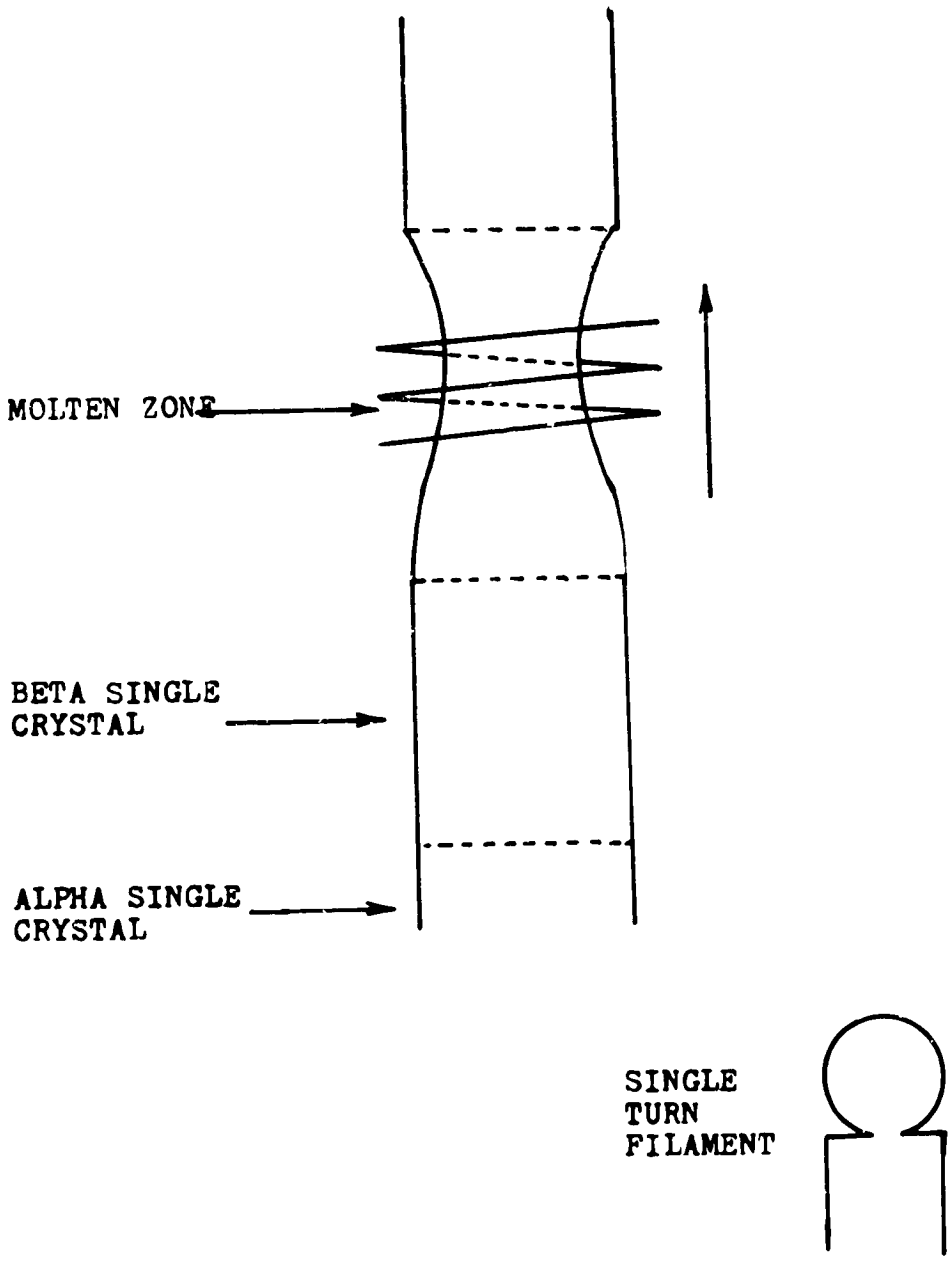

Fig. 38 - Single crystal growth

condition. Upon changing to a three-turn filament, a more uniform heating, as compared to a single-turn filament, was attained and the stability of the melt zone was improved.

Both the width and the concavity of the zone were important factors in controlling the stability of the molten zone. The concavity should be such that the tangent of the melt surface, at the bottom melt-solid interface, is vertical as shown in Fig. 38, otherwise the grown rod would either become bigger or smaller. The width of the zone should be stable with the heat input. This could best be achieved by very slowly increasing the power until a stable condition is reached.

The yield was relatively low compared with Cass et al.,[122] who used high purity titanium as starting material. Three 4-cm single crystal sections were obtained out of 1.5 m of original rod.

The crystals grown had their axes about 70° from the [0001] direction with one exception, which had [0001] as its axis. This growth mode with the basal plane containing the growth direction is a common one for pure HCP crystals and is presumably related to the anisotropy of thermal conductivity. That is, the crystal orientation that can most effectively conduct the heat from the transformation interface will be favored.

Cass et al.[122] indicated that with a relatively fast scan rate there was no redistribution of the solute atom. Post-growth chemical analysis of Ti-4Al crystals showed that aluminum was uniformly distributed longitudinally.

Finally, single crystal sections were cut from the rod, the sections were vacuum sealed in a quartz capsule and were annealed at 1080 K for 24 hours to remove any remaining small crystals and to remove any possible nonuniformity in composition. The vacuum was better than 1.3×10^{-5} N/m^2 (10^{-7} torr) before sealing the capsule. The impurity content of the materials used in this study are listed in Table XVIII. Hereafter the purchased crystal will be referred to as the high purity crystal and the laboratory prepared crystal will be referred to as the commerical purity crystal.

Table XVIII - Impurity Content of the Material Used in This Study

	C (ppm)	O (ppm)	N (ppm)	H (ppm)
High Purity Crystal	40	60	35	< 0.1
Commercial Purity Crystal	150	665	51	2

SPECIMEN PREPARATION

All single crystal specimen preparation was done using a spark cutter manufactured by Metal Research Group Corporation. The spark cutter was also equipped with a planing device which consisted of a rotating wheel for sparking away the specimen surface. The specimen is positioned on a planing table during the sparking (see Fig. 39). A procedure provided by the manufacturer ensures that the table top and the wheel surface are parallel. The manufacturer claims the accuracy of planing a flat surface to be better than $\pm$ 0.0002 mm/cm ; therefore, it is an excellent device for preparing parallel surfaces. During the cutting and planing, the crystal was immersed in kerosene, which is used as a dielectric. The temperature of the kerosene was kept constantly at about 303 K during the operation. There are seven power ranges on the spark cutter, the smaller the range the finer the finished surface. The finest finished surface, using the smallest range, was actually comparable to a surface prepared for metallography.

The crystal was first mounted on a goniometer and the orientation of the crystal determined by the Laue x-ray back-reflection method. With the proper maneuvering of the goniometer, the top and bottom surfaces of a cubic specimen can be cut with a predetermined orientation. After the top and bottom surfaces were prepared, the other four surfaces were carefully planed. The final cube specimens measured about 4.76 mm with all surfaces having the finest finish.

The top surface of the cube was checked for hardness with a microhardness tester. This served also to identify individual crystal load axes and to check any variation in hardness or contamination by oxygen. The Vickers hardness indentor with 3 kg load was used for this purpose. Results showed that the high purity purchased crystals had a Vickers hardness of 88 and that the laboratory produced crystals had a Vickers hardness of 120. There was very little variation among crystals of the same loading axis.

HYDROGENATION

Hydrogenation was done by gaseous charging at elevated temperatures. The specimens were first degreased with acetone and were handled with instruments only thereafter. After weighing, the specimens were placed in quartz capsules with a narrow opening. The volume of the capsule was then measured by injecting acetone into the narrow opening. These capsules were then connected to a vacuum system, evacuated to better than $1.3 \times 10^{-}$ N/m (10^{-} torr), back filled with predetermined pressures of hydrogen and sealed. Hydrogen pressure was measured by an α-tron gauge. The apparatus is shown in Fig. 40. Purified hydrogen of 99.95% purity and less than 20 ppm oxygen was used. This gas was further purified by passing it through a liquid nitrogen cold trap before back filling the capsules. The sealed capsules were then heated at 1080 K for one hour to allow for hydrogen absorption; the rate of absorption

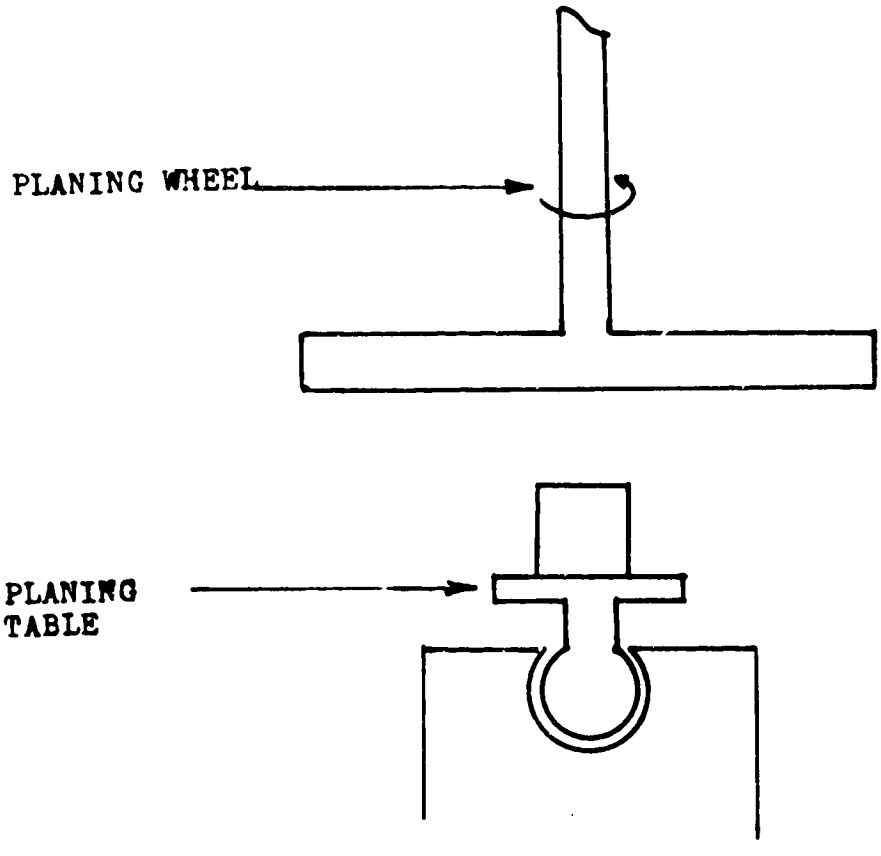

Fig. 39 - Planing setup. The movement of the planing wheel is controlled electronically, the progress of planing is monitored by a micrometer attached to the unit.

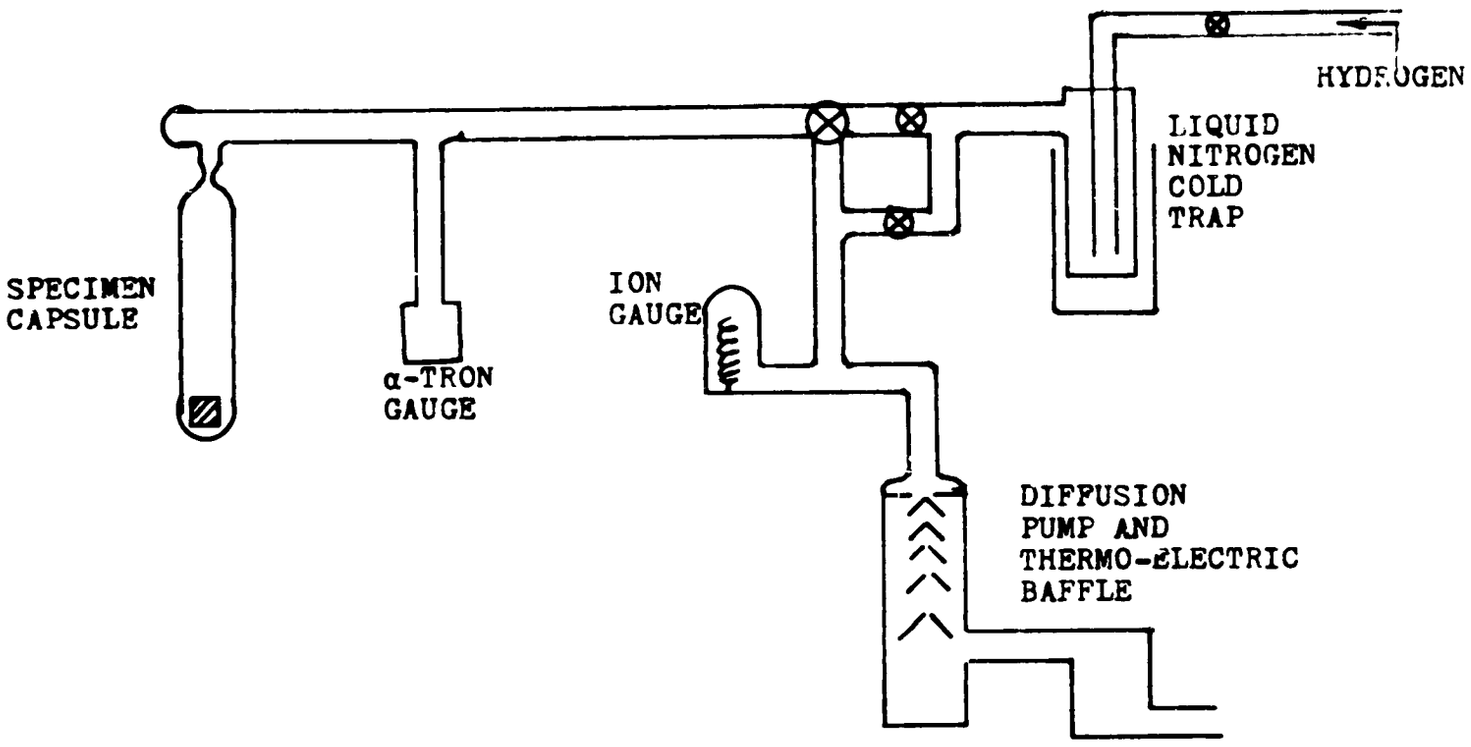

Fig. 40 - Hydrogenation apparatus

is very fast at 1080 K. Lenning et al.[87] used similar hydrogenation method and estimated the time required for complete absorption for the 17 mm diameter specimens at the pressure of 1.33×10^{2}-1.33×10^{3} N/m^2 (1-10 torr) to be about 15-30 minutes. After the gas was absorbed the specimens were furnace cooled to 980 K and were maintained at that temperature for one hour to homogenize hydrogen in the specimens. Specimens were furnace cooled to room temperature after homogenization.

Two specimens were checked for oxygen and nitrogen analyses. One specimen was subjected to the above treatment except no hydrogen was charged, the other specimen was not subjected to the above treatment. Results showed that there was approximately 3 ppm oxygen and nitrogen pick-up during the hydrogenation treatment. Statler,[123] using the same hydrogenation method, showed that accurate predetermined hydrogen concentrations could be achieved by this method (less than 5% error). After hydrogenation the precise orientation of all specimens were rechecked by the Laue back reflection method. The orientations were never more than 3° from the predetermined orientations.

COMPRESSION TEST

The top and bottom surfaces of the specimens were again planed after hydrogenation in preparation for the compression tests employing the Instron machine. A compression load with an accuracy of 1% of the full scale was used. The load cell was calibrated before each use. A crosshead speed of 0.005 cm/min, corresponding to a strain rate of 1% per minute was used. No lubricant was applied between the specimen and the compression anvil. Little barrelling was observed with or without lubricant. Load-displacement curves were recorded electronically on a strip chart recorder. Yield stresses and work hardening rates were calculated from these curves.

The design of the load cell used in this work did not allow for self-aligning of the compression table. However a self-aligning type of table which did not have the load capacity for the specimens in the present work was used on scaled-down specimens (1/4 size) to check the possible error introduced because of this lack of self-aligning capability. The scaled-down specimen was first compressed beyond yielding using the load cell with the self-aligning table, and then compressed further using the load cell with the fixed table to determine whether yielding would continuing at the same load. The result of this checking showed that yielding did occur at the same load. Thus, it is not expected that the non-self-aligning machine introduced any significant error.

Before starting the compression tests, two surfaces of each specimen, not top or bottom, were electropolished. These surfaces were examined carefully by optical microscopy for evidence of hydride precipitation and also for surface markings, all of which were recorded. After the compression test, these surfaces were again examined and the

angles between the edge of the top surface and twin planes and slip traces were recorded. Information obtained from the surfaces of the compressed crystal was plotted on the stereographic projection of each crystal and the twin and slip systems were identified.

HYDRIDE DETERMINATION

The room temperature hydrogen solubility was stated earlier to be about 21 ppm. It was thought that hydrogen solubility of single crystals might be higher because of the lack of grain boundaries for the nucleation of hydride. Thus, five crystals charged with 20, 50, 100, 150 and 200 ppm were examined for hydride.

Specimens were mounted and electropolished. The hydride phase, when present, was slightly elevated from the titanium matrix, therefore, merely adjusting the aperture diaphragm, which enhanced the contrast, would show the hydride phase. Hydride phase could also be seen using polarized light without etching the specimen. In general, hydrides were brighter than the matrix under polarized light. Etching was avoided because past experiences have shown that hydride needles form easily during etching. An interesting observation on the electropolished specimens were parallel lines of pits. The orientation of these lines on stereographic projections of the crystals showed that they followed the trace of one of the $\{10\bar{1}0\}$ planes intersecting the surface. Why they followed one of the $\{10\bar{1}0\}$ planes and not the other was not clear. A scanning electron micrograph of these pits is shown in Fig. 41.

FOIL PREPARATION

After the compression test, specimens were sliced with a diamond wafering blade into 0.5 mm thick slices for electropolishing to produce transmission electron microscopy foil. The electrolyte used was a mixture of 390 cc methyl alcohol, 350 cc 1-butanol, and 60 cc perchloric acid which was maintained at 243 K in a bath of dry ice in methonal. The polishing technique was the commonly phrased jet technique which employs two jet streams of electrolyte propelled by a small motor. The jets constantly wash the specimen surface. A voltage of about 28 volts was used.

Transmission electron microscopy studies were done using a Philips 300 electron microscope. All examinations were conducted at an accelerating voltage of 100 kV.

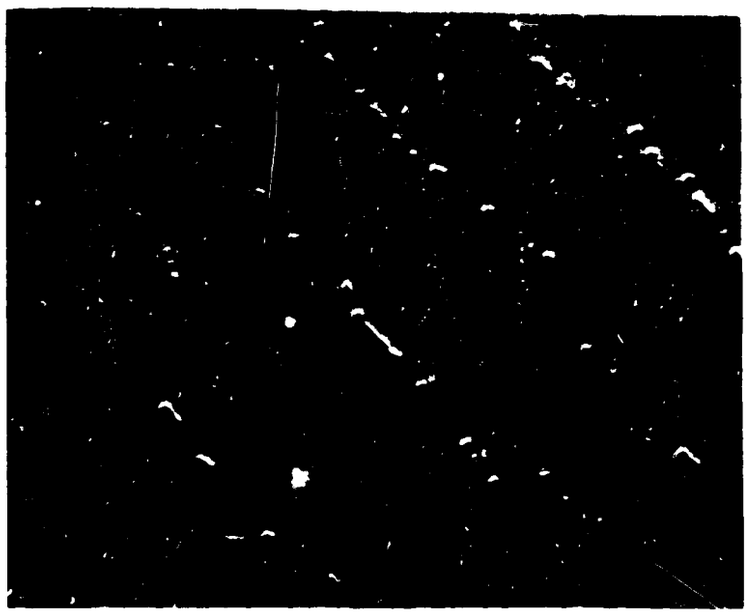

Fig. [illegible] - [illegible] of an electron micrograph of a [illegible] vinylidene chloride crystal. 100X

RESULTS

HYDROGEN SOLUBILITY

Specimens of commercial purity charged to 20, 50, 100, 200 ppm of hydrogen were examined for evidence of hydride and those with 50 ppm or more of hydrogen were found to contain hydride plates. Figure 42 shows hydride in a specimen containing 50 ppm of hydrogen. Figure 43 shows the absence of hydride plates in a specimen containing 20 ppm of hydrogen. The hydride plates in the specimen containing 50 ppm of hydrogen precipitated on two habit planes which were identified as the $\{10\bar{1}0\}$ and the $\{10\bar{1}1\}$ planes. High purity single crystals, containing 20 and 50 ppm of hydrogen, were also examined by the same technique. The difference in oxygen and nitrogen contents of the two purities of single crystals did not seem to affect either the hydrogen solubility or hydride habit planes.

Compression tests revealed the effects of hydrogen solubility. The nominal work hardening rates of specimens 5 to 12 are shown in Table XIX. The work hardening rates of commercial purity specimens 5, 7, 8, and 9, containing less than 20 ppm hydrogen, are about 906 MN/m^2; whereas, the work hardening rate of specimen 6, containing 22 ppm hydrogen, is 1357.3 MN/m^2. All of these specimens have the same orientation with respect to the loading axis, the only difference is hydrogen content. High purity specimens 10, 11 and 12 also show the same tendency. The work hardening rate of specimen 12 containing 20 ppm hydrogen is 1202.46 MN/m^2; whereas, specimens 10 and 11, containing less than 20 ppm hydrogen, have a work hardening rate of about 1045.7 MN/m^2. The higher work hardening rates of specimens containing more than 20 ppm of hydrogen can only be explained on the basis of the precipitation of very fine hydride particles during cooling. Hydride particles would block dislocations and cause the observed higher work hardening rate. Based on these data hydrogen solubility in pure titanium at room temperature is slightly less than 20 ppm.

Table XIX - Critical Resolved Shear Stress and Nominal Work Hardening Rate of the $\{10\bar{1}0\}1/3\langle 11\bar{2}0\rangle$ Slip System

Specimen	(O + N) (ppm)	H (ppm)	Critical Resolved Shear Stress (MN/m^2)	Nominal Work Hardening Rate (MN/m^2)
5	706	2	42.6	895.7
7	706	7	46.3	909.4
8	706	11	49.5	907.5
9	706	17	49.6	923.1
6	706	22	52.5	1357.3
10	95	< 0.1	13.4	1069.2
11	95	12	15.4	1033.9
12	95	20	17.7	1202.5

Fig. 42 - Hydride needles in a crystal containing 50 ppm of hydrogen. 1530X

Fig. 43 - Crystal containing 20 ppm of hydrogen 1530X

SLIP

Twelve specimens were prepared for the determination of the critical resolved shear stress of slip systems. Specimens 5 to 12 were for the study of the $\{10\bar{1}0\}1/3\langle 11\bar{2}0\rangle$ slip system. The loading axes were approximately halfway between the $[10\bar{1}0]$ and $[11\bar{2}0]$ poles. In this position the Schmid's factor is about 0.5 for one of the $\{10\bar{1}0\}1/3\langle 11\bar{2}0\rangle$ slip systems. Specimens 13 and 14 were prepared for study of the $\{0001\}1/3\langle 11\bar{2}0\rangle$ slip system. The loading axes for these specimens were halfway between the [0001] and $[11\bar{2}0]$ poles. Specimens 15 to 16 were prepared for study of the $\{10\bar{1}1\}1/3\langle 11\bar{2}0\rangle$ slip system. All the loading axes of these specimens are shown in Fig. 44, and in all cases they have a Schmid's factor of about 0.5 for the intended slip systems.

Critical resolved shear stresses were calculated from the load at 0.002 plastic strain. Results are shown in Tables XIX and XX which show that there is an increase in the critical resolved shear stress of the $\{10\bar{1}0\}1/3\langle 11\bar{2}0\rangle$ slip system with increasing hydrogen content from 2 to 22 ppm. Oxygen and nitrogen also increased the critical resolved shear stress for $\{10\bar{1}0\}1/3\langle 11\bar{2}0\rangle$ slip.

The crystallography of titanium is such that the $\{10\bar{1}0\}$ and $\{10\bar{1}1\}$ planes are very close to each other. The orientation of crystals prepared for the $\{10\bar{1}1\}1/3\langle 11\bar{2}0\rangle$ slip studies is such that it has a Schmid factor of 0.5 for the $\{10\bar{1}1\}1/3\langle 11\bar{2}0\rangle$ slip system and a Schmid factor of 0.424 for $\{10\bar{1}0\}1/3\langle 11\bar{2}0\rangle$ slip system; therefore, unless the ratio of the critical resolved shear stress for the $\{10\bar{1}1\}1/3\langle 11\bar{2}0\rangle$ slip system to the critical resolved shear stress for the $\{10\bar{1}0\}1/3\langle 11\bar{2}0\rangle$ slip system is less than 0.424/0.5, the $\{10\bar{1}1\}1/3\langle 11\bar{2}0\rangle$ slip system will not operate. This is what happened to specimens 15 and 16. After compression testing, the slip trace analysis showed that the $\{10\bar{1}0\}1/3\langle 11\bar{2}0\rangle$ slip system operated in preference to the $\{10\bar{1}1\}1/3\langle 11\bar{2}0\rangle$ slip system. Therefore, the critical resolved shear stress for $\{10\bar{1}1\}1/3\langle 11\bar{2}0\rangle$ slip is greater than 0.424/0.5 times the critical resolved shear stress for $\{10\bar{1}0\}1/3\langle 11\bar{2}0\rangle$ slip. The small amount of hydrogen in specimen 16 apparently did not raise the critical resolved shear stress of the $\{10\bar{1}0\}1/3\langle 11\bar{2}0\rangle$ slip system enough to enable the $\{10\bar{1}1\}1/3\langle 11\bar{2}0\rangle$ slip system to operate.

Specimen 13 and 14 are oriented for $\{0001\}1/3\langle 11\bar{2}0\rangle$ slip. Basal slip did not occur in specimen 13 but was observed in specimen 14. Examination of the surfaces of specimen 14 showed slip steps following the traces of $\{10\bar{1}0\}$ and $\{0001\}$ planes. The appearance of $\{0001\}1/3\langle 11\bar{2}0\rangle$ slip steps were quite different from $\{10\bar{1}0\}1/3\langle 11\bar{2}0\rangle$ slip steps as shown in Fig. 45. $\{10\bar{1}0\}1/3\langle 11\bar{2}0\rangle$ slip steps are fine, much more dense and straight; whereas, $\{0001\}1/3\langle 11\bar{2}0\rangle$ slip steps are coarse, discrete and wavy. In specimen 14, the Schmid's factor for $\{10\bar{1}0\}1/3\langle 11\bar{2}0\rangle$ slip was 0.187 and the Schmid's factor for $\{0001\}1/3\langle 11\bar{2}0\rangle$ slip was 0.5; therefore, the critical resolved shear stress for the $\{0001\}1/3\langle 11\bar{2}0\rangle$ slip system should be 0.5/0.187 times the critical resolved shear stress of the $\{10\bar{1}0\}1/3\langle 11\bar{2}0\rangle$ slip system.

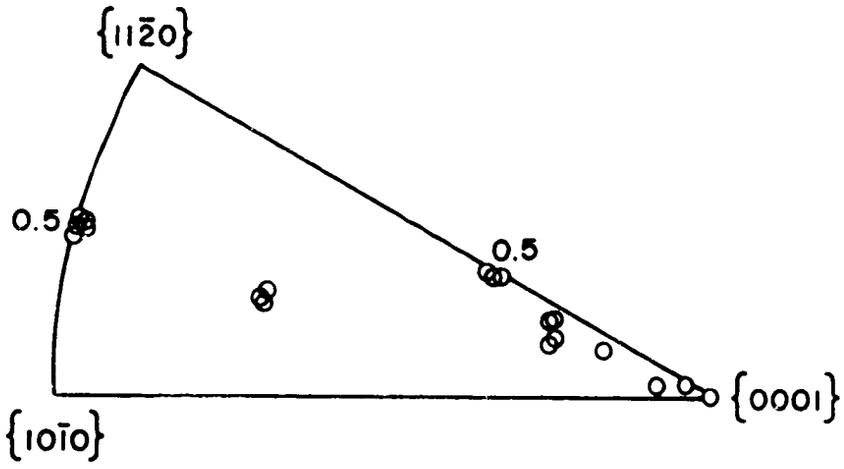

Fig. 44 - The orientations of loading axes of single crystal specimens.

Table XX - Results of the {0001}1/3⟨11$\bar{2}$0⟩ and the {10$\bar{1}$1}1/3⟨11$\bar{2}$0⟩ Slip System Study

Specimen	(O + N) (ppm)	H (ppm)	Intended Slip Plane	Observed Slip Plane	CRSS (MN/m^2)
13	95	< 0.1	0001	10$\bar{1}$0	14.7
14	95	15	0001	10$\bar{1}$0 0001	--
15	95	< 0.1	10$\bar{1}$1	10$\bar{1}$0	13.5
16	95	13	10$\bar{1}$1	10$\bar{1}$0	15.4

Fig. 49 - Prismatic slip steps (vertical); basal slip steps (horizontal) 130X

Specimen 13 had the same orientation as specimen 14, and yet the $\{0001\}1/3\langle 11\bar{2}0\rangle$ slip system did not operate in the specimen. This strongly suggests that the effect of the hydrogen atom in solution is not uniform to all three slip systems. Hydrogen seems to increase the critical resolved shear stress for the $\{10\bar{1}0\}1/3\langle 11\bar{2}0\rangle$ slip system more than for the $\{0001\}1/3\langle 11\bar{2}0\rangle$ slip system. Thirteen ppm of hydrogen in titanium apparently had decreased the ratio of the critical resolved shear stress of the $\{0001\}1/3\langle 11\bar{2}0\rangle$ slip system to the critical resolved shear stress of the $\{10\bar{1}0\}1/3\langle 11\bar{2}0\rangle$ slip system to less than 0.5/0.187.

A comparison between specimens 5-9 and specimens 10-12 reveals the effect of oxygen and nitrogen. The combined oxygen and nitrogen content is 700 ppm for commercial purity titanium crystals and 100 ppm for the high purity titanium crystal. The increase in oxygen and nitrogen not only increases the CRSS for the $\{10\bar{1}0\}1/3\langle 11\bar{2}0\rangle$ slip system, but also slightly decreased the work hardening rate of the $\{10\bar{1}0\}1/3\langle 11\bar{2}0\rangle$ slip system.

TWINNING

Specimens 1-4 and 17, 18 were prepared for twinning studies. They all have load axes 20-25° from the [0001] pole. The load-displacement curves for these specimens are typical of materials deformed by twinning. The curves start with the elastic region, and then along with an audible click, a sharp load drop or a flat region occurs at the moment of twin nucleation. The load, just before twin nucleation occurred, was used for calculation of the critical resolved shear stress for twin nucleation. Results are tabulated in Table XXI. It is clear from the table that hydrogen decreased the critical resolved shear stress for twin nucleation and oxygen and nitrogen have a similar effect.

Specimens 7, 9, 11 and 12 have their [0001] poles very close to the normal of one of the cube surfaces. These specimens, after compression testing for $\{10\bar{1}0\}1/3\langle 11\bar{2}0\rangle$ slip were reshaped to remove slight barrelling, electropolished, and then compressed normal to one of cube surfaces which had the [0001] pole close to the normal of the surface. The difference in load-displacement curves between specimens without preloading and specimens with preloading was the absence of the load drop or a flat region in the specimens with preloading. The displacement-load curves of preloaded specimens resembled the curves for crystals deformed by slip. The 0.2% offset yield and work hardening rate of these specimens are shown in Table XXII. Upon comparing the crystals with the same angle between the loading axis and the [0001] pole, it is seen that (1) the yield stress decreased with oxygen and nitrogen content, and (2) work hardening increased with oxygen and nitrogen content.

Table XXI - Critical Resolved Shear Stress and the Nominal Work Hardening Rate of the $\{11\bar{2}2\}\langle 11\bar{2}\bar{3}\rangle$ Twinning System

Specimen and Angle Between Loading Axis and [0001]	(O + N) (ppm)	H (ppm)	Critical Resolved Shear Stress (MN/m^2)	Nominal Work Hardening Rate (MN/m^2)
1 20.5°	706	2	56.3	2121.7
4 24°	706	2	57.8	2258.9
2 20°	706	10	54.9	2161.9
3 25°	706	21	50.9	2905.7
17 26°	95	< 0.1	72.5	1244.6
18 25°	95	22	58.8	1813

Table XXII - Yield Stress and Work Hardening Rate of Specimens with 2.5% Pre-Strain*

Specimen	Angle Between Leading Axis and [0001]	0.2% Offset Yield Stress (MN/m^2)	Nominal Work Hardening Rate (MN/m^2)
7	2°	243.2	1938.4
9	13°	207.2	2160.9
11	2°	178.4	1532.7
12	14°	156.6	1667.9

*These specimens were pre-strained 2.5% with $\{10\bar{1}0\}1/3\langle 11\bar{2}0\rangle$ slip operating, and then compressed for twinning study.

SURFACE EXAMINATION

After compression, specimens prepared for the $\{10\bar{1}0\}1/3\langle 11\bar{2}0\rangle$ slip study had $\{10\bar{1}0\}1/3\langle 11\bar{2}0\rangle$ slip steps and a limited number of $\{10\bar{1}2\}$ twins as shown in Fig. 46. In general, specimens containing more hydrogen had more twins. For example, specimens 5 and 6 had both been compressed about 6%, the subsequent surface examination revealed that specimen 6, containing 22 ppm hydrogen, had 30 twins whereas specimen 5, containing 2 ppm hydrogen, had no twins. Specimens containing the higher oxygen and nitrogen contents revealed the same tendency as specimens containing more hydrogen for the same amount of compressive strain.

Specimens prepared for the twinning study displayed $\{11\bar{2}2\}$ twins. Specimens 1, 2, 3, 4, 17, and 18 had $\{10\bar{1}0\}1/3\langle 11\bar{2}0\rangle$ slip traces in addition to $\{11\bar{2}2\}$ twinning. Specimens 7, 9, 11 and 12, after being compressed for the twinning study, showed $\{11\bar{2}2\}$ twins only. The slip observed in specimens 1, 2, 3, 4, 17 and 18 occurred after twin initiation. This is apparent in the load-displacement curves in that only the elastic region is observed prior to twin initiation.

Interestingly, along with $\{11\bar{2}2\}$ twins, there was always some type of slip on the twin and parent boundary and in front of the edge of the twin as shown in Fig. 47. These slip traces were analyzed and found to be the $\{10\bar{1}1\}$ type of slip. The orientation relationship of this slip to the $\{11\bar{2}2\}$ twins with which they are associated is shown in Figs. 48 and 49. The fact that $\{10\bar{1}1\}1/3\langle 11\bar{2}0\rangle$ slip is not a favorable slip system strongly suggests that it is associated with twin growth and it has a different Burgers vector. Transmission electron microscopy studies reveal that these dislocations have $1/3\langle 11\bar{2}3\rangle$ type of Burgers vector, which is the same as the shear direction for $\{11\bar{2}2\}$ twinning. Figure 50 shows these dislocations gliding away from the twin-parent boundary on $\{10\bar{1}1\}$ planes. Backofen et al.[72] suggested that this $\{10\bar{1}1\}1/3\langle 11\bar{2}3\rangle$ slip provided the strain forming in front of the $\{11\bar{2}2\}$ twin.

These $\{10\bar{1}1\}$ type of slip traces were observed only on one side of twin-parent boundaries as shown in Fig. 51, which would suggest that twin growth was actually operating only on one side of twin-parent boundary, contrary to the general belief.

DISCUSSION

SLIP

The least-square fitting of straight lines of the critical resolved shear stress for $\{10\bar{1}0\}1/3\langle 11\bar{2}0\rangle$ slip vs. hydrogen content was used and the result are illustrated in Figs. 52 and 53. Hydrogen increases the critical resolved shear stress of the $\{10\bar{1}0\}1/3\langle 11\bar{2}0\rangle$ slip system in both the commercial purity specimens and the high purity specimens.

Fig. 40 - The surface of a specimen showing prismatic slip bands and $\{10\bar{1}2\}$ twins. 130X

Fig. 41 - $\{10\bar{1}1\}$ slip traces in front of the edges of $\{11\bar{2}2\}$ twins. 130X

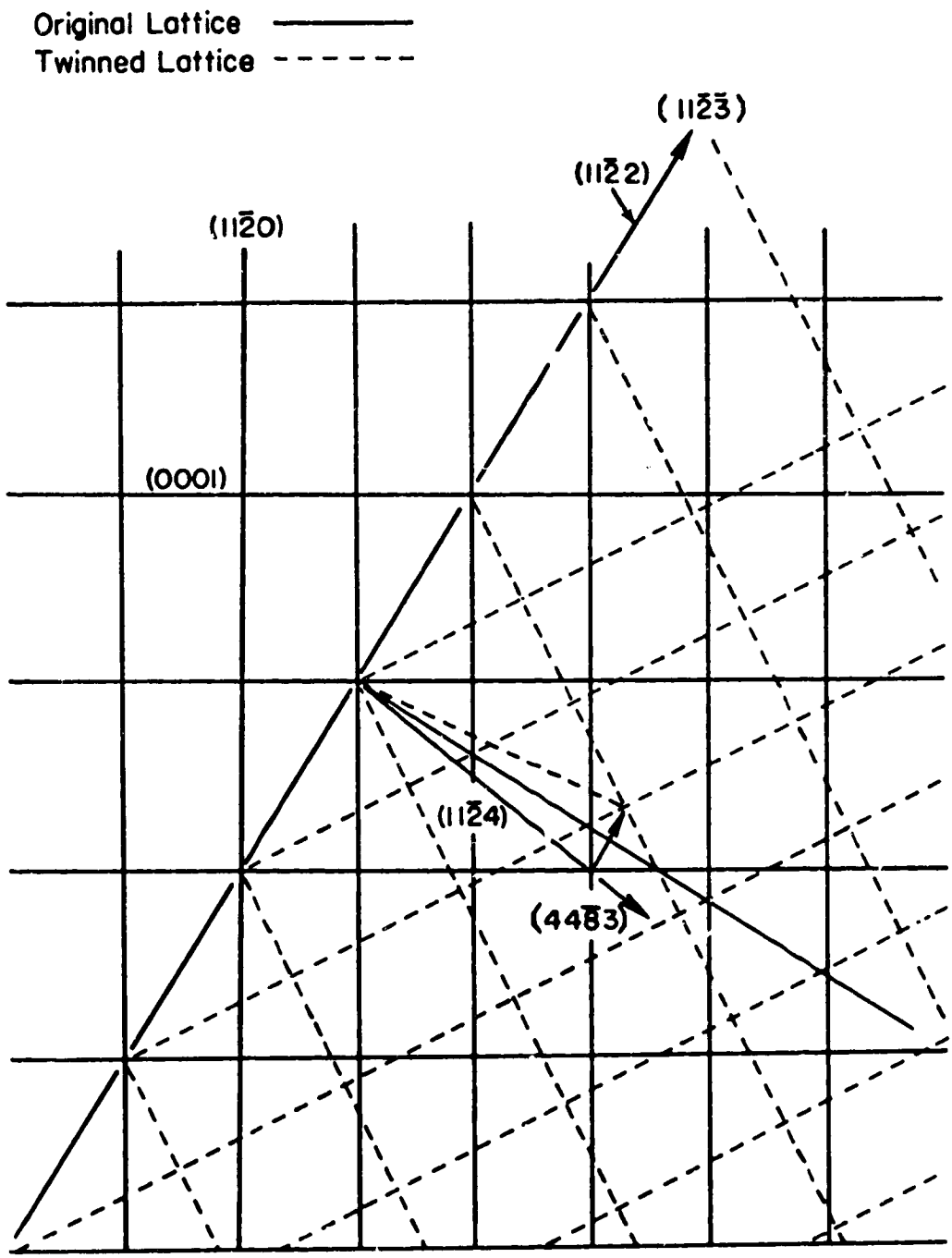

Fig. 48 - The relationship between the (11$\bar{2}$2) twin and the parent crystal.

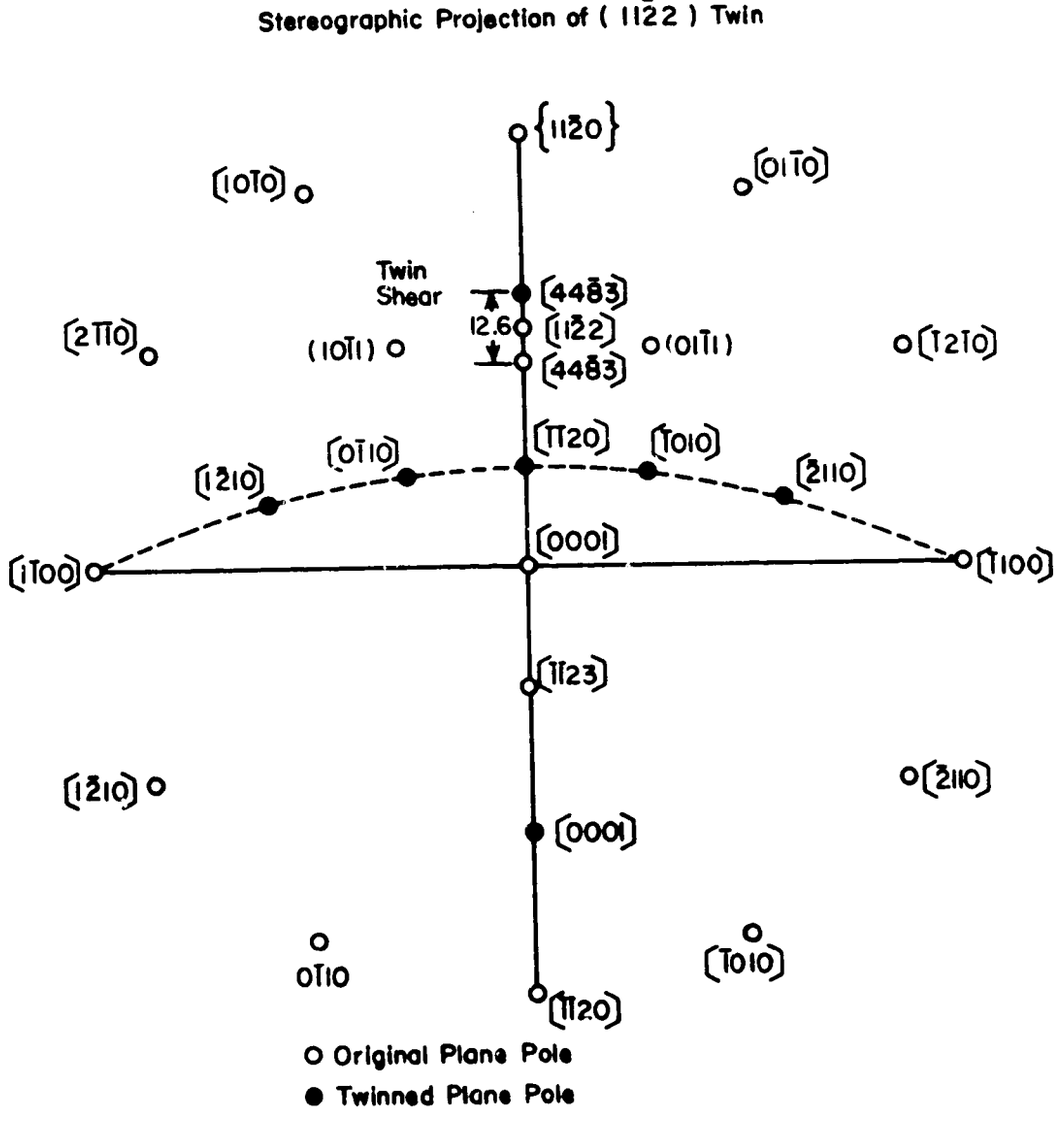

Fig. 49 - The stereographic projection of the (11$\bar{2}$2) twinning. The (10$\bar{1}$1) and (01$\bar{1}$1) are the two slip planes observed along the twin-parent boundary.

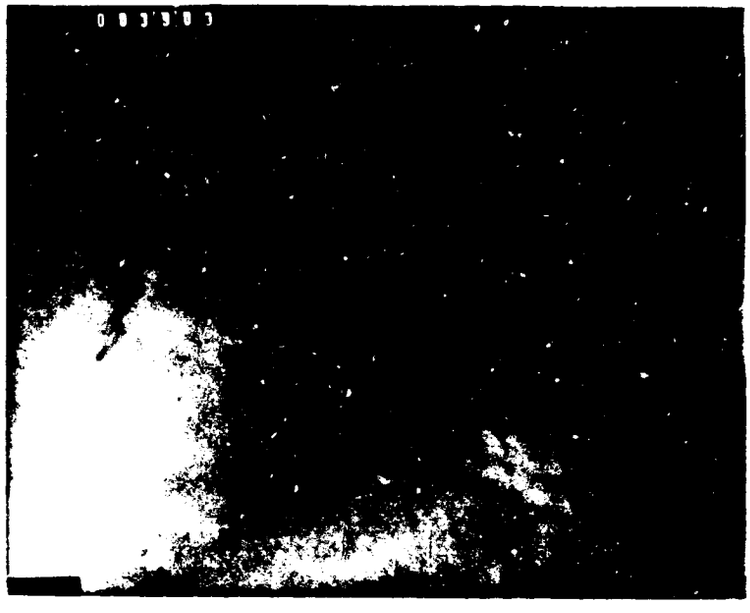

Fig. 50 - Dislocations moving away from the twin-parent boundary. Trace analysis shows that they move on $\{10\bar{1}1\}$ plane and dark field analysis show that they have $1/3\langle 11\bar{2}3\rangle$ Burgers vector. One twin-parent boundary is below the figure, one twin-parent boundary is to the left of the fig ~e. 30,000X

Fig. 51 - The $\{10\bar{1}1\}$ slip traces on one side of the $\{11\bar{2}2\}$ twins 130X

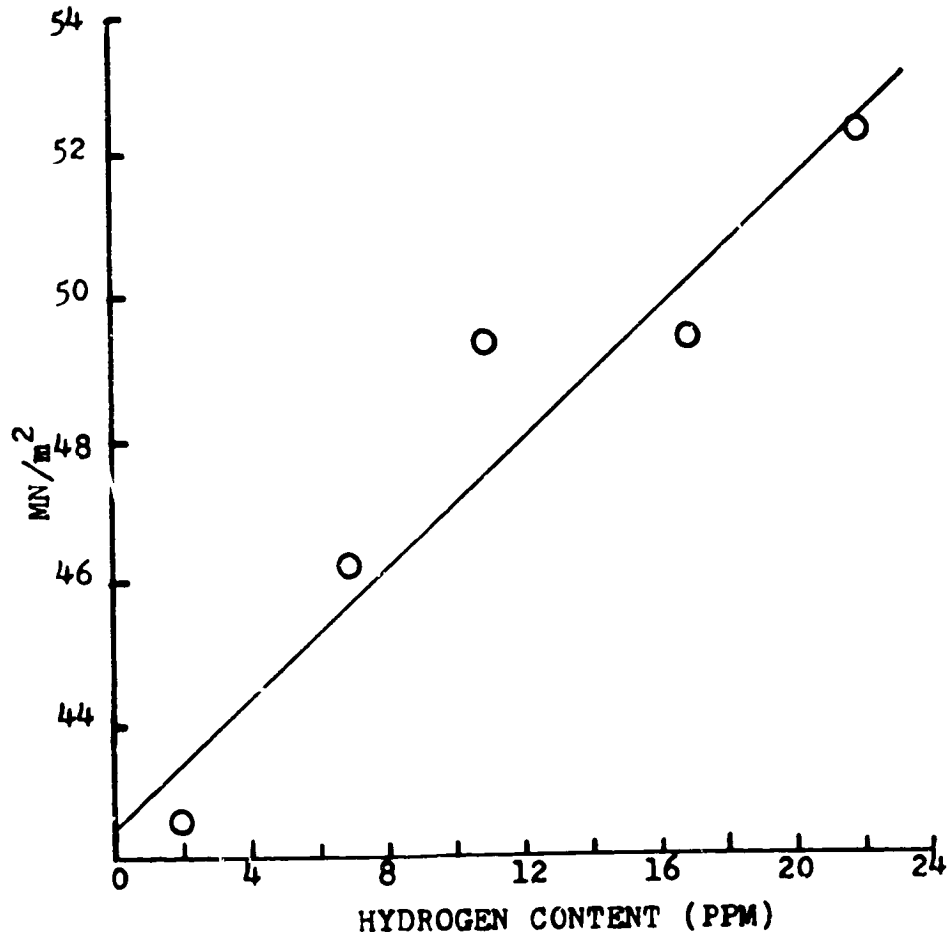

Fig. 52 - The critical resolved shear stress of $\{10\bar{1}0\}1/3\langle 11\bar{2}0\rangle$ slip system vs. hydrogen content in commercial purity titanium specimens

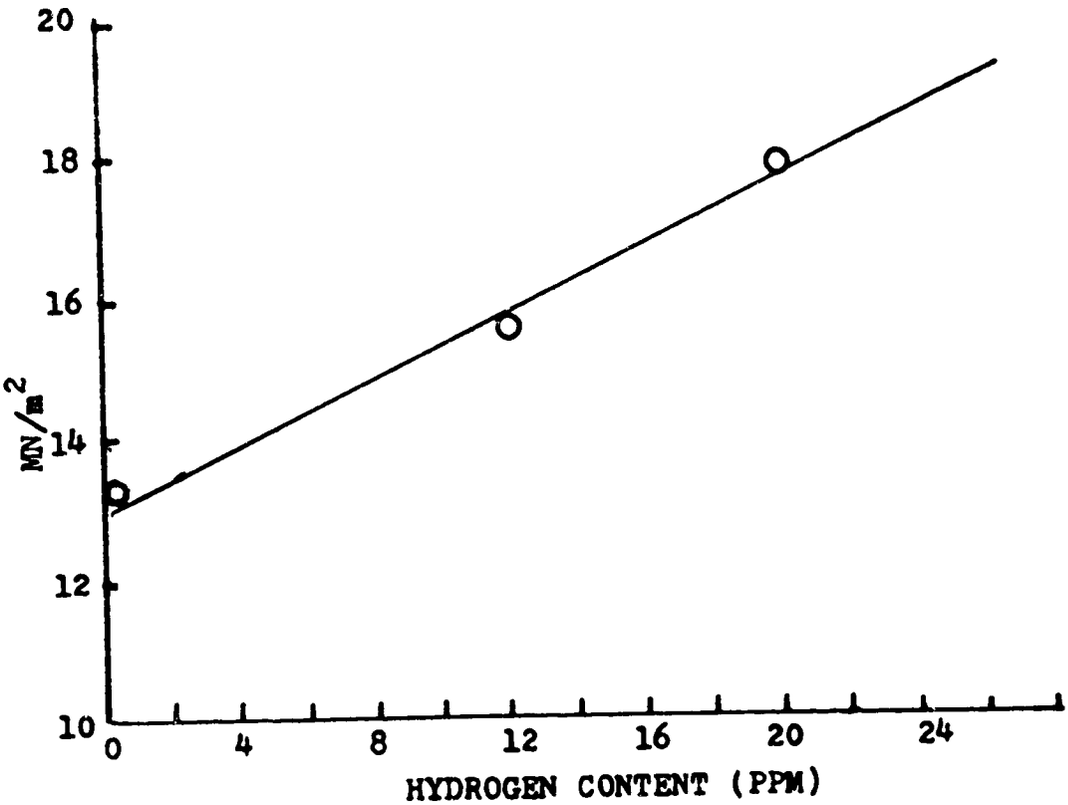

Fig. 53 - The critical resolved shear stress of $\{10\bar{1}0\}1/3\langle 11\bar{2}0\rangle$ slip system vs. hydrogen content in high purity titanium specimens

The slope of this curve for high purity specimens seems to be less than the slope for commercial purity specimen.

The increase in yield stress in α titanium with increasing hydrogen in solution was noted by Lenning.[108] No explanation was given for this phenomenon. Churchman[65] proposed a mechanism to explain the increase in critical resolved shear stress with increasing oxygen and nitrogen contents. His mechanism was based upon oxygen and nitrogen atoms being occupied in octahedral sites in α titanium, and in so doing provided friction for gliding of $\{10\bar{1}0\}$ planes.

Hydrogen atoms also occupy octahedral sites. The model such as proposed by Churchman certainly can be applied to interstitial hydrogen atoms in α titanium to account for the increase in CRSS of prism slip. However, this model can not explain why the $\{10\bar{1}0\}1/3\langle 11\bar{2}0\rangle$ slip system is strengthened more than the $\{0001\}1/3\langle 11\bar{2}0\rangle$ slip system by interstitial hydrogen atoms. Oxygen and nitrogen atoms preferentially strengthened the $\{10\bar{1}0\}1/3\langle 11\bar{2}0\rangle$ slip system over the $\{0001\}1/3\langle 11\bar{2}0\rangle$ and $\{10\bar{1}1\}1/3\langle 11\bar{2}0\rangle$ slip systems. (The preference of $\{10\bar{1}0\}1/3\langle 11\bar{2}0\rangle$ slip over $\{10\bar{1}1\}1/3\langle 11\bar{2}0\rangle$ slip can be explained by the same mechanism by showing that only half of the interstitial atoms in octahedral sites are effective in providing friction for $\{10\bar{1}1\}1/3\langle 11\bar{2}0\rangle$ slip). Churchman[65] explained the preference of prism slip over basal slip by showing that atoms in octahedral sites are obstacles for dissociation of dislocations on the basal plane (for details check the literature survey section). However, recent slip trace studies[121] and transmission microscopy studies[120] have all supported the contention that dislocations on the basal plane do not dissociate into partial dislocations since (1) the calculated stacking fault energy on the basal plane is about 300 erg/cm^2, too high for dislocation dissociation, (2) the slip steps of basal slip showed considerable cross slip, and (3) partial dislocations have never been seen in α titanium. All of this evidence suggests that the mechanism proposed by Churchman to explain the preferential strengthening of $\{10\bar{1}0\}1/3\langle 11\bar{2}0\rangle$ slip over $\{0001\}1/3\langle 11\bar{2}0\rangle$ slip was not based on the correct assumption.

Based upon the present observations, a possible mechanism is purposed to explain why $\{0001\}1/3\langle 11\bar{2}0\rangle$ slip was affected less than $\{10\bar{1}0\}1/3\langle 11\bar{2}0\rangle$ slip by interstitial atoms in octahedral sites. The nature of the basal plane is such that it contains all three $1/3\langle 11\bar{2}0\rangle$ Burgers vectors, while other planes contain only one of the three $1/3\langle 11\bar{2}0\rangle$ Burgers vectors. Thus screw dislocations on the basal plane can easily cross slip through any of the other slip planes when they reach an obstacle. Cass[121] showed that almost all dislocations observed on basal planes are screw dislocations. The observations on basal planes in the present study are shown in Fig. 54 were dislocations lined up parallel to their Burgers vector. These screw dislocations have the $1/3\langle 11\bar{2}0\rangle$ type of Burgers vector, and they frequently reacted to form the third Burgers vector through the reaction of $1/3[11\bar{2}0] + 1/3[1\bar{2}10] = 1/3[2\bar{1}\bar{1}0]$. This is probably due to the Peierls stress in the lattice forcing the dislocations to line up along the $\langle 11\bar{2}0\rangle$ directions.

Fig. 54 - Dislocations arrangement in pure titanium shows that they line up parallel to the $\langle 11\bar{2}0 \rangle$ directions 30,000X

Therefore, it is believed that the ability of dislocations to cross slip on the basal plane or to move away from the obstacle is the reason why basal slip is affected much less than prism slip. The wavy nature of basal slip and the straight nature of prism slip observed in this study support this mechanism.

Another possible reason for the above results is that screw dislocations interact with shear stress fields only, while edge dislocations interact with both hydrostatic and shear stress fields. The octahedral site in α titanium is not a symmetrical site; therefore, interstitial atoms in the octahedral sites will cause both hydrostatic and shear stress fields. Screw dislocations on basal planes will only interact with the shear component of the stress field, whereas dislocations on prism planes will interact with both stress fields. Consequently, dislocations on basal planes are affected less by the addition of interstitial atoms.

The slight increase in work hardening rate in high purity specimens may be due to the very low critical resolved shear stress for $\{10\bar{1}0\}1/3\langle 11\bar{2}0 \rangle$ slip as compared with other slip systems; therefore, at the stress of plastic deformation cross slip to other slip systems could not occur. This would make obstacles more effective in comparison with commercial purity specimens where difference in critical resolved shear stress between slip systems are less.

Comparing Fig. 52 and Fig. 53, it is seen that the high purity specimens have a smaller slope. The effect of hydrogen on the CRSS of prism slip is less in high purity specimens. This could be the result of a slight change in the size of octahedral sites. Small amounts of oxygen and nitrogen are known to cause a slight expansion of the c vector in pure titanium. Calculating according to Finley's data,[104] there is a 0.05% expansion in the c vector between the commercial purity titanium and high purity titanium in this study. Thus, there should be a better fit of the hydrogen atom in octahedral sites of high purity titanium, since the hydrogen atom is smaller than the octahedral site. Therefore, hydrogen is less effective as a strengthener in high purity specimens.

TWINNING

The critical resolved shear stress for $\{11\bar{2}2\}\langle 11\bar{2}\bar{3}\rangle$ twins in commercial purity titanium vs. hydrogen content is shown in Fig. 55. The straight line (least-square fitting) is based on the data in Table XXI. The effect of hydrogen apparently is to lower the critical resolved shear stress for twin nucleation. This decrease is probably directly related to the increase in the critical resolved shear stresses for slip.

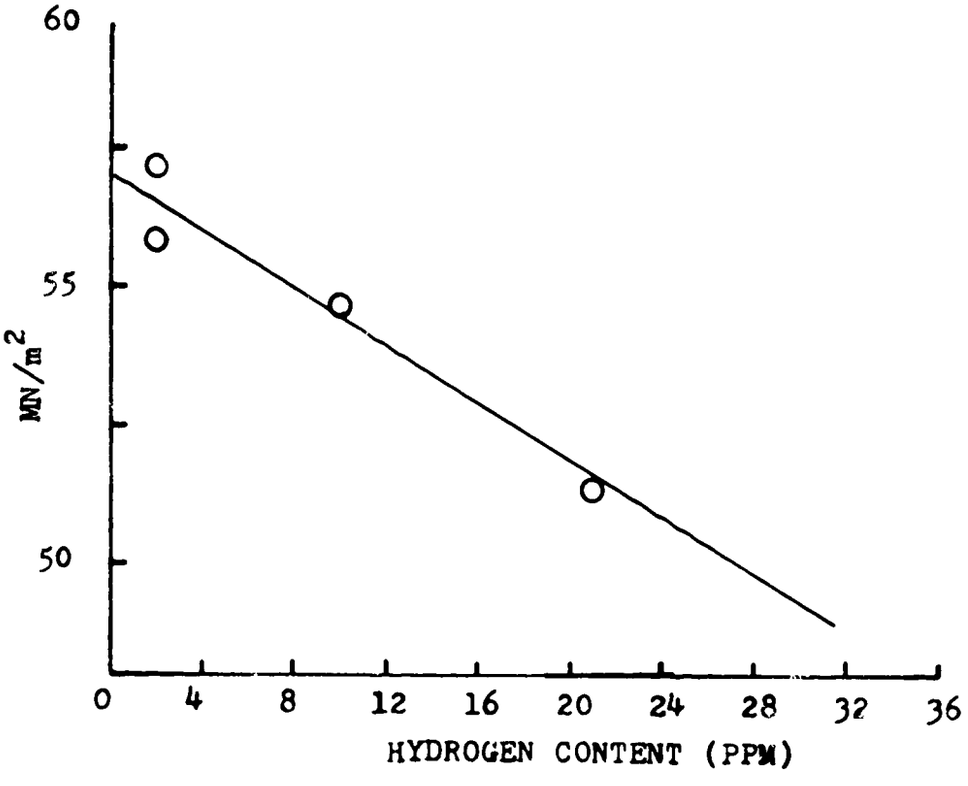

Fig. 55 - The critical resolved shear stress of $\{11\bar{2}2\}\langle 11\bar{2}\bar{3}\rangle$ twinning system vs. hydrogen content in commercial purity titanium specimens.

Earlier in this report it was shown that an increase in yield stress, either by a change in temperature or by a change in strain rate, would decrease the critical resolved shear stress for twin nucleation. It is generally believed that slip is a pre-requisite for twin nucleation, and microscopic movement of the dislocations cause dislocation pile-ups or tangles, together creating stress concentrations in the metal. These stress concentrations serve as nuclei for twin nucleation. If dislocations move away from these stress concentrations easily, or if the critical resolved shear stress is low for slip, the critical stress for twin nucleation at these stress concentrations will not be reached. By this mechanism, interstitial hydrogen and oxygen both increased the critical resolved shear stress for slip, and they both decreased the critical resolved shear stress for twin nucleation.

Twin growth is primarily a process of twin dislocation glide on the twin plane into the parent matrix. The Burgers vectors of these twin dislocations do not equal the lattice vectors; their main function is to provide the shear observed in a twin. Uniformity of the material has an effect on twin growth. The purer and the less strained the material, the easier it will be for twin growth. If the work hardening rates of crystals with the same orientations are compared, this would appear to be true for the present study. For example, crystals 7 and 11 in Table XXII have the same orientation; the work hardening rate is 1938 MN/m^2 for crystal 7 and 1532.7 MN/m^2 for crystal 11.

Twin nucleation and twin growth are two processes with opposite tendencies. Twin growth requires less stress where twin nucleation requires higher stress. For example, work hardened crystals have no difficulty in twin nucleation but require higher stresses for twin growth. These work hardened crystals must have created twin nuclei during the previous deformation, and subsequent deformation is merely a twin growth process. The yield stress shown in Table XXII is primarily the stress for twin growth, therefore, the stress decreased with the impurity of the material.

At this point, it is important to compare slip to twinning processes:

	slip $\{10\bar{1}0\}1/3\langle 11\bar{2}0\rangle$	twinning $\{11\bar{2}2\}\langle 11\bar{2}\bar{3}\rangle$
nucleation	not necessary	necessary
deformation by	dislocation movement	twin dislocation movement
CRSS	9.8 - 58.8 MN/m^2	39.2 - 68.6 MN/m^2
strain	uniform	highly concentrated
high temperature	easier	nucleation difficult
high strain rate	more difficult	nucleation easier
presence of impurity	more difficult	nucleation easier

Two important characteristics of twinning which have a direct relation to the embrittlement phenomenon should be pointed out. First, there is a highly concentrated deformation in twinning as compared with slip. Lenning[108] pointed out the direct relationship between severe impact embrittlement and the presence of a high volume fraction of twins at low temperature. Westlake[113] pointed out that the intersection of twins or slip with hydride initiated cracks in the hydride, but cracks were observed at the intersections of slip and hydride only after considerable deformation. Second, at the condition when slip is difficult, such as high strain rate or low temperature, twinning occurs. One would expect that when slip is difficult twin growth should be impeded, but such is not the case. Therefore, twin dislocations which have much smaller Burgers vectors than perfect dislocations are affected much less by the unfavorable condition for slip than are perfect dislocations. For example, the material at a crack tip is work hardened and under biaxial stress, therefore dislocation movement is impeded. Thus, this should be a favorable condition for twinning to occur. As a matter of fact, Bell and Cahn[129,130] showed that twinning did not occur in zinc single crystals under slow tensile loading, but twins were evident along the fracture surface.

The high concentration of deformation associated with the twinning process in this investigation suggests that when twinning occurs in α titanium it will enhance any existing embrittling effect. It also suggests that the presence of hydride will not only block dislocations, but also will creates high stress concentrations in α titanium to initiate twinning.

It is interesting to compare the effect of interstitial oxygen and nitrogen to that of interstitial hydrogen. All three occupy the same interstitial sites and their influence on the mechanical properties of α titanium are, in general, similar in nature. There has been much work[125-128] done on the effect of interstitial oxygen and nitrogen, but little has been done on the effect of interstitial hydrogen, probably due to its low solubility in α titanium, as low as 20 ppm.

It is deceptive to look at the weight fraction of hydrogen, since it is the lightest atom in the periodic table, 20 ppm of hydrogen is about 0.1 at.%. (0.1 at.% oxygen is about 320 ppm. Therefore, a significant comparison between oxygen and hydrogen should be based upon atomic percent).

If one used the present data and assumed a linear behavior between the stresses vs. atomic percent of interstitials, the effects of oxygen and hydrogen would be as follows:

	Hydrogen MN/m^2/at.%	Oxygen MN/m^2/at.%
CRSS for $\{10\bar{1}0\}1/3\langle 11\bar{2}0\rangle$ slip	700.7	1557.22
CRSS for $\{11\bar{2}2\}\langle 11\bar{2}\bar{3}\rangle$ twinning	950.6	867.3

This comparison shows that the effect of hydrogen is as great as oxygen. It is known that a titanium, 2 at.% oxygen alloy has a yield stress four times higher than pure titanium. (2 at.% hydrogen will only be 400 ppm hydrogen.) Therefore, one would expect that α titanium supersaturated with several thousand ppm of hydrogen (for example, at stress corrosion crack tip) to be a very strong and hard material.

HYDROGEN EMBRITTLEMENT

The effect of interstitial hydrogen on the mechanical properties of titanium is continuous. The hydrogen embrittlement of titanium reported in the literature refers to an abrupt decrease in ductility when a certain hydrogen concentration is exceeded. Therefore, hydrogen, in solution, is not the culprit for this type of embrittlement; in fact, hydrogen, in solution, in this type of embrittlement studies could never have exceeded several hundred ppm because of hydride precipitation.

The existing theories on hydrogen embrittlement were introduced in the literature survey section. In brief, hydride precipitation is blamed for the embrittlement effects. This is undoubtedly of great importance, but mechanical twinning would play a more important role than these theories had indicated. It is suggested that the effect of hydride precipitation is two-fold, first, it causes high stress concentrations and initiates twinning, and second, it cracks at points where it is intersected by twins. The tendency for fast strain rate embrittlement, being most severe at impact strain rates and low temperatures, is consistent with the tendency for twinning.

Slow strain rate embrittlement is believed to be caused by strain-induced-hydride precipitation on $\{10\bar{1}0\}$ and $\{10\bar{1}1\}$ planes. Again, twinning should play an important role, as dislocations are blocked by hydride plates.

STRESS CORROSION CRACKING

Stress corrosion cracking is a general phenomenon which involves many materials and many environments. It is doubtful that one single mechanism could explain all combinations of material-environment failures of the stress corrosion type. This discussion is concerned mainly with the transgranular cracking of α titanium in environments containing hydrogen.

The stress corrosion cracking mechanism proposed by Boyd *et al.* is the most complete hydride theory existing and it appears to fit most of the observations on the cracking behavior of titanium in aqueous environments. Their proposed model assumes the reduction of hydrogen at or near the crack tip which is free of any oxide. This hydrogen then absorbs on the surfaces, and subsequently diffuses into the metal.

Strain induced hydride will then nucleate and grow rapidly along the active slip planes. Boyd et al.[131] suggested that these strain-induced hydrides effectively blocked the active slip planes and prevented the movement of glide dislocations. Therefore, stress concentration at the crack tip builds up and cleavage occurs on the plane with maximum tensile strain. Their model is shown in Fig. 56.

Mauney and Starke[132] have further refined the model of Boyd et al. to explain the rather unusual $\{10\bar{1}8\}$ or $\{10\bar{1}7\}$[133] fracture planes observed in stress corrosion cracks. They proposed that, as strain induced hydride precipitate on active slip planes, the less active slip system $\{11\bar{2}2\}1/3\langle 11\bar{2}3\rangle$ is allowed to operate, this caused dislocation pile-ups of the $1/3\langle 11\bar{2}3\rangle$ type. This would allow the application of Stroh's theory of fracture. Stroh[134] determined that the cleavage plane was the plane with the maximum tensile stress and, therefore, the most likely cleavage plane was the plane which made an angle of 70.5° with the pile-up's slip plane. By considering the angle between the poles of the $\{10\bar{1}7\}$ or $\{10\bar{1}8\}$ SCC cleavage habit plane and the pile-up's slip plane, a comparison to the Stroh theory can be made. For the $\{10\bar{1}7\}$ plane the angle is 70.76° and for the $\{10\bar{1}8\}$ plane the angle is 69.14°. This shows very good agreement between the theory and the observed cleavage plane. Mauney and Starke[132] pointed out that $\{11\bar{2}2\}$ type of twinning would have the same effect as $\{11\bar{2}2\}1/3\langle 11\bar{2}3\rangle$ slip.

The basic arguments against the above model are as follows: First, the plastic zone must have formed at the moment of crack burst, and the momentum of crack propagation is actually absorbed by this plastic zone. There is little, if any, dislocation movement after the plastic zone has formed; therefore, strain induced hydride will not form. It is known that formation of the strain induced hydride is largely the result of supersaturation of hydrogen brought about by a strong matrix suppressing the hydride precipitation, subsequently dislocation movement aids hydride precipitation. Hydrogen could have diffused in front of the crack tip only after the crack burst, and the work hardened material in front of the crack tip would no doubt suppress hydride precipitation more strongly than strain-free material. With little help from dislocation movement the extensive formation of strain induced hydride would seem to be doubtful.

Second, a successful model should provide a mechanism for resharpening of the crack tip. Near cleavage fracture could occur only under the condition of fast strain rate with a sharp crack as the trigger for the process, a good example would be the cutting of diamond. Titanium supersaturated with hydrogen is not an extremely brittle material under normal tensile loading. For example, Ti-5Al alloy[106] with 200 ppm of hydrogen (Ti-5Al with 200 ppm hydrogen is supersaturated) under normal tensile loading will show an elongation of 24% as compared with 22% for the same material with 50 ppm of hydrogen. Thus, the above model does not explain the near cleavage fracture observed in stress corrosion cracking.

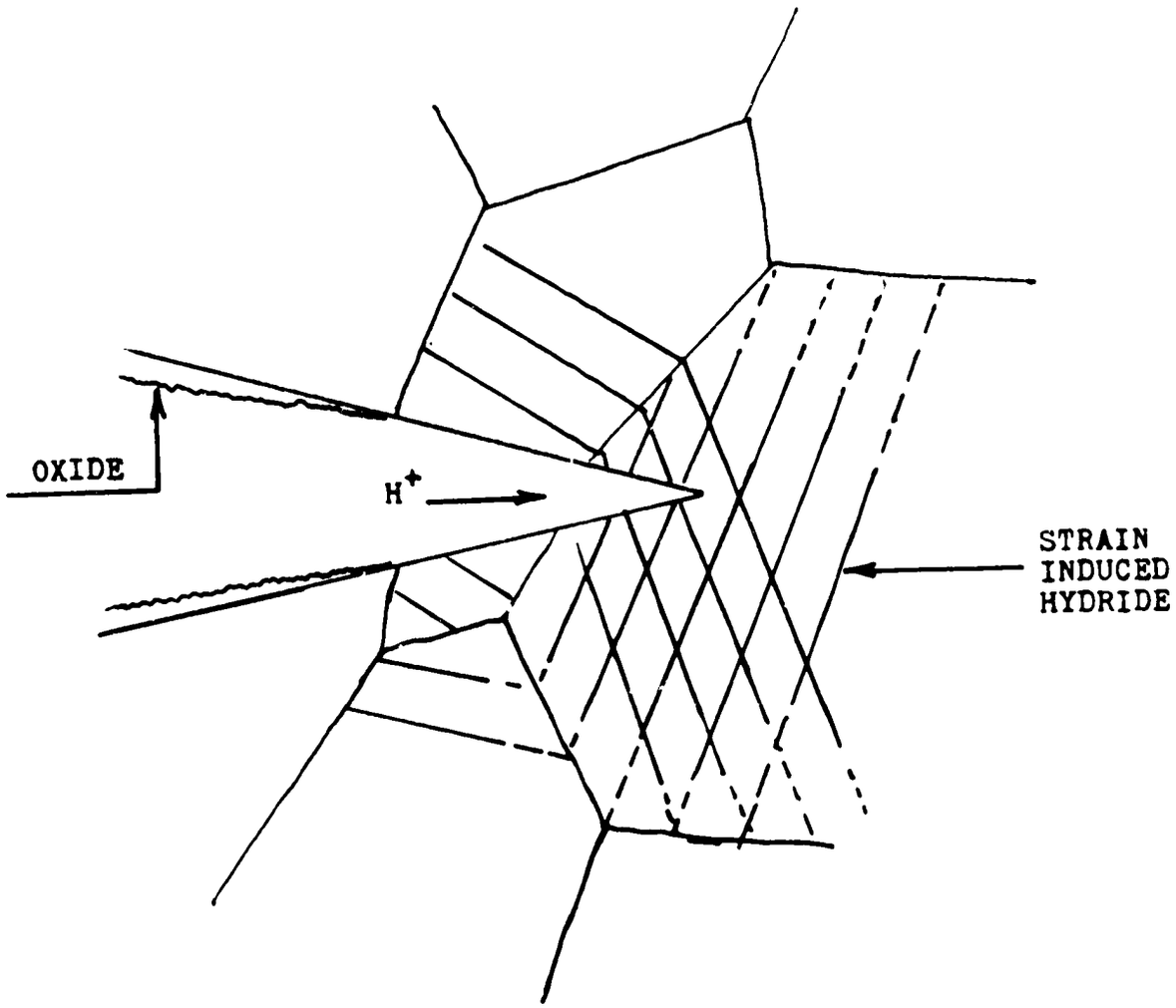

Fig. 56 - Stress corrosion cracking model proposed by Boyd et al.[131]

Third, $\{11\bar{2}2\}1/3\langle 11\bar{2}3\rangle$ slip has never been shown to be an important slip system. Stroh's fracture theory was primarily for anisotropic material and it might not be applicable for hexagonal structures. Stroh stated, "A crack should form when the group consists of about 1000 dislocation pile-ups under a stress of the magnitude occurring in a cold worked metal." It is doubtful that 1000 dislocations will pile-up against a single obstacle when strain induced hydride has precipitated extensively on the slip plane.

In stress corrosion cracking, it is generally agreed that embrittling elements--transported from the environment to the metal matrix--are the cause of the embrittlement. In aqueous solutions and methanol environments, this embrittling element is believed to be hydrogen.

There is no agreement as far as the actual mechanical processes are concerned. Among the various mechanical processes are: strain-induced-hydrides blocking dislocations, hydrogen-assisted cracking, hydrogen decreased cohension force between metal atoms, etc. There could be one unified mechanical mechanism to explain not only the stress corrosion cracking due to hydrogen, but also to explain stress corrosion cracking by oxygen and other embrittling agents, such as liquid metal, etc.

This study stresses the importance of twinning in the mechanical deformation of titanium. Through twinning, a more unified mechanism for stress corrosion cracking is possible. The following model involves twinning as a trigger for cleavage fracture. The model is presented stepwise as follows.

First, the freshly formed crack is arrested by the softer material which is free of embrittling element. The momentum of the crack propagation is absorbed by the plastic zone in front of the crack tip. The newly formed crack tip surface is free of any oxide.

Second, the hydrogen reduced on the surface starts to diffuse into the titanium matrix, but due to the highly work hardened matrix, hydride precipitation is suppressed and there will also be a lack of significant dislocation movement--hydride does not precipitate. Ti-8Al-1V-1Mo[31] requires over 800 ppm of hydrogen before spontaneous hydride precipitation occurs. In a work-hardened Ti-8Al-1V-1Mo, supersaturation of hydrogen as high as one or two thousand ppm is quite possible. Gray,[11] using the ion microprobe, found hydrogen concentrations of several thousand ppm below the surfaces of stress corrosion cracks of Ti-8Al-1Mo-1V. Ion microprobe distinguishes hydride from hydrogen,[146] therefore, the several thousand ppm of hydrogen is likely to be supersaturated hydrogen and not hydride. The diffusion rate under high dislocation density and high tensile stress should be faster than the ordinary diffusion rate, so the condition of supersaturation is established quickly.

Third, the several thousand ppm of hydrogen hardens the material to an extent that dislocation movement becomes extremely difficult.

During the formation of the plastic zone some twin nuclei had already formed, and with increasing hydrogen content the critical nucleation stress for twinning gradually decreases to a point where stress at the crack tip is capable of initiating twins. This is an ideal condition for twinning to occur with dislocation movement becoming extremely difficult due to work hardening, high concentration of hydrogen, and biaxial stress state.

Fourth, as twinning occurs, it creates a pure shear strain on the twin plane. The material immediately adjacent to the twin is subjected to the same pure shear strain, but of the opposite sense. The plane of principal normal strain is 45° away from the twin plane. The speed of twin formation is extremely fast, therefore, the plane 45° away from the twin plane is subjected to a high normal stress under fast strain rate. This strain can not be dissipated by plastic flow since the material has been hardened at this stage and the strain rate is very fast. Thus, near cleavage fracture occurs on this plane. Once near cleavage fracture occurs, it carries through the hardened material and finally stops at the ductile material. The process cycle then repeats. The model is shown schematically in Fig. 57.

The main role of twinning is a trigger for near cleavage fracture to occur. The high speed of formation and high concentration of strain are two excellent triggering mechanisms. It is not necessary to have a large amount of twinning for crack propagation, since it is necessary only to trigger the near cleavage fracture.

Fracture surfaces are known to have a high density of twins which are due mainly to a high overstress at the crack tip. Cox,[137] in his experiments, tried to relate the acoustic emission to transgranular crack propagation of zircaloys and he stated, "Metallography has confirmed that when this type of emission* is heard, there is evidence for transgranular cleavage facets having been generated in the specimen. However, there is also evidence for twins forming during the same period of the stress corrosion cracking, so that the cracking type of acoustic emission can not be unequivocally associated with either crack propagation or twinning." The only logical place for twin formation is at the crack tip. Boyd[138] et al. showed a picture of slip bands adjacent to a stress corrosion crack of Ti-8Al-1V-1Mo in aqueous environment. There was evidence of twinning.

Cleavage facets found in stress corrosion cracking of the α phase in titanium have been repetitively determined to have their normal only 12-17° from the [0001] pole[138] as shown in Fig. 58. The $\{11\bar{2}2\}\langle 11\bar{2}\bar{3}\rangle$ and $\{10\bar{1}2\}\langle 10\bar{1}\bar{1}\rangle$ twinning systems are the two most frequently observed twinning systems in titanium. According to the new model, the plane 45° away from the pure shear strain plane is the cleavage fracture plane. When calculated, the cleavage fracture plane for $\{11\bar{2}2\}\langle 11\bar{2}\bar{3}\rangle$

*Discontinuous type of acoustic emission

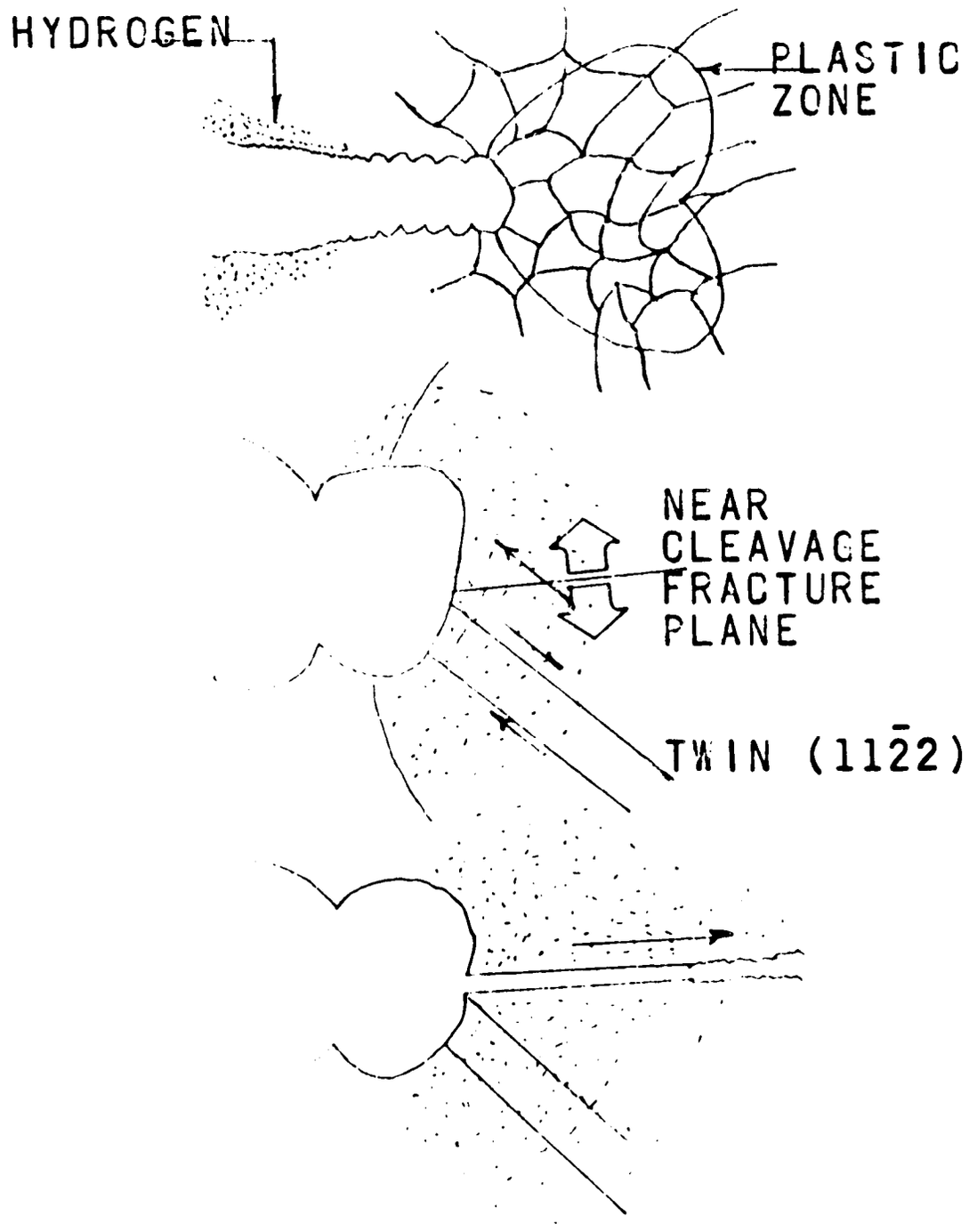

Fig. 57 - A model for the transgranular stress corrosion cracking in α titanium.

Step 1 - Right after crack burst crack tip is blunted and a plastic zone is formed.

Step 2 - Hydrogen diffused into the material, consequently it is hardened and the critical stress for twin nucleation is reduced.

Step 3 - High speed of the twin formation and concentrated strain triggers near cleavage fracture on a plane 45° from the twin plane. The crack propagates until arrested by the softer material.

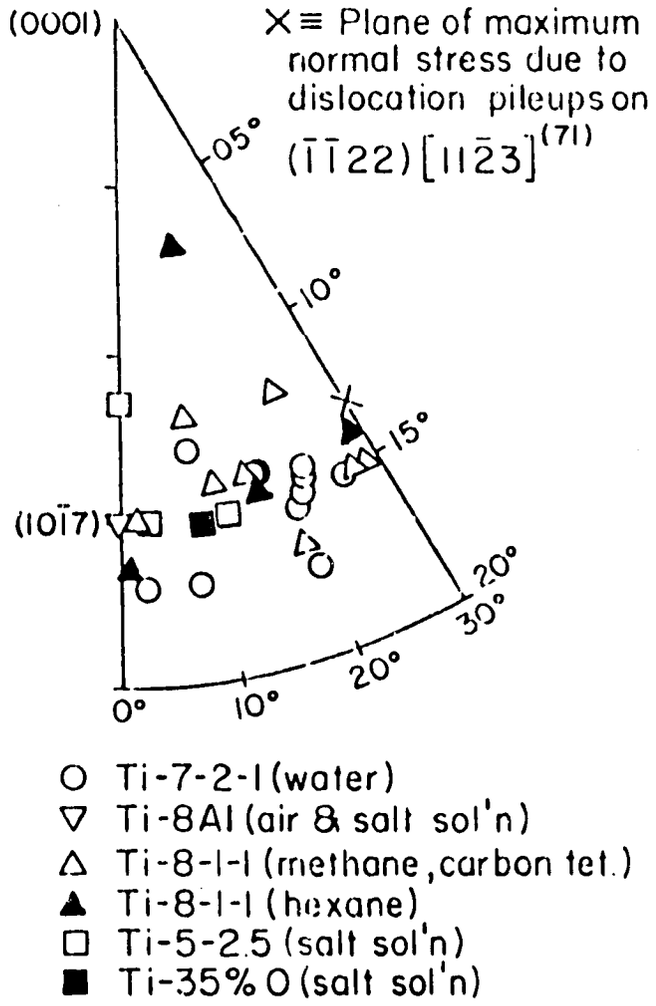

Fig. 58 - The orientation of the cleavage facets found in stress corrosion cracking of α titanium (ref. 138).

twinning is 13° from the [0001] pole, and the cleavage fracture plane for $\{10\bar{1}2\}\langle 10\bar{1}1\rangle$ twinning is 88° from the [0001] pole. The $\{11\bar{2}2\}\langle 11\bar{2}\bar{3}\rangle$ twinning occurs when compressed close to the [0001] pole or extended normal to the [0001] pole. The texture of α titanium has generally been found to have an orientation of the basal plane parallel to the metal flow direction and, in the case of sheet, the $\langle 10\bar{1}0\rangle$ direction is parallel to the rolling direction and the (0001) plane rotates 30° toward the transverse direction. Therefore, under tension the texture of α titanium sheet, wire and bar all favor the formation of $\{11\bar{2}2\}\langle 11\bar{2}\bar{3}\rangle$ twinning. Thus, the model explains the formation of the fracture facets observed.

Scully et al.[118] concluded from their experiments that, "The observed transgranular fracture can be caused either by hydrogen or by oxygen." This is illustrated in their stress corrosion experiments in which both hydrogen and oxygen caused the same type of brittle fracture.

In the present study both oxygen and hydrogen reduced the critical stress for twinning and also hardened the matrix; therefore, the new model can be applied to explain the embrittlement by oxygen and hydrogen in Scully's experiments.

In summary, there are two essential points in the new model. First, hydrogen reduces the critical resolved shear stress for twinning and hardens the material. Second, twinning with its high strain rate and concentrated strain triggers near cleavage fracture. This model has the following advantages:

(1) It is consistent with the discontinuous nature of crack propagation.

(2) It is a more unified mechanism, capable of explaining transgranular stress corrosion cracking caused by hydrogen, oxygen, or any other element which hardens titanium.

(3) It explains the observed fracture facets.

(4) It provides a trigger mechanism for the initiation of near cleavage fracture.

(5) Twinning is a localized phenomenon and it is compatible with the localized stress corrosion cracking phenomenon.

CONCLUSIONS

The effect of hydrogen on slip and twinning was determined for titanium single crystals.

Hydrogen increased the critical resolved shear stress for prism slip.

Hydrogen decreased the critical resolved shear stress for $\{11\bar{2}2\}\langle 11\bar{2}\bar{3}\rangle$ twinning.

The effects of oxygen on the critical resolved shear stresses for prism slip and $\{11\bar{2}2\}\langle 11\bar{2}\bar{3}\rangle$ twinning were qualitatively the same as for hydrogen.

Work hardening reduced the critical resolved shear stress for $\{11\bar{2}2\}\langle 11\bar{2}\bar{3}\rangle$ twinning.

$\{11\bar{2}2\}\langle 11\bar{2}\bar{3}\rangle$ twinning plays an important role in stress corrosion cracking.

APPENDIX

SAMPLE CALCULATIONS FOR HYDROGENATION PROCEDURE

$PV = nRT$ (ideal gas law)

$$R = 62.5 \frac{\ell - \text{mmHg}}{\text{deg - mole}}$$

$$n = \frac{a}{M} = \frac{\text{g of gas}}{\text{molecular weight}} = \frac{\text{g of gas}}{2}$$

Since backfilling pressure was at room temperature,

$T = 273 + 23 = 296$ K

$$a = \text{amount of gas in g} = \frac{(\text{wt\%})(\text{sample wt})}{100} .$$

If one sample weighed 7.2 g then

$$P = \frac{nRT}{V} + \frac{a}{2} \times 62.5 \times \frac{296}{V} .$$

For a desired level of 250 ppm hydrogen with the initial hydrogen content 10 ppm, 240 ppm hydrogen must be added;

$$P = \frac{9250\ a}{V} = \frac{9250(.00173)}{V} .$$

If the volume of the charging capsule is measured to be 82.5 ml then $P = \frac{9250(.00173)}{.0825} = 194$ mmHg. Thus the charging pressure should be raised to 194 mmHg and then the capsule sealed.

REFERENCES

1. R. C. May, F. H. Beck and M. G Fontana, "Stress Corrosion Cracking of Titanium Alloys," Report No. 9 NASA, Grant No. NGL 36-008-051, The Ohio State University Research Foundation, pp. 82-88 (1971).

2. E. L. Owen, F. H. Beck and M. G. Fontana, "Stress Corrosion Cracking of Titanium Alloys," Report No. 8, NASA, Grant No. NGL 36-008-051, The Ohio State University Research Foundation, pp. 96-97 (1970).

3. R. J. Smith and D. A. Otterson, "Tensile Properties of Titanium Electrolytically Charged with Hydrogen," NASA Technical Note TN D-6515.

4. P. E. Irving and C. J. Beevers, "Some Observations on the Deformation Characteristics of Titanium Hydride," J. Materials Science 7:1, January 1972, 23.

5. C. D. Beachem, "A New Model for Hydrogen-Assisted Cracking," Met. Tran. 3, February 1972, 437.

6. R. H. Ernst and J. W. Spretnak, Trans. Iron and Steel Institute of Japan, 9, No. 5, 1969, 361.

7. D. McGarry, Ohio State University, Met. Eng., M.Sc. Thesis, 1972.

8. A. K. Chakrabarti, "Characteristics of Plastic Instability in the Direction of Pure Shear," Ph.D. Dissertation, The Ohio State University, 1973.

9. N. D. Tomashov, R. M. Al'tovskii and M. Ya Kushnerev, Dokl. Akad. Nauk SSSR 141, 913 (1961).

10. N. D. Tomashov, R. M. Al'tovskii and M. Ya Kushnerev, Zavodskaya Laboratoriya 26, 298 (1960).

11. N. D. Tomashov, R. M. Al'tovskii and A. G. Arakelov, Dokl. Acad. Nauk. SSSR 121, 885 (1958).

12. N. D. Tomashov and E. M. Mirolyubov, eds., Corrosion of Metals and Alloys Collection No. 2, Israel Program for Scientific Translations: Jerusalem, p. 71 (1966).

13. R. Otsuka, Sci. Papers I.P.C.R. 54, 97 (1960).

14. R. C. May, F. H. Beck and M. G. Fontana, "Stress Corrosion Cracking of Titanium Alloys," Report No. 9, NASA, Grant No. NGL 36-008-051, The Ohio State University Research Foundation, pp. 4-9 (1971).

15. L. W. Berger, D. N. Williams, and R. I. Jaffee, "The Effect of Hydrogen on Mechanical Properties of Titanium and Titanium Alloys," Fourth Summary Report from Battelle Memorial Institute to Watertown Arsenal Laboratory, Contract No. DAI-33-019-505-ORD-(P)-1, July 31, 1955.

16. T. R. Beck, Proceedings of Conference on Fundamental Aspects of Stress Corrosion Cracking at The Ohio State University, R. W. Staehle, ed., NACE, Houston, 605, (1969).

17. D. T. Powell and J. C. Scully, Corrosion, 24, 151, (1968).

18. C. M. Chen, F. H. Beck, and M. G. Fontana, Corrosion, 27, 77, (1971).

19. J. A. S. Green and A. J. Sedricks, RIAS Technical Report 70-11C, Martin Marietta Corporation, October 1970.

20. M. G. Fontana et al., "Corrosion Cracking of Metallic Materials," Technical Report AFML-69-16, The Ohio State University to Air Force Materials Laboratory, Wright-Patterson Air Force Base, Ohio, February 1969.

21. B. F. Brown et al., "Marine Corrosion Studies," Third Interim Report of Progress, NRL Memorandum Report 1634, July 1969.

22. "A Study of the Stress Corrosion Cracking of Titanium Alloys in Sea Water With Emphasis on the Ti-6Al-4V and Ti-8Al-1Mo-1V Alloys," Research Report No. R471, Project No. 93002, Reactive Metals, Inc., October 18, 1965.

23. M. H. Peterson, B. F. Brown, R. L. Newbegin and R. R. Groover, Corrosion, 23, 142, (1967).

24. J. D. Jackson and W. K. Boyd, "Stress-Corrosion and Accelerated Crack-Propagation Behavior of Titanium and Titanium Alloys," DMIC Technical Note, Battelle Memorial Institute, Feb. 1, 1966.

25. I. R. Lane, Jr., I. J. Cavallars, and A. G. S. Morton, "Sea-Water Embrittlement of Titanium," Stress-Corrosion Cracking of Titanium, ASTM STP 397, Am. Soc. Testing Mater., 1966, p. 246.

26. S. R. Seagle, R. R. Seeley, G. S. Hall, "The Influence of Composition and Heat Treatment on the Aqueous Stress Corrosion of Titanium," Research and Development Report 492, Reactive Metals, Inc., March 15, 1967.

27. I. R. Lane and J. L. Cavallart, "Metallurgical and Mechanical Aspects of Sea Water Stress Corrosion of Titanium," Applications Related Phenomena in Titanium Alloys, ASTM STP 432, 1968, p. 147.

28. R. A. Wood, J. D. Boyd, and R. I. Jaffee, "The Effect of Composition on the Salt Water Stress-Corrosion Susceptibility of Titanium Alloys Containing Aluminum, Molybdenum, Vanadium, and Oxygen," paper presented at the Second International Conference on Titanium Alloys, May 2-5, 1972.

29. R. A. Wood, J. D. Boyd, D. N. Williams, and R. I. Jaffee, "The Effect of Alloy Composition on the Mechanism of Stress-Corrosion Cracking of Titanium Alloys in Aqueous Environments," Annual Summary Report to NASA, June 11, 1971 to June 10, 1972.

30. E. L. Owen, F. H. Beck, and M. G. Fontana, "Stress Corrosion Cracking of Titanium Alloys," NASA, Grant NGL 36-008-051, December 1970.

31. I. R. Lane, J. L. Cavallero, and A. G. S. Morton, "Fracture Behavior of Titanium in the Marine Environment," MEL R&D Phase Report 231/65, U. S. Navy Marine Engineering Laboratory, Annapolis, Maryland, 1965.

32. R. C. May, F. H. Beck, and M. G. Fontana, "Stress Corrosion Cracking of Titanium Alloys" NASA, Grant NGL 36-008-051, September 1971.

33. F. Cotterill, "The Hydrogen Embrittlement of Metals," Progr. Mater. Sci. 9, No. 4, (1961).

34. J. G. Morlet, H. H. Johnson, A. R. Troiano, J. Iron Steel Inst. 37, (1958).

35. J. D. Boyd, "Precipitation of Hydrides in Titanium Alloys," Trans. Am. Soc. Metals, 62, 977, (1969).

36. D. N. Williams, "Hydrogen in Titanium Alloys," TML Report No. 100, May 16, 1958.

37. G. A. Lenning, J. W. Spretnak, R. I. Jaffee, "Effect of Hydrogen on Alpha Titanium Alloys," Trans. AIME, Oct., 1956.

38. G. A. Lenning, L. W. Berger and R. I. Jaffee, "The Effect of Hydrogen on Mechanical Properties of Titanium and Titanium Alloys," Fourth Summary Report from Battelle Memorial Institute to Watertown Arsenal Laboratory, Contract No. DAI-33-019-505-ORD-(P)-1, July 31, 1955.

39. D. N. Williams, F. R. Schwartzberg, P. R. Wilson, W. M. Albrecht, M. W. Mallett, and R. I. Jaffee, "Hydrogen Contamination in Titanium and Titanium Alloys, Part IV: The Effect of Hydrogen on the Hydrogen in Titanium Alloys," WADC TR-54-616, March, 1957.

40. J. D. Boyd, F. H. Haynie, W. K. Boyd, R. A. Wood, D. N. Williams, and R. I. Jaffee, "The Effect of Composition on the Mechanism of Stress-Corrosion Cracking of Titanium Alloys in N_2O_4 and Aqueous and Hot-Salt Environments," Fifth Quarterly Progress Report from Battelle Memorial Institute to NASA, Contract No. NASr-100(09), February 29, 1968.

41. J. Spurrier and J. C. Scully, "Fractographic Aspects of the Stress Corrosion Cracking of Titanium in a Methanol/HCl Mixture," Corrosion, 28, No. 12, 453, (1972).

42. G. Sanderson and J. C. Scully, Corrosion Sci., 8, 541, (1968).

43. D. T. Powell and J. C. Scully, Corrosion, 25, 483, (1969).

44. J. C. Scully and D. T. Powell, Corrosion Sci., 10, 371, (1970).

45. D. A. Mauney, E. A. Starke, Jr., and R. F. Hockman, "Hydrogen Embrittlement and Stress Corrosion Cracking in Ti-Al Binary Alloys," Corrosion, 29, No. 6, 241, (1973).

46. V. J. Colangelo and M. S. Ferguson, "The Role of the Strain Hardening Exponent in Stress Corrosion Cracking of a High Strength Steel," Corrosion, 25, No. 12, 509, (1969).

47. C. D. Beachem, Trans. Am. Soc. Metals, 56, 318, (1963).

48. H. W. Hayden and S. Floreen, Acta Met., 17, 213, (1969).

49. N. H. Polakawski and S. Mostovy, Trans. Am. Soc. Metals, 54, 567, (1961).

50. Lo-Ching Chang, J. Mech. Phys. Solids, 3, (1955).

51. J. W. Spretnak, Trans. AIME, 236, 1639, (1966).

52. R. F. Recht, "Catastrophic Thermoplastic Shear," J. Appl. Mech., 189, (June 1964).

53. G. A. Lenning, J. Metals, 368, (March 1954).

54. M. J. Trzeciak, "Preparation and Analysis of Titanium-Hydrogen Standard Samples," DMIC, Memorandum 9, February 9, 1954.

55. J. F. Gloz, The Ohio State University, Ph.D. Dissertation, (To be published).

56. J. D. Boyd, P. J. Moreland, W. K. Boyd, R. A. Wood, D. N. Williams, and R. I. Jaffee, "The Effect of Composition on the Mechanism of Stress-Corrosion Cracking of Titanium Alloys in N_2O_4, and Aqueous and Hot-Salt Environments," Annual Report to NASA, Contract No. NASr-100(09), August 26, 1969, Battelle Memorial Institute.

57. R. H. Ernst, The Ohio State University, M.S. Thesis, 1967.

58. G. A. Lenning, M. S. Thesis, The Ohio State University, 1956.

59. J. D. Boyd, et al., (see Ref. 58), January, 1969.

60. A. T. Churchman, "The Slip Modes of Titanium and the Effect of Purity on Their Occurrence during Tensile Deformation of Single Crystals," Proc. Roy. Soc., A226, 216, (1954).

61. Shiro Kobayashi, Lecture Notes on Plasticity, Battelle Visiting Professor, The Ohio State University, 1967-68.

62. E. Parker, "Theory and Background of Fracture Mechanics," Chap. 1, Application of Fracture Toughness Parameters to Structural Metals, Metallurgical Society Conferences, Vol. 31, 1966.

63. F. R. Schwartzberg, The Ohio State University, M.S. Thesis, 1958.

64. R. L. Nolder, Technical Memorandum 043-47-1, Autonetics Division. North American Aviation, Inc.

65. A. T. Churchman, Proc. Roy. Soc., A226, 216, (1954).

66. F. C. Holden, H. R. Ogden and R. I. Jaffee, J. Metals, 5, 238, (1953).

67. D. N. Williams, and D. S. Eppelsheimer, J. Inst. Metals, 81, 553, (1953).

68. M. J. Blackburn, ASM Transaction, vol. 59, p. 694, 1966.

69. D. Shechtman, and D. G. Brandon, J. Material Sci. 8, 1233-1237, (1973).

70. A. G. Crocker, and M. Bevis, The Science, Technology and Application of Titanium, p. 453, Pergamon, 1970.

71. R. E. Reed-Hill, The Inhomogeneity of Plastic Def., p. 285, ASM, 1971.

72. N. E. Paten, and W. A. Backofen, Metall. Trans., 1, 2839-2847, (1970).

73. T. S. Liu, and M. A. Steinberg, J. Metal, 4, 1043, (1952).

74. R. E. Reed-Hill, Physical Metallurgy, Van Nostrand, 1964, p. 399.

75. G. F. Bolling, and R. H. Richman, Acta. Met., 13, 709-722, (1965).

76. G. F. Bolling, and R. H. Richman, Acta. Met., 13, 723-743, (1965).

77. G. F. Bolling, and R. H. Richman, Acta. Met., 13, 745-757, (1965).

78. R. N. Orava, G. Stone and H. Conrad, Trans. ASM, 59, 171-184, (1966).

79. R. L. Jones, and H. Conrad, Acta. Met., 15, 649-650, (1967).

80. A. M. Garbe, and R. E. Reed-Hill, Metall. Trans., 2, 2885-2888, (1971).

81. F. D. Rosi, and F. C. Perkins, J. Metals, 5, 1083-1084, (1953).

82. R. V. London, R. E. Edelman, and H. Markus, Trans. ASM, 59, 250-261, (1966).

83. E. O. Hall, Twinning and Diffusionless Transformations in Metals, p. 70, London, 1954.

84. N. Thompson, and D. J. Millard, Phil. Mag., 43, 421, (1952).

85. A. D. Mcquillan, J. Inst. Metals, 78, 249, (1950).

86. A. D. Mcquillan, J. Inst. Metals, 79, 371, (1951).

87. G. A. Lenning, C. M. Craighead, and R. I. Jaffee, AIME, 200, 367, (1954).

88. N. A. Tiner, T. L. Mackay, S. K. Asunmaa, and R. G. Ingersoll, Trans. ASM, 61, 195-202, (1968).

89. H. W. Worner, J. Inst. Metals, 81, 521, (1953).

90. N. E. Paton, B. S. Hickman, and D. H. Leslie, Metall. Trans., 2, 2791, (1971).

91. J. D. Boyd, Science Technology and Application of Titanium, p. 545, Pergamon, 1971.

92. G. A. Lenning, J. W. Spretnak, and R. I. Jaffee, Trans. AIME, 18, 1235, (1956).

93. G. Hagg, J. Phys. Chem., II, 433, (1930).

94. A. D. Mcquillan, Metallurgy of Titanium, New York Academic Press Inc., 1956.

95. H. L. Yakel, Acta. Cryst., 11, 46-51, (1958).

96. S. S. Sidhu, Acta. Cryst., 9, 101, (1956).

97. K. G. Barraclough and C. J. Beevers, J. Less-Common Metals, 35, 177-180, (1974).

98. T. S. Liu, and M. A. Steinberg, Trans. ASM, 50, 455, (1958).

99. G. Sanderson and J. C. Scully, Trans. AIME, 239, 1883, (1966).

100. M. R. Louthan, Jr., Trans. AIME, 227, 1166, (1963).

101. W. R. Holman, R. W. Grawfold, and F. Paredes, Jr., Trans. AIME, 233, 1836, (1965).

102. R. J. Wasilewski, and G. L. Kehl, Metallurgia XI, 50, 301, (1954).

103. D. N. Williams, B. G. Koehl, and E. S. Bartlett, J. Less-Common Metal, 19, 385-398, (1969).

104. W. L. Finley, J. Metals, 12, 280, (1950).

105. B. A. Kolachev, Hydrogen embrittlement of nonferrous metals, Jerusalem, Israel Program for Scientific Translations, 1968, p. 124.

106. V. A. Livanov, B. A. Kolachev, and A. A. Buhanova, The Science, Technology and Application of Titanium, Pergamon, 1970, p. 561.

107. P. Cotterill, "The Hydrogen Embrittlement of Metals," Progr. Mater. Sci., 9, 205, (1961).

108. G. Lenning, M.S. Thesis, The Ohio State University, 1956.

109. D. N. Williams, J. Inst. Metal, 91, 147, (1962).

110. N. A. Tiner, and T. L. Mackay, NASA, Report SM-49105-F3, 1968.

111. H. R. Gray, NASA, TM-D-5000, 1969.

112. Irving and Beavers, J. Mater. Sci., 7, 23-30, (1972).

113. D. G. Westlake, Transquarterly ASM, 56, 1-10, (1963).

114. O. Z. Rylski, Dept. of Mines and Technical Surveys, Mines Branch, Ottawa, Canada, PM-203 (CAN), 1958.

115. C. J. Beeners, The Science, Technology and Application of Titanium, Pergamon, 1970, p. 535.

116. C. D. Beachem, Metall. Trans., 3, 437, (1972).

117. H. R. Gray, Corrosion, 28, 47, (1972).

118. J. Spurrier, and J. C. Scully, Corrosion, 28, 453, (1972).

119. D. A. Mauney, E. A. Starke, and R. F. Hochman, Corrosion, 29, 241, (1973).

120. P. B. Price, Electron Microscopy and Strength of Crystals, Interscience, 1961, pp. 41-129.

121. T. R. Cass, The Science, Technology and Application of Titanium, Pergamon, 1970, p. 459.

122. T. R. Cass, R. W. Quinn and W. R. Spencer, J. Crystal Growth, 2, 413, (1968).

123. Section II of this report.

124. P. B. Hirsch, A. Howie, R. B. Nicholson, and D. W. Pashley, Electron Microscopy of Thin Crystals, Butterworths, 1965.

125. W. R. Tyson, The Science, Technology and Application of Titanium, Pergamon, 1970, p. 479.

126. H. Conrad, Canad. J. Phys., 45, 581, (1967).

127. R. I. Jaffee, H. R. Ogden and D. J. Maykuth, Trans. AIME, 188, 1261, (1950).

128. E. C. Burke, J. Metals, 4, 295, (1952).

129. R. L. Bell, and R. W. Cahn, J. Inst. Metals, 86, 433-438, (1958).

130. R. L. Bell, and R. W. Cahn, Acta. Met., 1, 752-753, (1953).

131. J. D. Boyd, P. J. Mouland and W. K. Boyd, Battelle Memorial Institute to NASA, Contract No. NASA-100-(09), 1969.

132. D. A. Mauney, and E. A. Starke, Corrosion, 25, 177, (1969).

133. M. J. Blackburn, and J. C. Williams, Paper presented at the Conference on the Fundamental Aspects of Stress Corrosion Cracking, Columbus, Ohio (1967).

134. A. N. Stroh, Proc. Roy. Soc., A223, 404-414, (1954).

135. A. R. Troiano, Trans. ASM, 52, 54, (1960).

136. F. H. Beck, and M. G. Fontana, NASA, Report 12, Grant No. NGL 36-008-051, 1972.

137. B. Cox, Corrosion, 30, 191-199, (1974).

138. J. D. Boyd, Metall. Trans., 4, 1037-1045, (1973).

139. W. R. Tyson, The Science, Technology and Application of Titanium, Pergamon, 1970, p. 479.

140. Anderson, Jillsoh, and Dunbar, J. Mater. Sci., 8, 1233, (1973).

141. Levine, Trans. AIME, 236, 11558, (1966).